Investigations into the Optically Stimulated Luminescence Response of Various Materials

by

William Geoffrey West

A dissertation submitted in partial fulfillment
of the requirements for the degree of
Doctor of Philosophy
(Nuclear Engineering and Radiological Sciences)
in the University of Michigan
2011

Doctoral Committee:

Professor Kimberlee J. Kearfott, Chair
Professor Rodney C. Ewing
Professor Ronald M. Gilgenbach
Professor Zhong He
Joseph A. Miklos

For Dad

ACKNOWLEDGEMENTS

I would like to thank my mother, Margie, for never letting me give up and always believing in me.

Sincere thanks also to my advisor, Professor Kimberlee Kearfott, for keeping me out of law school and reminding me of why I became a scientist in the first place. Additional thanks also to those individuals that helped this research along the way: Andrew Kalchik and Sara Bernal, my dedicated lab partners, for many long nights of work; Dr. Benjamin Warner and David Morris of Los Alamos National Laboratory for helping me to better understand radiation dosimetry and optics; and Dr. David Jordan for his help with all thing electrical and for mentoring me while I mentored him. A special thanks to Peggy Gramer, for always lending an ear and wise counsel when times were tough.

Finally, I want to thank my wife, Jennifer, for pushing me to finish what I started and for betting the farm on me.

PREFACE

In the summer of 2002, as the world – and the United States in particular – were still adjusting to a world in which the threat of nuclear terrorism appeared to have increased dramatically, I was busy preparing to leave my job as a medical physicist and enter law and business school (to attain a JD/MBA) at the University of Michigan. This was a career change that I had been planning for many years and I had only to sign the acceptance papers and arrange my move. As I contemplated my new career direction, I received a remarkably timely phone call from Professor Kimberlee Kearfott, who had been my Master's degree advisor several years prior. She mentioned that there was a project forming around the idea of using optically stimulated luminescence (OSL) techniques to improve our ability to detect illicit radiological materials, and that she thought that I might be interested. I told her that I had other plans in the works, but to tell me more since it sounded intriguing.

Over the course of an hour-long conversation, we discussed the importance of this type of work, the technical challenges, and the opportunities. Though the University of Michigan had a long history of groundbreaking research in the area of thermoluminescence dosimetry, OSL technology was relatively new and this area of scientific inquiry had not yet been explored at this institution. However, we both believed that if suitable materials could be indentified and techniques developed, it would permit a greater degree of ease and sophistication in extracting dose information from a

sample, and could potentially lead to novel applications yet unimagined. We believed that it was important to make every attempt to advance the state of knowledge in this field and that a significant need existed in analyzing materials for potential use in OSL applications that had never been evaluated before.

By the end of this phone call, I had decided to change my plans for law and business school and pursue a Ph.D. instead. I wanted to do something that would, in some small way, advanced the science of radiation detection and characterization; and perhaps lead to additional research and/or applications that would improve the safety and security of every peace-loving person on our planet.

This dissertation is the final product of my research. It documents a series of initial experiments undertaken to learn optimal OSL techniques and to produce novel information regarding basic OSL properties of numerous materials; details the design, construction and testing of a custom OSL reader; and reveals the results of a set of final experiments intended to more fully characterize the OSL behavior, including fading properties, of a set of promising materials.

I hope you, the reader, find value in its contents.

TABLE OF CONTENTS

DEDICATION ii

ACKNOWLEDGEMENTS iii

PREFACE iv

LIST OF FIGURES vii

LIST OF TABLES x

CHAPTER 1: Introduction 1

CHAPTER 2: The Sunlight OSL Response of a Commercially Available α-Al_2O_3:C Personnel Dosimetry Material 29

CHAPTER 3: The Optically Stimulated Luminescence of Various Known Thermoluminescent Materials 45

CHAPTER 4: An Affordable Optically Stimulated Luminescent Dosimeter Reader Utilizing Multiple Excitation Wavelengths 71

CHAPTER 5: OSL Investigation of KBr, $CaSO_4$:Tm, $CaSO_4$:Dy, $CaSO_4$:Dy+P, LiF:Mg,Cu,Na,Si and LiF:Mg,Cu,Si 126

CHAPTER 6: Conclusions 193

LIST OF FIGURES

Figure

1.1 Thermoluminescence (TL) glow curve for LiF:Mg,Cu,Na,Si 6 h after irradiation to 500 mGy with a 120 kVp x-ray beam. 6

1.2 Energy-level diagram showing the possible optical absorption transitions in a semiconductor.. 12

1.3 Photo-ionization cross-section versus incident photon energy as predicted by the Lucovsky theoretical model. 17

1.4 Graphical depiction of the continuous-wave optically stimulated luminescence (CW-OSL), linearly-modulated OSL (LM-OSL) and pulsed OSL (POSL) readout techniques, shown from top to bottom. 21

2.1 OSL response of a-Al_2O_3:C samples exposed to varying durations of direct sunlight……..... 34

2.2 Peak OSL signal of a-Al_2O_3:C in units of equivalent dose versus total direct sunlight exposure. 35

2.3 OSL response of a-Al_2O_3:C samples exposed to varying durations of direct sunlight after receiving a 15 mGy beta dose..... 36

2.4 Peak OSL signal of a-Al_2O_3:C versus duration of 100,000 lux direct sunlight exposure..37

2.5 Solar radiation spectrum for direct light at both the top of the Earth's atmosphere and at sea level..... 39

3.1 Optically stimulated luminescence (OSL) response during infrared light (λ = 830 nm) stimulation of unirradiated samples..... 53

3.2 Optically stimulated luminescence (OSL) response during blue light (λ = 470 nm) stimulation of unirradiated samples..... 54

3.3 Optically stimulated luminescence (OSL) response during infrared light (λ = 830 nm) stimulation of samples irradiated to 15 mGy. 55

3.4 Optically stimulated luminescence (OSL) response during blue light (λ = 470 nm) stimulation of samples irradiated to 15 mGy. 55

3.5 Optically stimulated luminescence (OSL) response during infrared light (λ = 830 nm) stimulation of samples irradiated to 1.5 Gy..... 56

3.6 Optically stimulated luminescence (OSL) response during blue light (λ = 470 nm) stimulation of samples irradiated to 1.5 Gy..... 57

3.7 Optically stimulated luminescence (OSL) peak signal height versus dose for $CaSO_4$:Tm. 58

4.1 Basic layout of the optically stimulated luminescence (OSL) reader. 77

4.2 Light emitting diode (LED) source assembly and iris plate with iris. 81
4.3 'Exploded view' of the main optically stimulated luminescence (OSL) reader components.. 88
4.4 Rendering of the optically stimulated luminescence (OSL) reader emission filter housing. 89
4.5 Rendering of the optically stimulated luminescence (OSL) reader sample holder assembly. 91
4.6 Circuit diagram of the excitation power supply. 96
4.7 Circuit diagram of the cooling fan/vacuum pump control system……..……..98
4.8 Photograph of the optically stimulated luminescence (OSL) reader case when closed……. 99
4.9 Screenshot of the optically stimulated luminescence (OSL) reader software interface……..... 103
4.10 Block diagram of the optically stimulated luminescence (OSL) reader software interface…..... 104
4.11 Circuit diagram of the photomultiplier tube (PMT) gating circuit. 107
4.12 Graph showing the results of the single channel analyzer (SCA) setup testing……..... 110
4.13 Graph showing the results of the iris position optimization testing..... 112
4.14 Optically stimulated luminescence (OSL) output graph from the OSL reader for samples of Luxel™ irradiated to 250 mGy and 500 mGy using Cs-137 gamma rays……..... 114
5.1 Corrected optically stimulated luminescence (OSL) curves for KBr irradiated to 500 mGy dose in air using 120 kVp x-rays, at 6 h post-irradiation..... 144
5.2 Corrected peak signal (CPS) curves for KBr irradiated to 500 mGy dose in air using 120 kVp x-rays. 144
5.3 Peak signal minus end signal (P-E) curves for KBr irradiated to 500 mGy dose in air using 120 kVp x-rays..... 145
5.4 Ratio of peak optically stimulated luminescence (OSL) signal minus end signal (P-E) values for KBr under red light excitation (λ = 625 nm) versus green light excitation (λ = 530 nm)..... 146
5.5 Thermoluminescence (TL) glow curves for KBr powder irradiated to 500 mGy dose in air using 120 kVp x-rays. 146
5.6 Corrected optically stimulated luminescence (OSL) curves for $CaSO_4$:Tm irradiated to 500 mGy dose in air using 120 kVp x-rays, at 6 hours post-irradiation. ... 147
5.7 Corrected average signal (CAS) curves for $CaSO_4$:Tm irradiated to 500 mGy dose in air using 120 kVp x-rays. 148
5.8 Corrected peak signal (CPS) curves for $CaSO_4$:Tm irradiated to 500 mGy dose in air using 120 kVp x-rays..... 148
5.9 Corrected average signal (CAS) output ratios for $CaSO_4$:Tm irradiated to 500 mGy dose in air using 120 kVp x-rays, as a function of time elapsed since irradiation. 149
5.10 Thermoluminescence (TL) glow curves for $CaSO_4$:Tm irradiated to 500 mGy dose in air using 120 kVp x-rays. 150
5.11 Corrected optically stimulated luminescence (OSL) curves for $CaSO_4$:Dy irradiated to 500 mGy dose in air using 120 kVp x-rays, at 6 hours post-irradiation. ... 151

5.12 Peak signal minus end signal (P-E) curves for $CaSO_4$:Dy irradiated to 500 mGy dose in air using 120 kVp x-rays. 151
5.13 Thermoluminescence (TL) glow curves for $CaSO_4$:Dy irradiated to 500 mGy dose in air using 120 kVp x-rays. 152
5.14 Corrected optically stimulated luminescence (OSL) curves for $CaSO_4$:Dy+P irradiated to 500 mGy dose in air using 120 kVp x-rays, at 6 hours post-irradiation. ... 153
5.15 Thermoluminescence (TL) glow curves for $CaSO_4$:Dy+P irradiated to 500 mGy dose in air using 120 kVp x-rays. 154
5.16 Corrected optically stimulated luminescence (OSL) curves for LiF:Mg,Cu,Na,Si irradiated to 500 mGy dose in air using 120 kVp x-rays, at 6 hours post-irradiation. 155
5.17 Corrected average signal (CAS) curves for LiF:Mg,Cu,Na,Si irradiated to 500 mGy dose in air using 120 kVp x-rays. 156
5.18 Corrected peak signal (CPS) curves for LiF:Mg,Cu,Na,Si irradiated to 500 mGy dose in air using 120 kVp x-rays. 156
5.19 Corrected average signal (CAS) output ratios for LiF:Mg,Cu,Na,Si irradiated to 500 mGy dose in air using 120 kVp x-rays. 157
5.20 Afterglow optically stimulated luminescence (OSL) curves for LiF:Mg,Cu,Na,Si irradiated to 500 mGy dose in air using 120 kVp x-rays, at 6 hours post-irradiation. 158
5.21 Thermoluminescence (TL) glow curves for LiF:Mg,Cu,Na,Si irradiated to 500 mGy dose in air using 120 kVp x-rays. 159
5.22 Corrected average signal (CAS) curves for LiF:Mg,Cu,Na,Si, irradiated to 500 mGy dose in air using 120 kVp x-rays, with only green, cyan, blue and royal blue curves shown…… 160
5.23 Corrected optically stimulated luminescence (OSL) curves for LiF:Mg,Cu,Si irradiated to 500 mGy dose in air using 120 kVp x-rays, at 6 hours post-irradiation. ... 161
5.24 Corrected optically stimulated luminescence (OSL) curves for LiF:Mg,Cu,Si, irradiated to 500 mGy dose in air using 120 kVp x-rays, at 30 days post-irradiation. ... 162
5.25 Corrected average signal (CAS) curves for LiF:Mg,Cu,Si irradiated to 500 mGy dose in air using 120 kVp x-rays. 163
5.26 Afterglow optically stimulated luminescence (OSL) curves for LiF:Mg,Cu,Si irradiated to 500 mGy dose in air using 120 kVp x-rays, at 5 days post-irradiation. 164
5.27 Total integrated optically stimulated luminescence (OSL) afterglow signal for LiF:Mg,Cu,Si irradiated to 500 mGy dose in air using 120 kVp x-rays, as a function of time since irradiation. 165
5.28 Ratio of LiF:Mg,Cu,Si integrated optically stimulated luminescence (OSL) afterglow signals for green, cyan and blue light excitation relative to royal blue light excitation, as a function of time since irradiation. 166
5.29 Thermoluminescence (TL) glow curves for LiF:Mg,Cu,Si irradiated to 500 mGy dose in air using 120 kVp x-rays. 167

LIST OF TABLES

Table

3.1 Thermal annealing parameters used for material samples.……..……51
4.1 Light emitting diode (LED) emission specifications. 79
4.2 Digital acquisition (DAQ) board digital channel assignments..... 98

CHAPTER 1

INTRODUCTION

Optically stimulated luminescence (OSL) dosimetry relies upon the illumination of an irradiated sample with light to produce a stimulated emission of light proportional to the radiation dose which previously caused trapping of electrons in the material[1]. OSL has become an accepted personnel dosimetry method during the past 15 years, as evidenced by the success of a commercially-available dosimeter based upon anion-defective, carbon-doped aluminum oxide, or α-Al_2O_3:C (Luxel®, Landauer, Inc., 2 Science Road, Glenwood, Illinois, 60425-1586, USA, custserv@landauer.com, +1 800 323 8830, www.landauer.com). The use of OSL dosimeters versus other choices, such as thermoluminescent dosimeters (TLDs) or film-based dosimeters, is attractive for a number of technical reasons, including: 1) the current material of choice for this application, α-Al_2O_3:C, is highly sensitive in that it emits a large amount of stimulated luminescence per unit of radiation dose absorbed[2-8]; 2) the optical readout method is fast and relatively simple[5, 9]; and 3) the OSL technique lends itself to repeat readout of samples since, unlike thermal stimulation as used in TLDs, optical stimulation can be activated and deactivated very quickly, allowing fast readout of the dose information without a significant depopulation of the dosimetric traps[10]. Although OSL dosimeters are frequently susceptible to light-induced fading[11-13], maintaining the material in a

light-tight container during use does not present a significant problem in most applications.

In addition to its application in the area of personnel dosimetry, the OSL phenomenon is widely used in the dating of geologic samples[4, 14-22] and has been investigated and used for a variety of other applications, including remote dosimetry[23], retrospective dosimetry[14, 24-27] and medical dosimetry[28-30]. In most of these applications, the material employed is either α-Al_2O_3:C or a natural material such as quartz (SiO_2) or feldspar ($KAlSi_3O_8$, $NaAlSi_3O_8$, or $CaAl_2Si_2O_8$).

This dissertation documents a series of research and development activities exploring the OSL response of various materials, either to document the properties of materials never before studied for OSL, or to provide useful additional information regarding materials already investigated to some degree. In order to appreciate and comprehend the results and significance of the findings herein, it is essential for the reader to have a basic understanding of the theoretical underpinnings of OSL. This chapter provides a primer on OSL theory and concludes by outlining the objectives and organization of the dissertation.

THEORY

Physical Processes

OSL

OSL is the light emitted from an irradiated insulator or semiconductor as a result of exposure to light. The intensity of the OSL signal is a function of how much ionizing radiation was absorbed by the material. During irradiation of a suitable material, ionization of valence electrons and the consequent creation of electron-hole pairs occur. Pre-existing defects within the material then localize the free electrons and holes into 'traps'. The energy of both electrons and holes in these traps lies within the forbidden gap between the valence band and conduction band of the material. Subsequent illumination of the irradiated sample with light leads to absorption of energy by the trapped electrons, allowing them to transition from the localized trap into the delocalized conduction band. Subsequent recombination of these freed electrons with localized holes results in radiative emission and luminescence. This is the OSL signal, and it is generally accompanied by photoconductivity, since the process leads to the presence of electrons in the conduction band during illumination.

When discussing the OSL phenomenon, it is useful to have a basic understanding of solid state physics, crystal structure and electronic transport theory. While a complete review of these topics is beyond the scope of this dissertation, a brief review of material defects is salient. Defects can be of various types. There are interstitial defects, where an

atom is located within the crystal structure at a point not normally occupied; substitution defects, where a dopant atom replaces an atom of the bulk crystal material at a particular location; and vacancy defects, where an atom normally present in the material structure is missing. In addition, there are numerous other types of defects in both crystals and amorphous compounds, including complex defects consisting of multiple defect types, e.g., an association of a dopant atom with a vacancy defect[31]. For the purposes of this document, it is helpful to understand one type of defect in particular: the F-center.

An F-center is a type of crystallographic defect in which an anionic vacancy in a crystal is filled by one or more electrons, the number depending on the charge of the missing ion in the crystal. Electrons in such a vacancy tend to absorb light in the visible spectrum such that a material that is usually transparent becomes colored; thus the origin of the name, F-center, which comes from the German word farbe, meaning color. The greater the number of F-centers, the more efficiently the compound will absorb light of a particular wavelength and the more intense will be the color of the compound. F-centers may be produced in a crystal by heating the material in the presence of an atmosphere of the metal that constitutes the material[31], or by chemically substituting a dopant for one of the primary lattice atoms to deform the normal crystal structure. In addition, ionizing radiation can produce F-centers. The F-center is a particularly important defect in this context because its predilection to absorb optical energy results in a likelihood of OSL behavior.

While other defect types do come into play in the various electron-hole transport mechanics associated with OSL, a complete understanding of those defects is not as important as a more general understanding of energy level diagrams and the phenomena

that are associated with the various types of charge transitions amongst these energy levels. Besides OSL, there are a number of other transition phenomena possible in insulators and semiconductors and it is valuable to understand those other phenomena to know how they differ from, and relate to, OSL. These related phenomena are described below.

Thermoluminescence

Thermoluminescence (TL) or thermally stimulated luminescence (TSL), is the phenomenon, or technique, whereby charges trapped at defect sites during irradiation are released upon heating of the sample, thereby producing luminescence. TL and OSL differ only in the mechanism used to free the trapped charges. The recombination processes are identical. Thermoluminescence has been used as a dosimetry technique for longer than OSL and a great deal more published research into its use is available. It is widely used in virtually all areas of radiation dosimetry, and its application continues to be studied and improved.

In TL, the sample to be read out is typically heated from room temperature to a maximum temperature, T_m, at a specific heating rate, R. During this heating process, an irradiated TL material emits light in proportion to the radiation dose. This light is emitted with changing intensity corresponding to the excitation of charge carriers in various traps in the material. As the temperature increases, the resultant greater lattice vibrational intensity excites charge carriers in deeper and deeper traps to the point that they are delocalized and can undergo radiative recombination. The luminescence intensity is

plotted as a function of time and, by association, temperature to produce what is known as a 'glow curve'. An example of a glow curve is presented as Figure 1.1. Once the sample reaches the maximum temperature, the sample may be maintained at that temperature until the luminescence fades to a minimal level, or the heating may be suspended. In addition, the sample may also then be subsequently 'annealed' at an even higher temperature for a period of time for the purpose of clearing out, i.e., depopulating, all of the traps in the material.

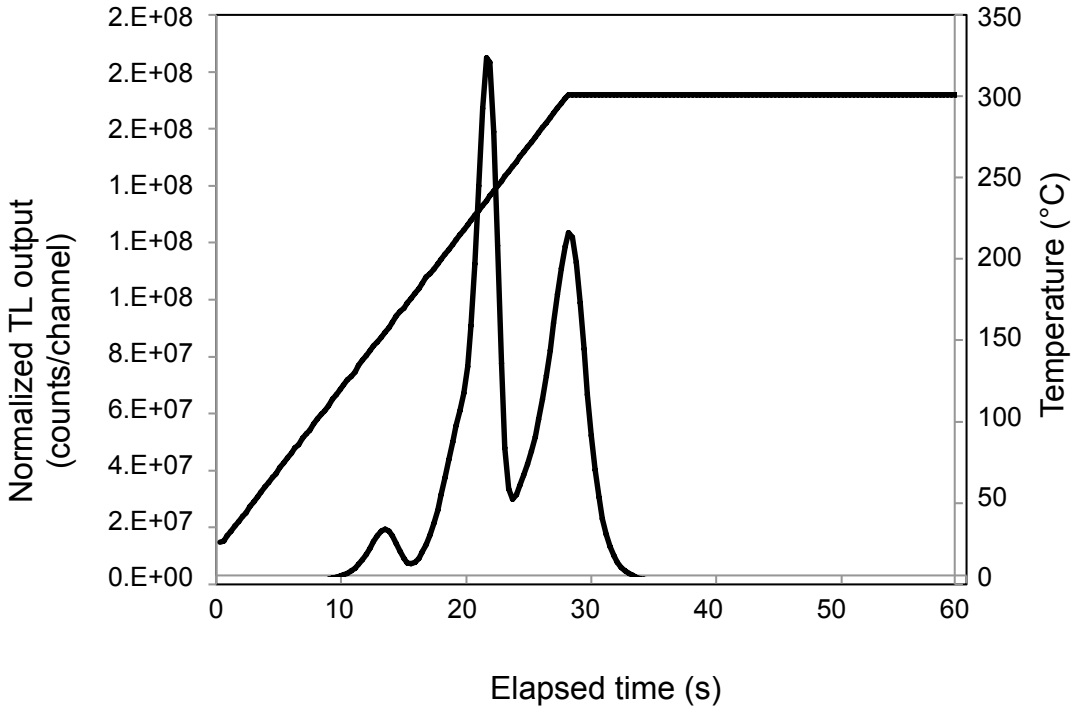

Figure 1.1: Thermoluminescence (TL) glow curve for LiF:Mg,Cu,Na,Si 6 h after irradiation to 500 mGy with a 120 kVp x-ray beam. The dashed line shows the temperature and the solid line is the TL signal intensity.

In a TL glow curve, the position, i.e., temperature, of a TL peak and its thermal stability are dictated by both the energy level, E, of the corresponding trap and its s value, i.e., the attempt-to-escape frequency factor[32]. It is this combination of E and s that dictates the temperature of the peak. If the traps in a material are of roughly equal s, the lower-temperature peaks correspond to lower-energy, i.e., shallower, traps in the material. Additionally, the lower the TL peak temperature, the greater the degree of fading of the peak over time at room temperature. This is a result of charge carrier 'leakage' due to thermal excitation of charge carriers from the shallow trap into the conduction band, for electrons, or into the valence band, for holes. The fading of these low-temperature peaks is normally considered a confounding factor in dosimetry applications, since the focus is on accurately estimating radiation dose irrespective of the time elapsed since irradiation. In TL, because of the inherently probabilistic nature of thermal excitation, the peaks corresponding to the traps have an associated width and therefore closely-spaced peaks may overlap and be difficult to resolve. This is another confounding factor in TL dosimetry and frequently necessitates the use of complex curve-fitting and deconvolution procedures, performed using computer software, to determine the relative charge populations of various traps in the material.

Since there is a direct correlation in the underlying physics of the TL and OSL processes, there is also a correlation between a materials' TL behaviors and OSL behaviors. Because of this, the substantial body of published TL research informs not only the investigation of OSL materials, but also aids in their identification. Specifically, if a material exhibits TL, it may also exhibit OSL. Since materials exhibiting TL are already known to have band gap energy levels that are populated during exposure to

radiation, and also known to emit light during the electron-hole recombination process, the only additional question is whether trap ionizations can be produced using optical excitation instead of thermal excitation. The answer to this question depends on the details of each material's molecular structure and will be discussed in greater detail later in this chapter.

Photoluminescence

One related phenomenon easily confused with OSL is photoluminescence (PL). PL involves the optical excitation of an electron in the ground state of a defect site to an excited state within that same defect site. This type of transition is referred to as an 'intra-center' transition since it does not involve the delocalization of electrons or holes in the material. Following excitation, the electron undergoes radiative relaxation back to the ground state and luminescence is produced. The intensity of this luminescence is proportional to the concentration of excited defects. Unlike OSL, PL is generally not dependent upon irradiation of the sample – it is an intrinsic property of the unirradiated material. Also unlike OSL, since no ionization occurs – i.e., charge carriers are not delocalized – there is no associated photoconductivity. One other difference between PL and OSL is that in PL, the wavelength of the luminescence is always longer than that of the excitation light since some of the excitation photon energy is lost to thermal excitation of the sample. The difference in the incident and emitted wavelengths is called the Stokes shift. With OSL, the emitted light may have *either* a longer or a shorter wavelength than the incident light due to the fact that the recombination process occurs at

a different defect site than the excitation process and therefore the energies are not directly related.

Delayed OSL (DOSL)

During OSL readout, once the stimulation light is turned off, the emitted luminescence typically decays at a rate corresponding to the luminescence centers in the material. Since the recombination process depends upon charge carriers moving through the material and finding an unpaired mate, and also since there is an associated metastable nature to the excited states in the defect sites, there is an associated delay after illumination as the stimulated luminescence is emitted. The rate of recombination, and therefore the intensity of the OSL signal, can be approximated as a first-order process with a time constant dependent upon the specific characteristics of the material. An example of this behavior can be seen in Al_2O_3:C, in which there are F-centers with an excited state half-life of 35 ms at room temperature[33-34]. However, in some Al_2O_3:C samples, and in various other materials, a much longer lifetime is observed. In these cases, the OSL signal decays much more slowly than one would expect due to either normal recombination or to re-trapping of the freed charges. In Al_2O_3:C, this decay has been fitted to two exponentials, the faster decay being due to the intrinsic F-center luminescence lifetime. The other decay component is significantly slower, exhibiting a half-life of 545 ms at 25 °C. However, unlike the fast component, this slow component has been shown to be highly temperature-dependent[34]. This temperature dependence indicates that the slower component results from the re-trapping of charges in very

shallow traps, which are then cleared out thermally at room temperature. As such, though this process has been labeled 'delayed' OSL or DOSL[35], it can also be regarded as room-temperature TL occurring subsequent to optical stimulation.

Photo-transferred thermoluminescence (PTTL)

As the previous section illustrates, DOSL involves the optically induced transfer of charges from deep traps that are not susceptible to room temperature TL, to shallow traps that are. DOSL is one form of a more general class of phenomena known as PTTL. In addition to DOSL, PTTL also covers those processes where the shallow traps into which the charge carriers are deposited after optical stimulation are not so shallow that the charge carriers are delocalized from them at room temperature. In this case, after optical stimulation, the material is left in a stable state where it can subsequently be examined using traditional TL techniques – or, for that matter, OSL techniques, in which case the process is called photo-transferred OSL or PTOSL – to extract information. PTTL behavior is found in many luminescence dosimetry materials and is a frequently important, sometimes confounding process in OSL research and development.

In a typical example of how PTTL behavior might be observed during OSL experimentation, let us imagine an irradiated sample read out using TL up to a certain temperature T. During that readout, all traps in the material with energy levels less than the corresponding thermal activation energy of T are emptied, such that an immediate re-read of the sample using TL procedures up to temperature T would yield no remaining signal. Let's say that the material is then exposed to a light source for some period of

time. If the material exhibited PTTL, one could then re-read the sample using TL up to the same temperature T, and luminescence would result, as there would have been an optical transfer of charge from deep traps not thermally annealed to shallow traps accessed during the TL examination. In this case, without knowing about the PTTL process in the material, the experimenter may have assumed that the material had received a dose of ionizing radiation between the first and second TL readouts. In this way, PTTL can be confounding. On the other hand, PTTL can be a useful tool for investigating the optical absorption and transition processes that occur in OSL materials during illumination. In addition, if properly known and characterized, the PTTL behavior of a material can be harnessed for use as a dosimetry method since, like OSL, the PTTL signal intensity is proportional to both the original dose of radiation and the intensity of the optical excitation. However, it is generally preferable to simply use TL or OSL techniques for dosimetry purposes.

Summary of Optical Absorption Transitions

It is helpful in understanding, and discriminating amongst, the various possible optical processes above, to employ a visual metaphor. As such, an energy-level diagram showing the various possible optical absorption transitions is presented as Figure 1.2. This figure shows the seven different possible light-induced electron transitions in a semiconductor: ionization, exciton formation, defect ionization, intra-center excitation, and trap ionization.

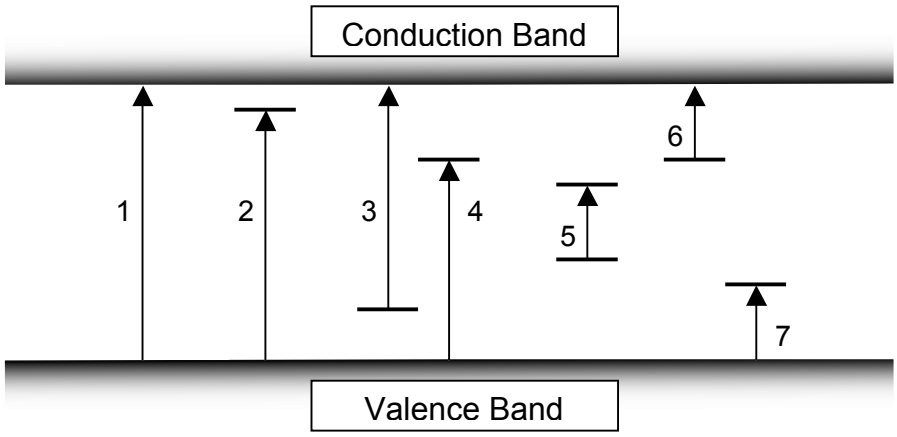

Figure 1.2: Energy-level diagram showing the possible optical absorption transitions in a semiconductor. The possible transitions are: (1) ionization; (2) exciton formation; (3, 4) defect ionization; (5) intra-center excitation; and (6, 7) trap ionization.

Ionization of electrons directly out of the valence band, designated as transition type 1 in Figure 1.2, is typically not possible at optical wavelengths for insulators such as Al_2O_3, which has a band gap of ~6.6 eV[36], as well as semiconductors with very wide band gaps. However, it can be important for semiconductors such as ZnSe[1], which has a band gap of 2.7 eV[37].

Exciton formation, labeled transition type 2 in Figure 1.2, results in a localized charge which can then lead to OSL and/or TL, but this type of transition generally only occurs at vacuum ultraviolet wavelengths and is therefore not usually important in dosimetry applications[1].

Defect ionizations, shown as transition types 3 and 4 in Figure 1.2, are where an incident photon is energetic enough to cause ionization at a defect site within the material, but not necessarily energetic enough to cause ionization in the bulk crystal

structure. This optical transition essentially accomplishes the same purpose as the irradiation phase of the OSL method, using somewhat less energy. Subsequent to this type of transition, trapping of the electron may occur, leading to the possibility of later OSL and/or TL. As with transition type 2, these transitions would typically require photon energies corresponding to ultraviolet stimulation wavelengths and would not be desired transitions for dosimetry applications.

Intra-center transitions or excitations, designated as transition type 5 in Figure 1.2, involve the excitation of an electron in a defect from a ground state to an excited state. This type of transition is the genesis of PL, which is produced by the subsequent radiative relaxation of the excited electron back to its ground state. As discussed previously, since this transition type does not involve the transport of charge from one defect site to another, or elevate electrons into the conduction band, this is not an OSL phenomenon. If the defect itself was caused by the irradiation of the material, however, this would be called radiophotoluminescence (RPL) instead of PL. While RPL could be used to determine the radiation dose to a material, unlike the OSL method, where defects are not induced by the irradiation but merely populated, there would be no way to 'reset' the material back to its original unirradiated condition using optical methods. One additional consideration for transition type 5 is that if the temperature is sufficiently high and the excited defect state is sufficiently close in energy to the bulk material conduction band energy, then thermal ionization of the excited state electron can occur, leading to subsequent TL. This phenomenon has been exploited in certain geologic dating applications where reuse of the sample is unnecessary[38-39].

Finally, trap ionizations, shown as transition types 6 and 7 in Figure 1.2, constitute OSL. These transitions are made possible by the initial trapping of electrons and holes at defect sites during irradiation, followed by the release of those trapped charges by absorption of light energy. The subsequent recombination of the electrons and holes results in OSL emission. It is worth mentioning that these types of transitions are also the mechanism behind phototransfer mechanisms such as PTTL, as well as optical bleaching of TL and/or OSL signals – that is, when light exposure 'clears' or optically anneals a sample.

Mathematical Description

The intensity of the OSL signal at any given time is related to the rate at which the charge carriers are excited from defect traps and experience recombination. The rate at which charge carriers are excited from the traps is a function of the concentration of trapped charges in the material. In the simplest case of first-order behavior, this rate is linearly proportional to the trapped charge concentration. If one plots the intensity of the luminescence as a function of time, as is customary for OSL readouts, a characteristic luminescence-versus-time curve results. In the simplest case of a material with a single trap with first-order kinetics, this curve follows a simple exponential decay function. The integral of the luminescence-versus-time curve is related to the trapped charge concentration, which is, in turn, proportional to the absorbed radiation dose. This methodology is the basis for the use of OSL measurement for radiation dosimetry. In addition to the induced luminescence signal being proportional to the initial dose of

radiation absorbed, this signal is also a function of the intensity and wavelength of the optical stimulation. How these parameters affect the luminescence signal is discussed below.

For OSL to occur, it is first necessary for an optical absorption to occur that stimulates charge carriers out of a trap, or optically ionizes them. The probability of optical ionization, p, of any given trap is simply the product of the incident light intensity and the probability that the trap will ionize by stimulation with a photon of this light. This is described by the following equation[1]:

$$p(E) = \Phi\sigma(E) \tag{1}$$

where Φ is the optical stimulation intensity and $\sigma(E)$ is the photoionization cross-section for interaction of the trap with an incident photon. E is the energy of the individual photons of incident light. Since the photoionization cross-section for a trap is a function of the photon energy of the incident light, the probability of trap ionization depends on the photon energy. It is important to note here that p does not predict in full the OSL light output of a material. If the material is opaque to its own emitted OSL light, or does not possess radiative recombination processes, the output OSL signal will be reduced or eliminated. In any case, if a material produces OSL, p will be proportional to the OSL output and is therefore an important parameter to understand.

The photoionization cross-section σ, as a function of incident photon energy E, can be either calculated theoretically or determined empirically. Several models exist to calculate the shape of this function and these models make different underlying

assumptions about trap structures, energy transitions, and other physical processes. Though a thorough review of the different models is beyond the scope of this introduction, it should be said that no one model created to date fully describes the photoionization behavior of every trap in every material. It is also important to note that all models predict the following behavior: that trap ionization does not occur below a threshold optical activation energy, E_o, and that as the photon energy increases beyond this threshold, the photoionization cross-section increases quickly. Where the models differ is in exactly how fast this cross-section increases with energy, and also whether continued increases in photon energy result in a sustained high cross-section, or whether the cross-section begins to decrease again and to what extent. One model frequently used for dosimetric materials, due to its high level of predictive value for wide-band-gap insulators commonly used as dosimetry materials, is described by the following equation[40]:

$$\sigma(h\upsilon, E_o) \propto \left[\frac{4(h\upsilon - E_o)E_o}{(h\upsilon)^2}\right]^{3/2} \quad (2)$$

where h is Planck's constant, υ is the frequency of the incident photon and E_o is the threshold optical ionization energy of the trap.

In this model, the photoionization cross-section reaches its maximum when the photon energy is twice the trap threshold energy and then declines very slowly at higher photon energies. A graph showing this function is presented as Figure 1.3.

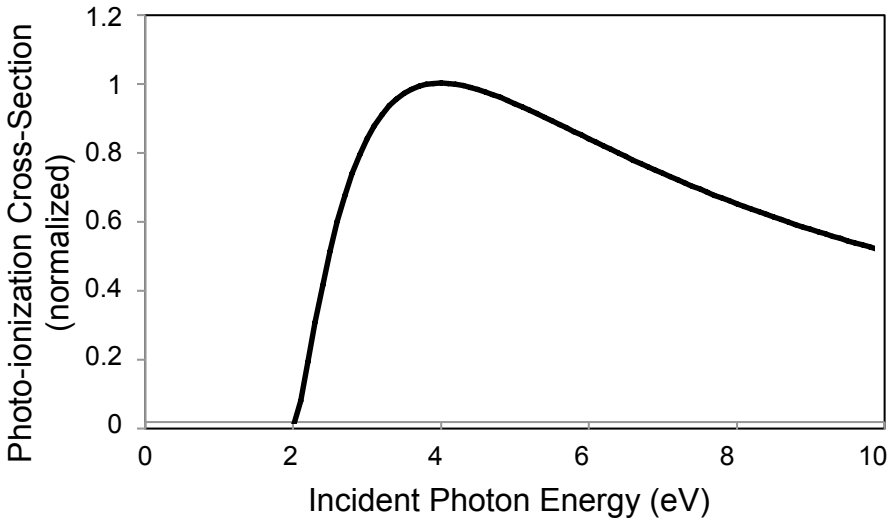

Figure 1.3: Photo-ionization cross-section versus incident photon energy as predicted by the Lucovsky theoretical model. In this graph, the threshold optical ionization energy E_o has been set to 2 eV.

In addition to predictive models, the shape of the photoionization cross-section curve can also be determined experimentally. In one method, the photoconductivity of a sample is measured during illumination, as the wavelength of the incident light source is increased, typically using a scanning monochromator. In another method, the OSL output intensity is measured as wavelength is increased. In either case, since both the photoconductivity and the OSL signal of a material are directly proportional to the photoionization cross-section, these techniques yield the latter.

It is interesting to note that since the photoionization cross section for a given trap has a minimum activation energy, and since the probability of OSL signal resulting from the trap rises quickly with the photon energy above that threshold, this suggests a method for reading, or emptying, traps in a material individually. If the excitation light is scanned from long wavelength to short wavelength, it is possible to produce an OSL

signal from progressively deeper traps. Unlike with TL, one can thus produce a signal from a shallow trap without producing any signal from, or affecting, a deeper trap even if that deeper trap is similar in energy level. This characteristic results in a benefit to OSL over TL in being able to clearly discriminate closely-spaced traps in a material by use of careful wavelength selection. It is this particular technique that is employed in Chapter 5 of this dissertation to examine the fading behavior of different traps in several OSL materials.

The Relation between OSL and TL Mechanics

It is useful when comparing a material's TL and OSL behavior to understand the relation between the thermal activation energy of a trap, E_t, and the trap's optical activation energy, E_o. The optical ionization energy is not equal to the thermal activation energy since some of an excitation photon's energy is converted in phonon energy, or lattice vibrations. As such, the optical ionization energy is somewhat greater than the thermal activation energy, according to the following equation[32]:

$$E_o = E_t + E_{ph} \tag{3}$$

where E_{ph} is the phonon energy.

The phonon energy is calculated using the following equation:

$$E_{ph} = S\hbar\omega_p \quad (4)$$

where S is the Huang-Rhys factor and ω_p is the phonon vibration frequency of the material. These parameters are material properties generally determined experimentally using a variety of crystallographic material testing techniques, such as x-ray diffraction and scattering.

The thermal activation energy, E_t, is the amount of energy required to excite an electron from one energy level, as shown on a classical energy level diagram, to a higher level. This value, if not already known for a specific trap, can be estimated using TL techniques. By noting the temperature in the TL glow curve at which the maximum TL signal is emitted, one can estimate this thermal activation energy. The relation linking these two values[32], is as follows:

$$E_t \approx 25kT_m \quad (5)$$

where E_t is the average thermal activation energy (or trap depth) of the peak in units of eV. k is Boltzmann's constant, 8.62×10^{-5} eV K^{-1}. T_m is the temperature of the peak at its maximum in units of K. This relation yields only an approximate value since the heating rate, the attempt-to-escape frequency factors, and the thermal conductivity of the material, affect the exact value of T_m in the material. However, without knowledge of attempt-to-escape frequency factors, which may be determined using thermally

stimulated conductivity (TSC) experimentation[41], the relation provides a starting point for linking the TL output of a material to known defect states in that material.

By understanding the relationship between E_t, E_o and T_m, it becomes possible to use both the TL and OSL techniques to partially validate the results of the other, and also to form a more complete picture of a material's energy level structure and mechanisms.

Readout Methods

Three different readout methods are common in the OSL literature: continuous-wave OSL (CW-OSL), linearly modulated OSL (LM-OSL) and pulsed OSL (POSL). The methods differ by the manner in which the excitation light source is modulated (or not modulated) to optically excite the sample. In CW-OSL, the excitation light source is turned on for a single readout period and its intensity is held constant throughout the readout. The OSL output signal is collected concurrently with the sample excitation so that a system of filters, monochromators, and/or other frequency-selecting apparatus are needed to ensure that the excitation light is prevented from stimulating the OSL reader detection system to an extent that the OSL signal cannot be resolved. In LM-OSL, the excitation light source is ramped up from zero intensity to maximum intensity in a linear fashion. Like with CW-OSL, the OSL signal is collected during the sample excitation, so apparatus must be employed to prevent detection of the incident excitation light signal. POSL involves the repeated pulsing of the excitation light on the sample and relies on the fact that the electron-hole recombination process is not instantaneous. The OSL signal is detected only between pulses by the use of shutters or electronic gating circuits. This

technique eliminates the need for filters or other frequency-selecting equipment such that the detection efficiency is maximized. A relatively intense light source able to be switched on and off quickly is required for this technique – lasers or high-powered LEDs are typically employed – and the pulsing should be fast enough to ensure that most of the OSL signal is emitted after that incident light source is switched off and the detection system switched on. Figure 1.4 gives a graphical representation of these three methods.

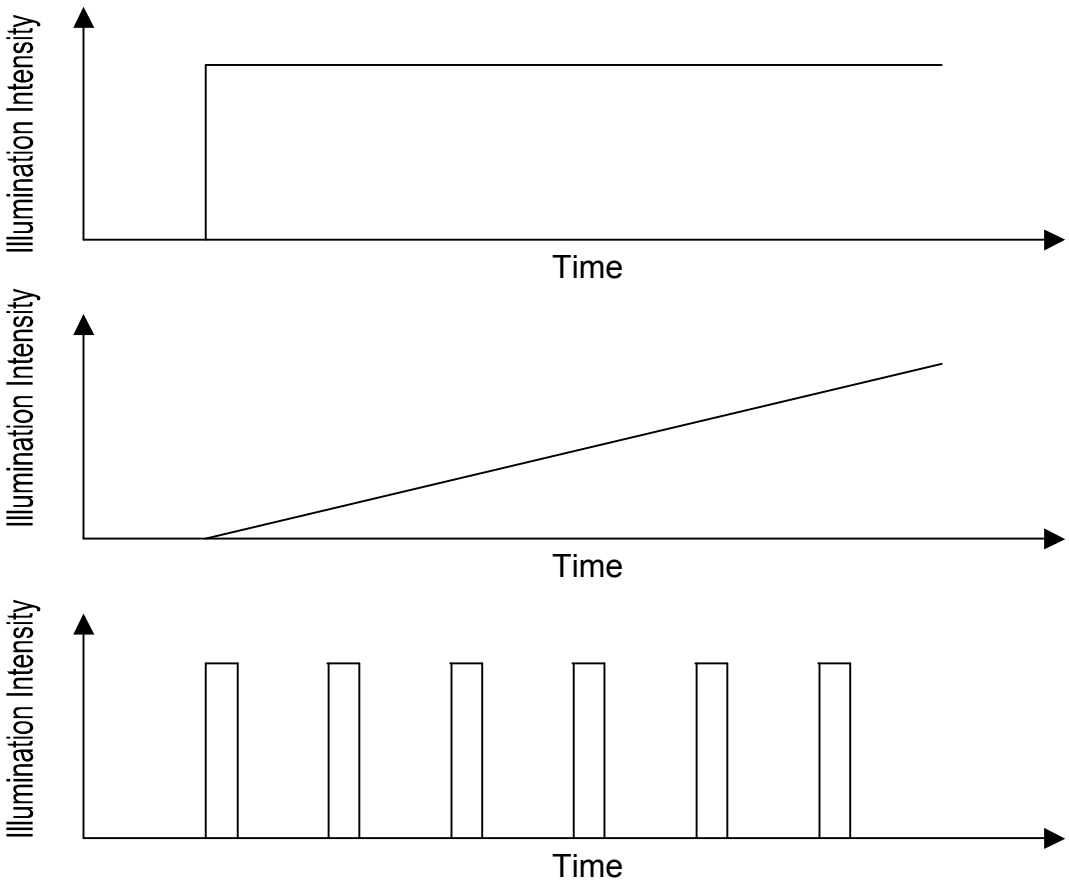

Figure 1.4: Graphical depiction of the continuous-wave optically stimulated luminescence (CW-OSL), linearly-modulated OSL (LM-OSL) and pulsed OSL (POSL) readout techniques, shown from top to bottom.

The methods differ in their optimal applications. CW-OSL is the simplest method to employ experimentally and is best where there is substantial difference in the incident light wavelength and the emitted OSL signal wavelength of the sample. LM-OSL can be useful when it is desired to permit the maximum amount of dose operating range for OSL apparatus – the readout can be suspended if the OSL signal approaches the saturation point of detection electronics. POSL is more complex to implement due to the need for fast timing electronics and/or mechanical components, but can permit the greatest possible dose sensitivity.

Now that an understanding of the physical principles and methodologies of OSL have been discussed, it is appropriate to address the specific objectives of this dissertation, as well as to describe the organization of this document.

OBJECTIVES AND ORGANIZATION OF THE DISSERTATION

Because of the substantial utility of α-Al_2O_3:C, and the prevalence of OSL techniques in geologic dating, a great deal of published research has focused on α-Al_2O_3:C and natural materials, while relatively little published data are available on the OSL properties of other conventional TL materials that may also exhibit OSL. In addition, a thorough, quantitative analysis of the OSL response of α-Al_2O_3:C to sunlight has not been published. As such, a series of experiments was conducted on the following substances: α-Al_2O_3:C, CaF_2:Mn, $Li_2B_4O_7$:Cu, LiF:Mg,Ti, KBr, $CaSO_4$:Tm, $CaSO_4$:Dy, $CaSO_4$:Dy+P, LiF:Mg,Cu,Na,Si and LiF:Mg,Cu,Si. The initial experiments used commercially-available OSL readers to investigate several of the materials, to determine

which of these materials exhibited OSL behavior to a degree to warrant further investigation, and to inform the design process of a custom-built OSL reader for later experiments. In addition, the sunlight OSL response of α-Al_2O_3:C was investigated and documented, providing additional information about this important OSL material. This experiment also allowed for experience to be gained by the author on OSL experimental methods and instrumentation capabilities, and provided a reference standard for OSL dose sensitivity for later experiments. Once these initial experiments were completed, a custom OSL reader was designed and constructed that would allow the use of additional excitation wavelengths of stimulation light to query samples. The capability to utilize numerous excitation wavelengths in this research was desired in the interest of producing information regarding the minimum and optimal wavelengths needed to excite OSL in the samples. Additionally, it was desired to investigate the extent to which OSL and TL behaviors in these materials were correlated. By using multiple excitation wavelengths, it was hoped that low-energy electron traps in the materials, corresponding to low-temperature TL peaks, could be investigated independently of higher-energy traps. Since commercial OSL readers typically employ only one or two excitation wavelengths [9, 42-47], a custom reader was necessary to produce these data. This research effort was also subject to a very modest budget, necessitating that the OSL reader be built at a cost roughly 1/10 that of commercially-available readers. Once the OSL reader, which permits CW-OSL operation, was completed and acceptance testing performed to validate its performance specifications, OSL signals from each material that showed promise in the initial results, as well as some new materials, were measured in response to seven excitation wavelengths from 625 nm to 455 nm, at twelve time periods post-irradiation

from 6 h to 120 d. The magnitude and fading behaviors of the OSL response of each material were then analyzed and results documented.

Each of the following chapters consists of a research paper documenting one step in the course of this research effort: initial investigations and experimentation using commercial materials and systems; OSL analysis of several TL materials to identify candidates for further exploration; design, construction and testing of the OSL reader; and final experimentation to document the OSL properties of new materials. In the sum of their parts exists both findings as well as new questions. It is hoped that in producing both, this dissertation will, in small measure, advance the body of science.

REFERENCES

1. Bøtter-Jensen, L., McKeever, S. W. S. and Wintle, A. G. Optically stimulated luminescence dosimetry. (Amsterdam, The Netherlands: Elsevier Science B.V.) (2003) ISBN 0444506845.

2. Kristianpoller, N., Oster, L. Optically stimulated luminescence in anion-defective carbon doped alpha-Al_2O_3 crystals. Radiation Effects and Defects in Solids. 134, 311-313 (1995).

3. McKeever, S. W. S., Akselrod, M. S. and Markey, B. G. Pulsed optically stimulated luminescence dosimetry using α-Al_2O_3:C. Radiat. Prot. Dosim. 65, 267-272 (1996).

4. Bøtter-Jensen, L. and McKeever, S. W. S. Optically stimulated luminescence dosimetry using natural and synthetic materials. Radiat. Prot. Dosim. 65, 273-280 (1996).

5. Bulur, E. and Göksu, H. Y. Pulsed optically stimulated luminescence from α-Al_2O_3:C using green light emitting diodes. Radiat. Meas. 27, 479-488 (1997).

6. Bøtter-Jensen, L., Larsen, N. A., Markey, B. G. and McKeever, S. W. S. Al_2O_3:C as a sensitive OSL dosimeter for rapid assessment of environmental dose rates. Radiat. Meas. 27, 295-298 (1997).

7. Akselrod, M. S., Lucas, A. C., Polf, J. C. and McKeever, S. W. S. Optically stimulated luminescence of Al_2O_3. Radiat. Meas. 29, 391-399 (1998).

8. McKeever, S. W. S. and Akselrod, M. S. Radiation dosimetry using pulsed optically stimulated luminescence of Al_2O_3:C. Radiat. Prot. Dosim. 84, 317-320 (1999).

9. Bøtter-Jensen, L., Mejdahl, V. and Murray, A. S. New light on OSL. Quaternary Geochronology. 18, 303-309 (1999).

10. Yoder, R. C. A radiation measurement film employing optically stimulated luminescence technology. Landauer, I. Glenwood, Illinois. (2000).

11. Moscovitch, M., Tawil, R. A. and Svinkin, M. Light induced fading in α-Al_2O_3:C. Radiat. Prot. Dosim. 47, 251-253 (1993).

12. Walker, F. D., Colyott, L. E., Larsen, N. A. and McKeever, S. W. S. The wavelength dependence of light-induced fading of thermoluminescence from α-Al_2O_3:C. Radiat. Meas. 26, 711-718 (1996).

13. West, W. G., Kearfott, K. J. and Bernal, S. M. The sunlight OSL response of a commercially available α-Al_2O_3:C personnel dosimetry material. Radiat. Prot. Dosim. 119, 344-349 (2006).

14. Bøtter-Jensen, L., Markey, B. G. and Agersnap Larsen, N. Retrospective radiation dosimetry using optically stimulated luminescence on natural and synthetic materials. (Horn, Austria: Berger) (1996).

15. Stoneham, D., Bailiff, I. K., Petrov, S., Botter-Jensen, L., Goeksu, Y. and Jungner, H. Retrospective dosimetry: The development of an experimental methodology using luminescence techniques. (Luxembourg, Luxembourg) (1996).

16. Banerjee, D., Boetter-Jensen, L. and Murray, A. S. Retrospective dosimetry: Estimation of the dose to quartz using the single-aliquot regenerative-dose protocol. Applied Radiation and Isotopes. 52, 831-844 (2000).

17. Kanemaki, M., Ninagawa, K., Yamamoto, I., Nakagawa, M., Wada, T., Yamashita, Y. and Endo, K. Red thermoluminescence of volcanic glass fractions from tephras. International Journal of Radiation Applications and Instrumentation. Part D. Nuclear Tracks and Radiation Measurements. 18, 81-88 (1991).

18. Bøtter-Jensen, L., Jungner, H. and Mejdahl, V. Recent developments of OSL techniques for dating quartz and feldspars. Radiation Protection Dosimetry (UK). 47, 643-648 (1993).

19. Banerjee, D. Optical stimulated luminescence (OSL) dating. (Lucas Heights, Australia: Australian Institute of Nuclear Science and Engineering) (1999).

20. Bailey, R. M., Adamiec, G. and Rhodes, E. J. OSL properties of nacl relative to dating and dosimetry. Radiat. Meas. 32, 717-723 (2000).

21. Huett, G. and Jaek, I. Advances in the luminescence dating: The optically stimulated luminescence based procedures and their physical background. Proceedings of the Estonian Academy of Sciences: Geology. 50, 214-232 (2001).

22. Stokes, S. and Fattahi, M. Red emission luminescence from quartz and feldspar for dating applications: An overview. Radiat. Meas. 37, 383-395 (2003).

23. Takaki, S., Ikeya, M. and Yamanaka, C. Remote TL and OSL for asteroid and meteorite study. Radiat. Meas. 27, 393-397 (1997).

24. Bøtter-Jensen, L. Development of optically stimulated luminescence techniques using natural minerals and ceramics, and their application to retrospective dosimetry. Risø-R-1211(EN). Roskilde, Denmark. (2000).

25. Inrig, E. L., Godfrey-Smith, D. I. and Khanna, S. Optically stimulated luminescence of electronic components for forensic, retrospective, and accident dosimetry. Radiat. Meas. 43, 726-730.

26. Bailiff, I. K. The use of ceramics for retrospective dosimetry in the Chernobyl exclusion zone. Radiat. Meas. 24, 507-511 (1995).

27. Hashimoto, T., Hong, D. G. and Takano, M. Retrospective dosimetry at JCO using luminescence from ceramics pieces and quartz grains. Advances in ESR Applications. 18, 197-202 (2002).

28. Akselrod, M. S., Bøtter-Jensen, L. and McKeever, S. W. S. Optically stimulated luminescence and its use in medical dosimetry. Radiat. Meas. 41, S78-S99 (2006).

29. Gaza, R., McKeever, S. W. S., Akselrod, M. S., Akselrod, A., Underwood, T., Yoder, C., Andersen, C. E., Aznar, M. C., Marckmann, C. J. and Bøtter-Jensen, L. A fiber-dosimetry method based on OSL from Al_2O_3:C for radiotherapy applications. Radiat. Meas. 38, 809-812 (2004).

30. Gaza, R. and McKeever, S. W. S. A real-time, high-resolution optical fibre dosemeter based on optically stimulated luminescence (OSL) of KBr:Eu, for potential use during the radiotherapy of cancer. Radiat. Prot. Dosim. 120, 14-19 (2006).

31. Ashcroft, N. W. and Mermin, N. D. Solid state physics. (Belmont, California, USA: Brooks/Cole) (1976) ISBN 978-0-03-083993-1.

32. Randall, J. T. and Wilkins, M. H. F. Phosphorescence and electron traps. I. The study of trap distributions. Proceedings of the Royal Society of London. Series A, Mathematical and Physical Sciences. 184, 365-389 (1945).

33. Springis, M., Kulis, P., Veispals, A. and Tale, I. Photo- and thermostimulated processes in α-Al_2O_3. Radiat. Meas. 24, 453-456 (1995).

34. Markey, B. G., Colyott, L. E. and McKeever, S. W. S. Time-resolved optically stimulated luminescence from α-Al_2O_3:C. Radiat. Meas. 24, 457-463 (1995).

35. Yoder, R. C. and Salasky, M. R. A dosimetry system based on delayed optically stimulated luminescence. Health Phys. 72, S18-S19 (1997).

36. Shiiki, K., Igarashi, M. and Kaijyu, H. Electronic structure of Al_2O_3 thin film studied using first-principle band calculation. Japanese Journal of Applied Physics. 42, 2 (2003).

37. Streetman, B. G. and Banerjee, S. Solid state electronic devices. Prentice Hall) (2000) ISBN 0-13-025538-6.

38. Hütt, G., Jaek, I. and Tchonka, J. Optical dating: K-feldspars optical response stimulation spectra. Quaternary Science Reviews. 7, 381-385 (1988).

39. Hütt, G. and Jaek, I. Photostimulated luminescence of some materials and its dosimetry applications. Nuclear Tracks and Radiation Measurements. 21, 95-98 (1993).

40. Lucovsky, G. On the photoionization of deep impurity centers in semiconductors. Solid State Communications. 3, 299-302 (1964).

41. Whitley, V. H., Agersnap Larsen, N. and McKeever, S. W. S. Determination of ionisation energies and attempt-to-escape factors using thermally stimulated conductivity. Radiat. Prot. Dosim. 100, 147-151 (2002).

42. Bortolot, V. J. A new modular high capacity OSL reader system. Radiat. Meas. 32, 751-757 (2000).

43. Bøtter-Jensen, L., Andersen, C. E., Duller, G. A. T. and Murray, A. S. Developments in radiation, stimulation and observation facilities in luminescence measurements. Radiat. Meas. 37, 535-541 (2003).

44. Bøtter-Jensen, L., Poolton, N. R. J., Willumsen, F. and Christiansen, H. A compact design for monochromatic OSL measurements in the wavelength range 380-1020 nm. Radiat. Meas. 23, 519-522 (1994).

45. Ford, R. M. and Hanify, R. D. A desktop OSL system for on-site dosimeter processing. Glenwood, IL. (2003).

46. Markey, B. G., Bøtter-Jensen, L. and Duller, G. A. T. A new flexible system for measuring thermally and optically stimulated luminescence. Radiat. Meas. 27, 83-89 (1997).

47. Markey, B. G., Bøtter-Jensen, L., Poolton, N. R. J., Christiansen, H. E. and Willumsen, F. A new sensitive system for measurement of thermally and optically stimulated luminescence. Radiat. Prot. Dosim. 66, 413-418 (1996).

CHAPTER 2

The Sunlight OSL Response of a Commercially Available α-Al_2O_3:C Personnel Dosimetry Material

ABSTRACT

Carbon-doped, anion-defective aluminum oxide has become a widely-used and effective medium for personnel dosimetry applications using optically stimulated luminescence (OSL) techniques. Though the commercial products currently using this material employ light-tight packaging to prevent light-induced effects on the OSL signal, the material could be employed in environments where package integrity cannot be assured. This paper reports on the results of an experiment performed to quantify the effects of sunlight exposure on α-Al_2O_3:C. Samples of commercially available Luxel® material were exposed to carefully-recorded levels of sunlight both before and after irradiations to determine the nature and magnitude of both activation and fading phenomena in this material. The results confirm that both fading and activation processes are seen in this material and indicate that the material reaches an equilibrium dose level in response to prolonged sunlight exposure equivalent to a dose of ~15 mGy under the experimental test conditions.

INTRODUCTION

Optically stimulated luminescence (OSL) has become a commercially successful dosimetry method during the past 10 y, as evidenced by the success of the Luxel® dosimeter manufactured and distributed by Landauer, Inc. In addition, the OSL phenomenon is widely used in the dating of geologic samples and has been proposed for a variety of other applications.

The use of OSL as a dosimetry method is attractive for a number of technical reasons, some of which are: 1) the current material of choice for this application, α-Al_2O_3:C, is highly sensitive in that it emits a large amount of stimulated luminescence per unit of radiation dose absorbed, 2) the optical read-out method is fast and relatively simple, and 3) the OSL technique lends itself to repeated read-out of samples. Unfortunately, the large photo-ionization cross-section that makes alumina such a sensitive OSL dosimeter also introduces some complexities to its behavior which must be accounted for: light-induced fading and activation. A number of studies have treated the effects of indoor and single-frequency light exposures on the material [1-3], and two studies have performed limited treatments of the effects of low-level 'daylight' exposure on this material[4-5]. In addition, a seminal investigation of the wavelength dependence of light-induced fading of the material using monochromatic excitation methods was performed by Walker, et al[6]. However, a quantitative and comprehensive study of the reaction of this material to direct sunlight exposure under controlled and repeatable conditions has not been performed to date. It is important for researchers and users of this material in real-world environments to know both the *magnitude and nature* of the

material's reaction to natural light to make informed choices regarding a variety of issues related to environmental or personnel dosimetry. Whether the material undergoes dosimetrically significant changes in 1 μs or 1 h is extremely important when a dosimetrist or physicist is attempting to determine whether a light exposure may or may not have occurred, analyzing a potential new application for the material that may involve natural light, or designing handling protocols for investigating or using this material in an outdoor setting. To date, no other study has provided this quantitative information in a controlled and fully-documented manner.

This experiment was designed to measure the amount of OSL signal fading due to direct sunlight exposure over several orders of magnitude immediately after a radiation exposure. In addition, this experiment also measured the amount of OSL signal induction caused by direct sunlight exposure on samples which had been previously bleached of their dosimetric OSL signal and were not subsequently irradiated. The results of this experiment may be used to better understand the effects of handling this material for even brief time periods in sunlit environments. In addition, this experiment also yields additional and potentially useful data for researchers interested in the phenomological characteristics of aluminum oxide's OSL behavior.

MATERIALS

Aluminum oxide (α-Al_2O_3:C) provided by Landauer, Inc. in the form of laminated Luxel® material was used for this experiment. Twenty individual samples of α-Al_2O_3:C were formed using a standard-size single hole punch to produce 6.35 mm (1/4") diameter

round samples from the Luxel® 'tape' provided. All samples were washed with ethyl alcohol to remove any potentially fluorescent contaminants before use.

METHODS

This experiment was performed at the Los Alamos National Laboratory Luminescence Geochronology Lab. The experimental setup consisted of a Risø Model DA-15 Automated OSL/Thermoluminescence (TL) Reader System. This reader allows continuous blue light stimulation centered at 470 nm. The reader also had an integral beta irradiator employing a pneumatically activated 1.48 GBq $^{90}Sr/^{90}Y$ source, capable of delivering ~15 mGy s^{-1} to a sample. The detection subsystem of this OSL/TL reader consists of a low-background bi-alkali photomultiplier tube with a quartz window, operated in photon counting mode. U-340 filters are employed to filter the emission spectrum and these filters transmit a light bandwidth centered at 340 nm, with a full-width half-maximum value of ~80 nm. For additional technical information regarding the specifications of this commercially available system, the reader is referred to the technical thesis regarding its development and construction[7].

Though the alumina samples had been previously exposed to both room light and low-level background radiation for several months prior to the testing, all samples were first 'cleared' using the OSL reader by stimulation with blue light until no remaining dosimetric OSL signal above background was detectable. Due to the laminated nature of the Luxel® material, a total thermal annealing of the material is not possible. As such, it would be expected that the tested material could have a small residual deep trap

population, a possibility which would also exist in a corresponding real-world scenario. Appropriate treatment and consideration of this deep-trap population is addressed in the Discussion section of this paper. It is noted that the OSL signal output from the clearing sequences verified that the accumulated dose on the material since receipt from the OSL material manufacturer was less than 2 mGy in all cases. After clearing, ten of the samples were irradiated to 15 mGy using the OSL reader's integral beta source. The other ten samples were not irradiated. All of the samples were then placed in identical, individually-labeled light-tight containers for transport from the laboratory to a suitably level and unobstructed outdoor location for the sunlight exposure. The sunlight exposures occurred on the grounds of Los Alamos National Laboratory during mid-summer at an elevation of ~2200 m (7277 ft) above sea level. Meteorological conditions during the sunlight exposures were sunny with little or no clouds in the sky and no cloud cover of the sun itself. The light levels for the sunlight exposure were measured using a Quantum Instruments Photometer LX possessing a current calibration certificate. The light level during the exposures was 100,000 lux (± 5000 lux). The outdoor ambient temperature during the exposures was 40°C. When exposed, the samples were placed flat on a solid white piece of paper. Samples (one each of the irradiated and non-irradiated batches) were exposed to 0, 1, 5, 15, 30, 60, 300, 900, and 1800 s of unfiltered direct sunlight, respectively. Anticipated 3600 s samples were not used because of approaching cloud cover near the end of the sunlight exposure period.

After sunlight exposure, the samples were returned to their light-tight containers for transport back to the laboratory darkroom and immediately read out using both the infrared and blue excitation sources. All of the read-outs were continuous-illumination

and programmed to last 150 s with sampling intervals of 0.2 s, for a total of 750 data points per read-out. The results of the read-out phases were collected by the OSL reader software and those data were analyzed and plotted.

RESULTS

Figure 2.1 shows a composite plot of the blue-light read-outs of the samples which were illuminated by sunlight without prior irradiation. This graph clearly shows that as sunlight exposures increase, the magnitude of the resulting OSL signals increase, up to a point. Furthermore, in overlaying a plot of a sample irradiated to 15 mGy with no sunlight exposure, it becomes evident that the OSL signal's readout 'half-life' for the sunlight-activated samples is considerably different from that of an irradiated sample of similar peak height. This discrepancy will be discussed further in the next section.

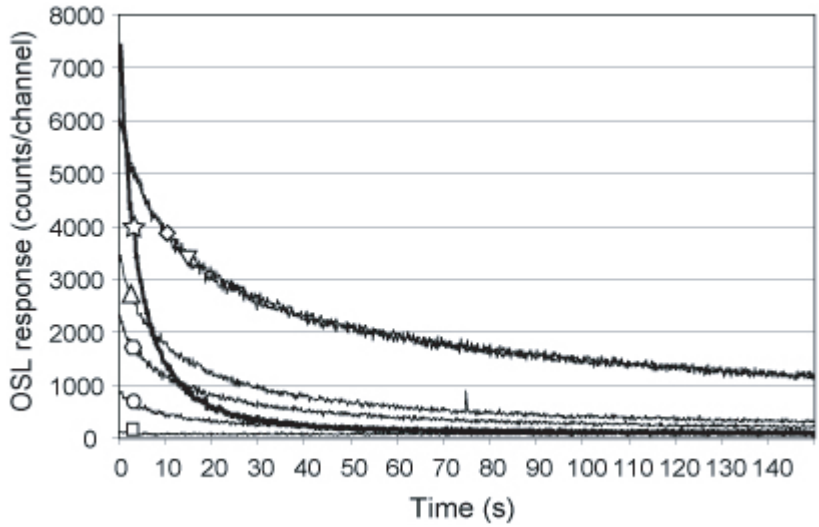

Figure 2.1: OSL response of a-Al_2O_3:C samples exposed to varying durations of direct sunlight. Results shown for blank (opened squares), 1 s (open circles), 5 s (open hexagons), 30 s (open triangles), 5 min (open diamonds), 30 min (open inverse triangles) and a comparison sample irradiated to 15 mGy but with no sunlight exposure (open stars).

It should be mentioned that two of the samples in this experiment (the 15 and 60 s samples that were not irradiated) were dropped during darkroom handling after sunlight exposure and, based on their measurements, it is presumed that they were flipped over before reading. The opaque nature of the Luxel® material resulted in readings which were ~30% lower than would be expected based on the general trend. Because these samples were considered to be compromised, their corresponding data points are not shown in the figures. Figure 2.2 shows the change in the peak OSL signal (an average of the first three OSL channel readings) versus the amount of sunlight exposure in units of equivalent exposure versus lux-hours.

Note that because of the different shape of the radiation-induced OSL curve versus the sunlight-induced OSL curve, the choice of what measurement (peak height, area, or some other value) to use for equating a dose to an OSL signal is somewhat

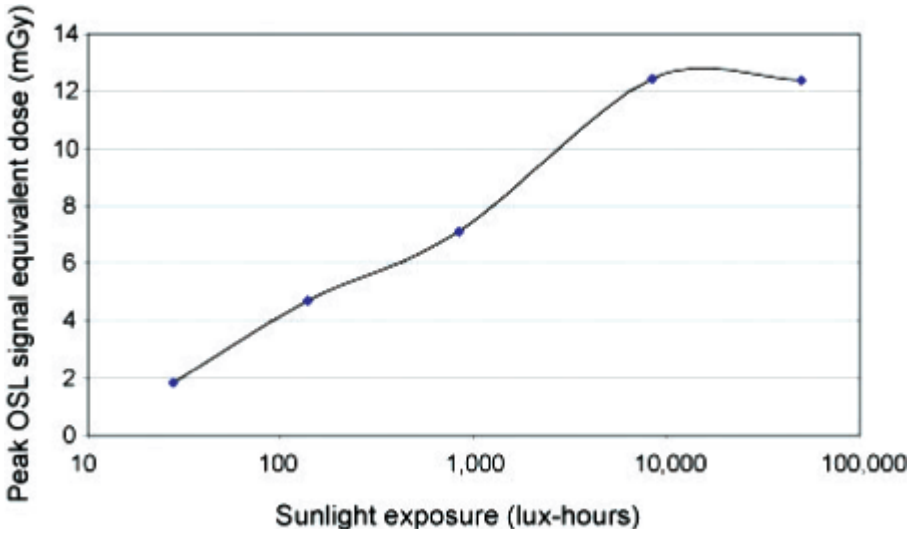

Figure 2.2: Peak OSL signal of a-Al_2O_3:C in units of equivalent dose versus total direct sunlight exposure.

arbitrary. For the purposes of this study, and since the total peak area for the longer-duration peaks cannot be measured, the peak height is used as the reference value. Using this method, the data show a potentially significant induction of OSL signal in aluminum oxide roughly equivalent to 12 mGy at maximum.

The next portion of our experiment was the study of the impact of direct sunlight exposure on samples which had been irradiated just prior to their exposure. Figure 2.3 shows a composite plot of the blue-light read-outs of these samples. The time axis of this plot was truncated to 60 s for readability. The graph clearly shows that as sunlight exposure increases, a more complex change in the magnitude and shape of the OSL signal results. A plot of the OSL signal peak height versus sunlight exposure time of both the previously-irradiated and non-irradiated samples is shown in Figure 2.4. These figures will be discussed in the next section.

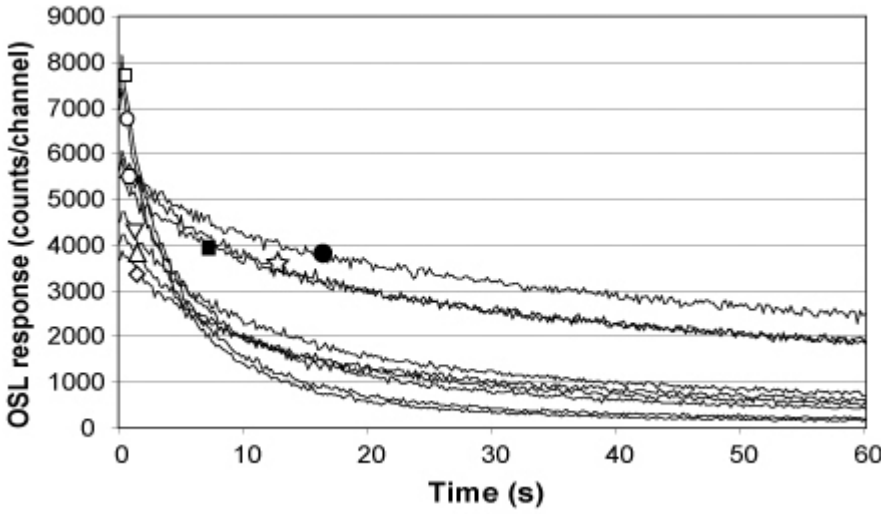

Figure 2.3: OSL response of a-Al_2O_3:C samples exposed to varying durations of direct sunlight after receiving a 15 mGy beta dose. Results shown for blank (open squares), 1 s (open circles), 5 s (open hexagons), 15 s (open triangles), 30 s (open diamonds), 1 min (open inverse triangles), 5 min (open stars), 15 min (closed circles) and 30 min (closed squares).

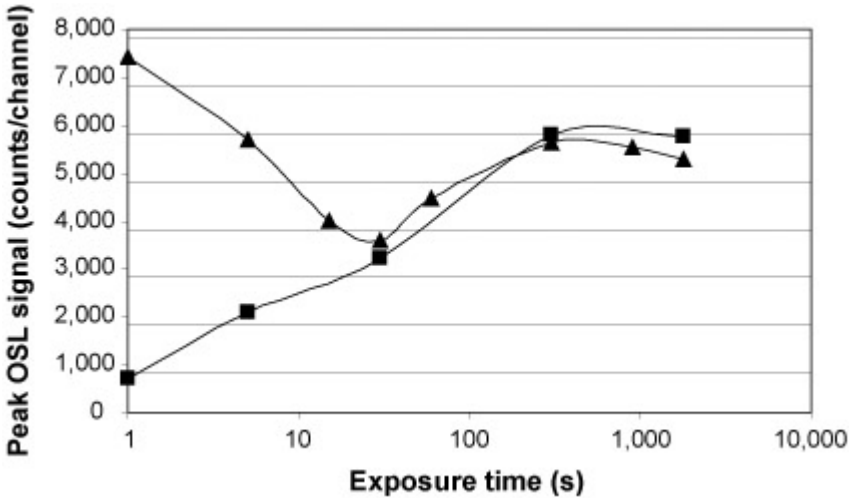

Figure 2.4: Peak OSL signal of a-Al_2O_3:C versus duration of 100,000 lux direct sunlight exposure. Samples which were bleached prior to sunlight exposures (closed squares). Samples which were bleached and then irradiated to 15 mGy prior to sunlight exposures (closed triangles).

DISCUSSION

Based on the results obtained, it appears that direct exposure to sunlight produces both immediate and significant light-induced fading and activation of this material in time periods on the order of seconds and at magnitudes on the order of mGy. These two processes appear to compete and eventually reach a saturation condition independent of whether the material had been dosed prior to sunlight exposure or not. This saturation condition may be a steady-state equilibrium condition though our sunlight exposures did not extend to time periods long enough to verify this possibility. The saturation condition under the experimental conditions was roughly equivalent to an absorbed dose in the material of 12 mGy, which could certainly prove to be a confounding effect on environmental or personnel dosimetry measurements. A previous study briefly treated the daylight-induced activation of α-Al_2O_3:C, but this study was

performed at a relatively low light level (300 lux) and it is not apparent whether the daylight was direct or indirect and whether it was filtered or unfiltered[5]. In addition, the material in that study had been exposed to a 2 Gy gamma dose and annealed to 600K immediately before the sunlight activation, resulting in a different initial condition for the material. This initial condition would not normally be expected to occur with the commercially available alumina-based dosimeter since the relatively low melting point of its polyester substrate precludes high-temperature thermal annealing. This previous study found an equivalent TL response of roughly 90 μGy at a daylight exposure of 100 lux-hours, which is roughly a factor of 45 lower than our data. Another study[4] examined the fading of α-Al_2O_3:C when exposed to daylight filtered by normal window glass for 8 h. This study found a residual OSL signal dose of <0.4 μGy. However, the ultra-violet (UV) filtering effect of the window glass as well as the possibility that the sunlight exposure was indirect and thus composed of a different spectral composition than direct sunlight could explain the difference in our signal induction findings. With respect to the well-documented importance of a material's dose 'pre-history' to its subsequent OSL behavior, our experiment was designed to more closely approximate the conditions expected from use of the as-found commercial product for a period on the order of months. It is noted that the low level of background radiation experienced by the samples prior to the experimentation was small with respect to both the dose used during the irradiation portion of the experiment, as well as the equivalent doses realized by prolonged exposure to sunlight. As such, the effect of this particular element of pre-history on the material's deep trap population, when compared with the effect from the

experiment itself, would be expected to be minor and of diminishing importance as the material approached an equilibrium condition.

Since sunlight consists of a complex spectrum of infrared, visible, and UV light, as shown in Figure 2.5[8], analysis of the interactions of the alumina with it will also be necessarily complex. While the light-induced fading stems from the same mechanisms that the OSL read-out process utilizes to empty the main dosimetry peak, the light-induced activation could result from one or a combination of two factors: 1) photo-transferred OSL (PTOSL) from deep traps, and 2) UV ionization of electrons at localized recombination centers[6, 9]. The former process has been documented to occur in this material with exposure to UV light of wavelengths between 200 and 350 nm[10], which

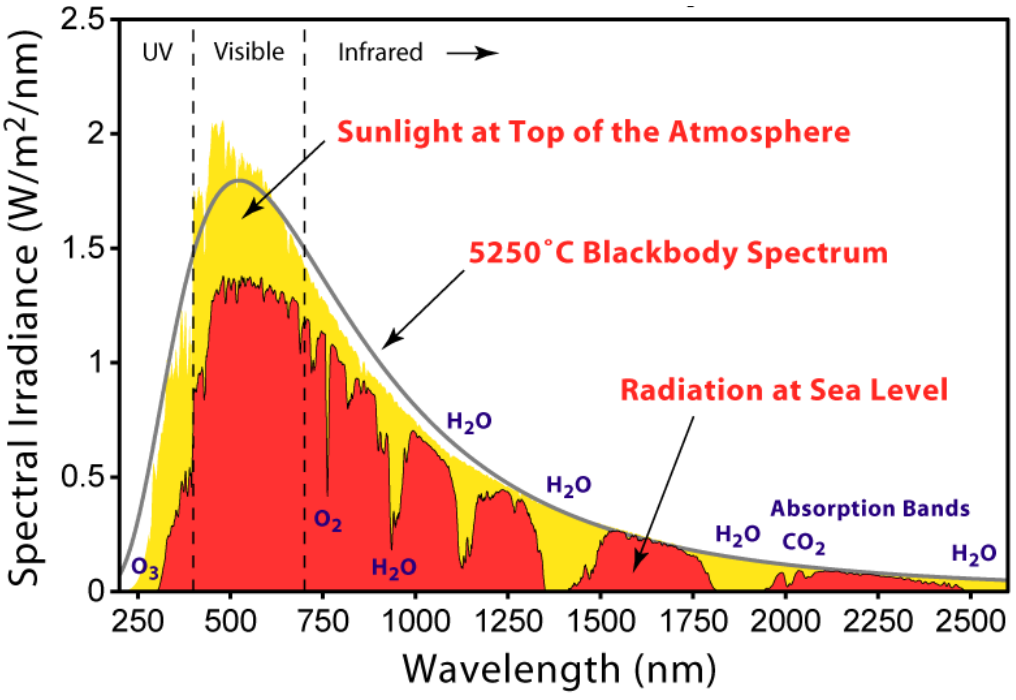

Figure 2.5: Solar radiation spectrum for direct light at both the top of the Earth's atmosphere and at sea level. As light passes through the atmosphere, some is absorbed by gases with specific absorption bands, also shown.

are certainly present in sunlight, and thus we can logically conclude that this phenomenon is at least partially responsible for our reaction behavior. The latter process appears to occur at photon wavelengths of less than ~300 nm and has also been documented in this material under laboratory conditions[11]. These wavelengths are on the very edge of the sunlight spectrum and are quite weak at sea level. However, as this experiment was performed at high elevation, some small light component in this range may have been present in the incident sunlight. Which of these processes is actually at work in this experiment, and to what relative degree, cannot be definitively derived from our experimental results. A detailed assessment of the relative contributions of these mechanisms is outside the scope of this study. However, the observed shape difference between radiation-induced and sunlight-induced OSL does provide an interesting clue into the physical processes at work in α-Al_2O_3:C. It has been previously stated that the 450K peak in aluminum oxide is actually a superposition of multiple traps of varying energy levels[6, 12]. As such, one possible explanation of this change in OSL signal readout half-life is that the sunlight is causing PTOSL that preferentially fills a deeper trap or 'slower' component of this peak. It seems reasonable to then predict that if the ratio of electrons trapped in the deeper trap level to those trapped in the shallower trap level(s) of this peak is higher for sunlight than for radiation, then the read-out process would be more gradual for the sunlight scenario. For this scenario to occur, however, would mean that the sunlight-induced PTOSL does not act through the same de-localized conduction band that ionized electrons operate in, since if it did it would be expected to be subject to the same branching ratios into the dosimetric traps. Instead, the PTOSL

would have to act through a tunneling or direct localized transference process in which the electrons are transported more directly from the deep trap to the deep dosimetric trap.

With regard to the PTOSL process, while the dose and annealing history of this material is well-known to affect subsequent photo-transferred TL measurements, it is noted that in spite of having been exposed only to background levels of radiation of less than 2 mGy, the commercially-available Luxel® α-Al_2O_3:C material used for this experiment was susceptible to sunlight-induced OSL. Whether this material has populated deep traps immediately post-production is not known, but these experimental results certainly allow this possibility.

The sunlight-induced fading results of the irradiated samples are compatible with the results of the non-irradiated activation experiment. Specifically, Figure 2.3 reveals a gradual transition over sunlight exposure time of the OSL signal from a simple radiation-induced shape to a sunlight-induced shape similar to those seen in Figure 2.1. Furthermore, it can be seen from Figure 2.4 that after ~30 s of sunlight exposure, the samples previously exposed to 15 mGy of beta radiation demonstrate a peak OSL signal height that is indistinguishable from the non-irradiated samples. This transition is consistent with the presence of two separate processes acting on the material, one tending to empty the dosimetric traps and one tending to fill them up in a different way. The magnitude of the fading is also of note in that the original OSL signal on our irradiated sample was depleted by ~50% after only 15 s of direct sunlight exposure. Finally, the fact that both the fading and activation processes seen in Figure 2.4 are roughly linear on a semi-log scale until saturation suggests a first-order process in both cases. In the case

of the activation process, this behavior supports the model of a finite number of deep trap electrons being directed into the dosimetric trap through PTOSL.

CONCLUSIONS

The primary purpose of this investigation was to evaluate the response of α-Al_2O_3:C in the form of Luxel® to sunlight in a realistic, experimentally repeatable, and carefully documented as-found condition. The experimental results indicate that light-induced OSL induction from direct sunlight exposure is not negligible in α-Al_2O_3:C in an environmental or personnel dosimetry scenario. Furthermore, the mechanism for charge transfer into the dosimetric traps during sunlight exposure results in significantly different OSL signal read-out characteristics than those produced by ^{90}Sr beta irradiation. The precise cause for this difference is as yet unknown and further research is indicated to answer this question. It has also been shown that sunlight-induced fading of the OSL signal in α-Al_2O_3:C happens in very short times frames under direct sunlight and results in erasure of the original radiation-induced signal and replacement with a sunlight-induced signal. Though this study confirms that convenient bleaching of the dosimetric OSL signal in α-Al_2O_3:C can be accomplished through the proper application of UV-filtered sunlight, it is not advisable to expose dosimetry samples to full-spectrum direct sunlight due to the apparently high UV activation sensitivity of this material.

ACKNOWLEDGEMENTS

This research would not have been possible without the cooperation and assistance of personnel at Los Alamos National Laboratories. In particular, we would like to thank Dr. David E. Morris, Dr. Benjamin P. Warner, Dr. Cathy J. Wilson, Dr. Kenneth Lepper, and Mr. Jeff Hoffman for their constructive comments and assistance with equipment provision and instruction during the course of this research activity. Also, we would like to thank Dr. Eduardo Yukihara for his assistance during the execution of this ongoing research effort. This research was supported, in part, by a U.S. Department of Homeland Security (DHS) Fellowship administered by the Oak Ridge Institute for Science and Education (ORISE) through an interagency agreement with the U.S Department of Energy (DOE). All opinions expressed in this paper are the author's and do not necessarily reflect the policies and views of DHS, DOE, or ORISE.

REFERENCES

1. Moscovitch, M., Tawil, R. A. and Svinkin, M. Light induced fading in α-Al_2O_3:C. Radiat. Prot. Dosim. 47, 251-253 (1993).

2. Rathbone, B. A., Endres, A. W. and Antonio, E. J. (Orlando, FL: Oak Ridge National Laboratory) (1994).

3. Musk, J. H. Time-dependent and light-induced fading in Victoreen model 2600-80 aluminum oxide thermoluminescence dosemeters. Radiat. Prot. Dosim. 47, 247-249 (1993).

4. Bøtter-Jensen, L., Banerjee, D., Jungner, H. and Murray, A. S. Retrospective assessment of environmental dose rates using optically stimulated luminescence from Al_2O_3:C and quartz. Radiat. Prot. Dosim. 84, 537-542 (1999).

5. Akselrod, M. S., Kortov, V. S., Kravetsky, D. J. and Gotlib, V. I. Highly sensitive thermoluminescent anion-defect alpha-Al_2O_3:C single crystal detectors. Radiat. Prot. Dosim. 33, 119-122 (1990).

6. Walker, F. D., Colyott, L. E., Larsen, N. A. and McKeever, S. W. S. The wavelength dependence of light-induced fading of thermoluminescence from α-Al_2O_3:C. Radiat. Meas. 26, 711-718 (1996).

7. Bøtter-Jensen, L. Development of optically stimulated luminescence techniques using natural minerals and ceramics, and their application to retrospective dosimetry. Risø-R-1211(EN). Roskilde, Denmark. (2000).

8. Rhode, R. A. Solar spectrum. (Wikimedia Commons) (2007).

9. Summers, G. P. Thermoluminescence in single crystal α-Al_2O_3. Radiat. Prot. Dosim. 8, 69-80 (1984).

10. Oster, L., Weiss, D., Kristianpoller, N. A study of photostimulated thermoluminescence in C-doped alpha-Al_2O_3 crystals. J. Phys. D Appl. Phys. 27, 1732-1736 (1994).

11. Kristianpoller, N., Rehavi, A., Shmilevich, A., Chen, R. Radiation effects in pure and doped Al_2O_3 crystals. Nucl. Instrum. Meth. B. 141, 343-346 (1998).

12. Moscovitch, M., Kaufman, M. M., Rodgers, J. E. and Niroomand-Rad, A. Ultra-low dose (100 nGy - 100 μGy) response of α-Al_2O_3:C. Radiat. Prot. Dosim. 47, 173-176 (1993).

CHAPTER 3

The Optically Stimulated Luminescence of Various Known Thermoluminescent Materials

ABSTRACT

Optically stimulated luminescence (OSL) techniques are widely utilized for diverse applications, including personnel, environmental and medical dosimetry, as well as for geologic dating. This paper reports on an investigation into the OSL properties of several known thermoluminescent materials. Samples of LiF:Mg,Ti, $Li_2B_4O_7$:Cu, $CaSO_4$:Tm, and CaF_2:Mn were irradiated to doses, in air, of 15 mGy, 150 mGy and 1.5 Gy and then analyzed using a commercially available OSL reader system to determine their luminescence response to blue and infrared light (IR) excitation, centered at 470 nm and 830 nm wavelengths, respectively. CaF_2:Mn did not show an OSL response after irradiation under IR or blue light stimulation; $Li_2B_4O_7$:Cu and LiF:Mg,Ti demonstrated very weak OSL signals and only under blue light excitation; and $CaSO_4$:Tm exhibited OSL under both IR and blue light stimulation at sensitivities roughly one order of magnitude less than the OSL response of α-Al_2O_3:C under the experimental excitation and emission conditions. Further investigation of the OSL properties of $CaSO_4$:Tm is indicated to determine an optimal OSL readout regime and to determine its OSL dose sensitivity and fading properties.

INTRODUCTION

Optically stimulated luminescence (OSL) dosimetry relies upon the illumination of an irradiated sample with light to produce a stimulated emission of light proportional to the radiation dose which previously caused trapping of electrons in the material[1]. OSL has become an accepted personnel dosimetry method during the past 15 y, as evidenced by the success of a commercially-available dosimeter based upon anion-defective, carbon-doped aluminum oxide, or α-Al_2O_3:C (Luxel®, Landauer, Inc., 2 Science Road, Glenwood, Illinois, 60425-1586, USA, custserv@landauer.com, +1 800 323 8830, www.landauer.com). The use of OSL dosimeters versus other choices, such as thermoluminescent dosimeters (TLDs) or film-based dosimeters, is attractive for a number of technical reasons, including: 1) the current material of choice for this application, α-Al_2O_3:C, is highly sensitive, in that it emits a large amount of stimulated luminescence per unit of radiation dose absorbed[2-8]; 2) the optical readout method is fast and relatively simple[5, 9]; and 3) the OSL technique lends itself to repeat readout of samples, since unlike thermal stimulation as used in TLDs, optical stimulation can be activated and deactivated very quickly, allowing fast readout of the dose information without a significant depopulation of the dosimetric traps[10]. An additional reason that α-Al_2O_3:C in particular was chosen as a dosimetry material for widespread use is the fact that it exhibits very little fading at room temperature over time, meaning that the accurate estimation of dose is not affected to a large degree by the amount of time elapsed between irradiation of the dosimeter and readout[7, 11]. Although OSL dosimeters are frequently susceptible to light-induced fading[12-14], maintaining the material in a

light-tight container during use does not present a significant problem in most applications.

In addition to its application in the area of personnel dosimetry, the OSL phenomenon is widely used in the dating of geologic samples[4, 15-23] and has been investigated and used for a variety of other applications, including remote dosimetry[24], retrospective dosimetry[15, 25-28] and medical dosimetry[29-31]. In most of these applications, the material employed is either α-Al_2O_3:C or a natural material such as quartz, i.e. SiO_2, or feldspar, namely $KAlSi_3O_8$, $NaAlSi_3O_8$, or $CaAl_2Si_2O_8$.

Because of the substantial utility of α-Al_2O_3:C, and the prevalence of OSL techniques in geologic dating, a great deal of published research has focused on α-Al_2O_3:C and natural materials, while relatively little published data is available on the OSL properties of other conventional TL materials that may also exhibit OSL. In the case of $Li_2B_4O_7$:Cu and $CaSO_4$:Tm, in spite of their use in commercially-available dosimeters, and the presence of substantial published TL data[32-41], no published research exists documenting their OSL properties. However, $CaSO_4$:Tm has recently been shown to produce a signal using phototransferred thermoluminescence techniques (PTTL) techniques[40]. PTTL is the measurement of a TL signal originating from shallow traps following the optical transfer of charge from deep traps to the shallow traps. Its presence in a TL material indicates that the material has an optically sensitive trap clearance mechanism and therefore may also exhibit OSL under appropriate excitation and detection conditions. $CaSO_4$:Tm is also known to be quite sensitive to light-induced fading[42], which suggests that its optical ionization cross section is high and therefore a good candidate for OSL.

In the case of LiF:Mg,Ti, there has been one published confirmation of an optically stimulated afterglow (OSA) from this substance, along with a characterization of the excitation and emission spectra relating to this afterglow[43]. However, no published data exist related to its OSL dose sensitivity or behavior in a conventional continuous-wave OSL (CW-OSL) measurement regime. In the case of CaF_2:Mn, there is a limited amount of published OSL research. As with LiF:Mg,Ti, there has been published confirmation of an OSA as well as characterization of the excitation and emission spectra of that signal[43]. Additionally, an experiment using broadband optical illumination and a delayed OSL (DOSL) technique has been published[44], as have some phototransferred thermoluminescence (PTTL) and OSL experiments reporting OSL excitation spectra for a single emission wavelength of 495 nm, but with no sensitivity information[45]. Finally, investigations of the material's sensitivity, annealing behavior and long-term OSL fading behavior using a highly specialized 'cooled' OSL technique have also been published[46-48].

This experiment seeks to expand upon this limited research and to more fully characterize these materials and supplement the prior art. Specifically, this experiment was designed to determine whether LiF:Mg,Ti; $Li_2B_4O_7$:Cu; $CaSO_4$:Tm; and CaF_2:Mn exhibit OSL when using narrow-band IR and blue light excitation in a room-temperature CW-OSL regime, and to what degree. Because the defined experimental setup, which stimulated with two wavelengths of light and detected in the ultraviolet (UV) region, does not examine the entire spectrum of possible excitation and emission wavelengths, this experiment is intended as an initial investigation into the promise of several of these materials as OSL dosimeters.

MATERIALS

The four commercially available TLD crystal types evaluated as part of this experiment were LiF:Mg,Ti (TLD-100, Harshaw Chemical Company, 29001 Solon Road, Cleveland, OH, 44139, USA), $Li_2B_4O_7$:Cu (Panasonic Industrial Company, 3 Panasonic Way, 7E-6, Secaucus, NJ, 07094, USA, radiationmeasurement@us.panasonic.com, +1 201 348 2517, www.panasonic.com), $CaSO_4$:Tm (Panasonic Industrial Company, 3 Panasonic Way, 7E-6, Secaucus, NJ, 07094, USA, radiationmeasurement@us.panasonic.com, +1 201 348 2517, www.panasonic.com), and CaF_2:Mn (TLD-400, Harshaw Chemical Company, 29001 Solon Road, Cleveland, OH, 44139, USA).

The LiF:Mg,Ti and CaF_2:Mn were in the form of loose 3.2 mm x 3.2 mm x 0.6 mm chips. The $Li_2B_4O_7$:Cu and $CaSO_4$:Tm material was originally in the form of small grains attached with an epoxy to dosimeter badge backings (UD-802AQ TLD badges, Panasonic Industrial Company, 3 Panasonic Way, 7E-6, Secaucus, NJ, 07094, USA, radiationmeasurement@us.panasonic.com, +1 201 348 2517, www.panasonic.com). The materials were carefully scraped from their respective backings and placed on 9.7 mm diameter stainless steel planchets with a non-fluorescing adhesive. This adhesive was verified as non-fluorescing by confirming that blank samples, containing only adhesive on the planchet, produced no detectable OSL output during the course of the experiment. The grains covered a circular surface area roughly the size of the chips. Samples of α-Al_2O_3:C (Luxel®, Landauer, Inc., 2 Science Road, Glenwood, Illinois, 60425-1586, USA, custserv@landauer.com, +1 800 323 8830,

www.landauer.com) were used as reference standards. Individual samples were formed using a hole punch to produce 6.35 mm diameter round samples from the clear polystyrene-laminated α-Al_2O_3:C ribbon provided. All samples were washed with ethyl alcohol, C_2H_5OH, to remove any potentially fluorescent contaminants before use.

METHODS

A flexible, commercially available automated OSL/TLD reader system was employed for the experiment (Model DA-15, Risø National Laboratory, Frederiksborgvej 399, P.O. Box. 49, 4000 Roskilde, Denmark, risoe@risoe.dtu.dk, +45 4677 4677, www.risoe.dtu.dk). This reader allows continuous blue light stimulation centered at 470 nm using clusters of 42 light emitting diodes (LEDs) (NSPB 500S, Nichia Corporation, 491 Oka, Kaminaka-Cho, Anan-Shi, Tokushima, 774-8601, Japan, +81 3 3456 3746, www.nichia.co.jp) collectively delivering 50 mW cm^{-2}. In addition, this unit features infrared (IR) stimulation capability, centered at 830 nm, using a 1 W IR laser diode delivering 300 mW cm^{-2}. The reader also had an integral beta irradiator employing a pneumatically activated 1.48 GBq $^{90}Sr/^{90}Y$ source, capable of delivering approximately 15 mGy s^{-1} to a sample. The detection subsystem of this OSL/TL reader consists of a low-background bi-alkali photomultiplier tube with a quartz window (Model 9235QB, ADIT Electron Tubes, 300 Crane Street, Sweetwater, Texas, 79556, USA, sales@electrontubes.com, +1 325 235 1418, www.electrontubes.com), operated in photon counting mode. High-pass filters (U340, Hoya Filters, 2-7-5, Naka-Ochiai, Shinjuku-ku, Tokyo, 161-8525, Japan, +813 39521151, www.hoyafilter.com) are

employed to filter the emission spectrum and these filters transmit a light bandwidth centered at 340 nm, with a full width at half maximum (FWHM) of approximately 80 nm[25].

Before the $CaSO_4$:Tm and $Li_2B_4O_7$:Cu samples were irradiated, they were annealed using the hot N_2 gas heating system of an automated TLD reader (Harshaw 6600, Thermo Fisher Scientific Inc., 81 Wyman Street, Waltham, MA, 02454, USA, +1 781 622 1000, www.thermoscientific.com). Before the CaF_2:Mn and LiF:Mg,Ti samples were irradiated they were annealed using the TLD heating element of the OSL reader. The annealing parameters for the TLD materials are given in Table 3.1. Ten α-Al_2O_3:C reference samples were also annealed prior to irradiation by exposure to blue

Table 3.1: Thermal annealing parameters used for material samples. This table indicates the equipment used as well as the heating parameters employed to anneal the samples of LiF:Mg,Ti; $Li_2B_4O_7$:Cu; $CaSO_4$:Tm; and CaF_2:Mn prior to subsequent irradiation and optically stimulated luminescence (OSL) readout.

Material	LiF:Mg,Ti (TLD-100)	$Li_2O_4B_7$:Cu	$CaSO_4$:Tm	CaF_2:Mn (TLD-400)
Equipment Used	Hot-gas TLD reader	OSL Reader	OSL Reader	Hot-gas TLD reader
Preheat Temperature (°C)	150	N/A	N/A	170
Preheat Time (s)	0	N/A	N/A	0
Heating Rate (°C s^{-1})	15	N/A	N/A	10
Maximum Temperature (°C)	300	N/A	N/A	370
Acquire Time (s)	16.7	N/A	N/A	26.7
Anneal Temperature (°C)	300	350	350	400
Anneal Time (s)	0	5	5	5

stimulation light in the OSL reader until no remaining dosimetric OSL signal above background was detectable. Owing to the laminated nature of the α-Al_2O_3:C sample material, a total thermal annealing of the material is not possible.

After annealing, all samples were kept in light-tight plastic 35 mm photographic film canisters (Eastman Kodak Company, 343 State Street, Rochester, NY, 14650, +1 585 724 4000, www.kodak.com) for transport to a darkroom, where the samples were prepared for irradiation and readout, as described above. The time elapsed between annealing and irradiation was 1 d. Once prepared, the samples were placed in the OSL reader and run through identical irradiation and readout protocols designed to examine the OSL response under both IR light and blue light after three different irradiations covering three orders of dosimetric magnitude. Specifically, this protocol consisted of the following consecutive steps: read with IR light; read with blue light; irradiate to 15 mGy; read with IR light; read with blue light; irradiate to 150 mGy; read with IR light; read with blue light; irradiate to 1.5 Gy; read with IR light, and read with blue light. The only exception to this protocol was in the case of the α-Al_2O_3:C samples, which were irradiated and read out at only the 15 mGy dose point, since it was projected that the high light output of this material could potentially saturate the instrument detection electronics at the 150 mGy and 1.5 Gy doses.

The irradiations were performed using the OSL reader's integrated $^{90}Sr/^{90}Y$ beta source and in each case a readout cycle occurred immediately thereafter. All of the readouts were programmed to last 50 s with sampling intervals or 'channels' of 0.2 s, for a total of 250 data points per readout. The samples were read out before the first irradiation in order to confirm that the annealing process had been successful in emptying

out any accessible traps. The results of the six readout phases per crystal sample were collected by the OSL reader software and those data were transferred to a spreadsheet program (Excel®, Microsoft Corporation, One Microsoft Way, Redmond, Washington 98052) for analysis and plotting.

RESULTS

Both the IR and blue readouts of all of the samples prior to any irradiation, as shown in Figures 3.1 and 3.2, showed only normal background count rates, i.e., count rates of approximately 10-20 counts per channel, thus verifying the success of the annealing processes.

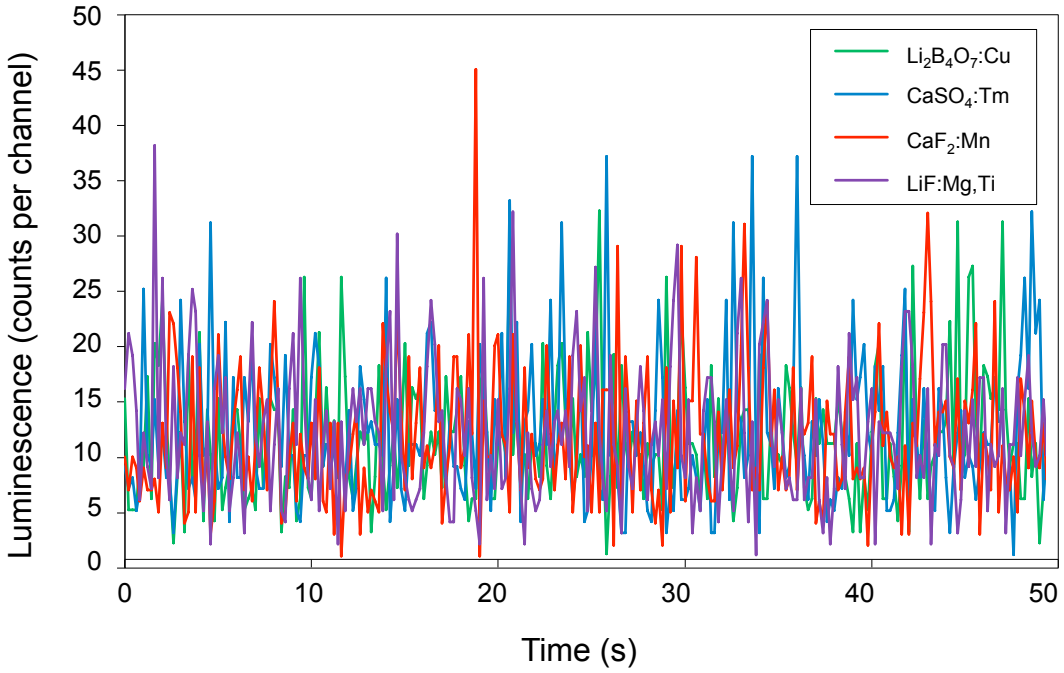

Figure 3.1: Optically stimulated luminescence (OSL) response during infrared light (λ = 830 nm) stimulation of unirradiated samples. Output is shown in counts per channel, with each channel representing 0.2 s.

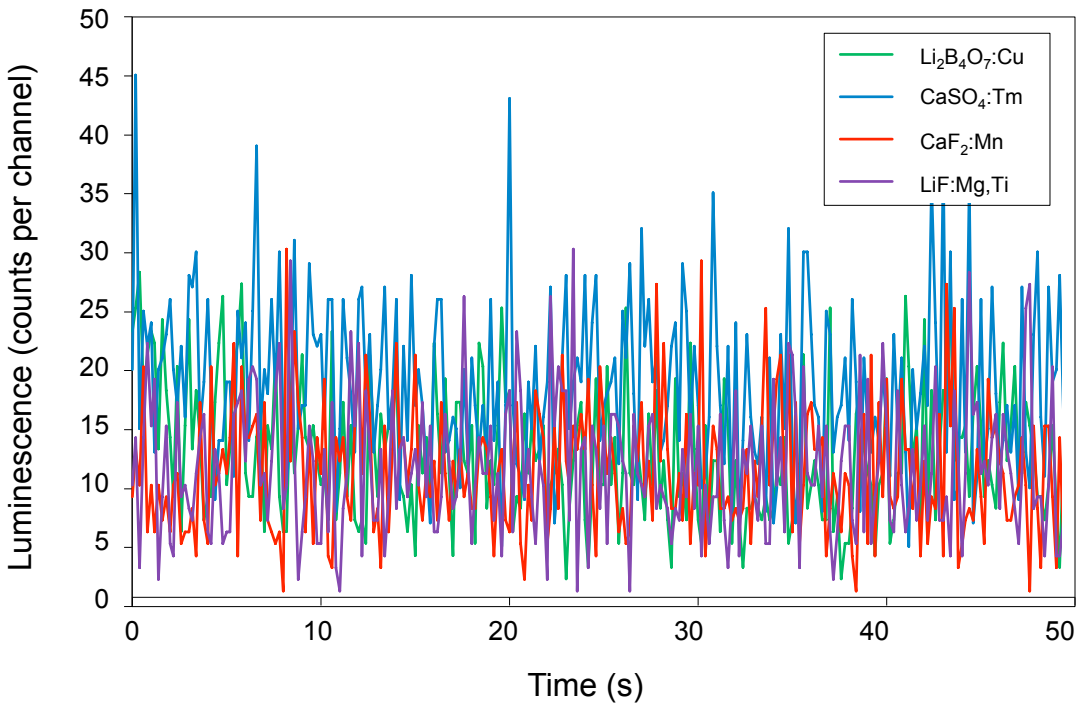

Figure 3.2: Optically stimulated luminescence (OSL) response during blue light (λ = 470 nm) stimulation of unirradiated samples. Output is shown in counts per channel, with each channel representing 0.2 s.

At the lowest dose used, 15 mGy, only the $CaSO_4$:Tm sample demonstrated an OSL signal above background count rates. This can be seen in Figures 3.3 and 3.4, which show the IR- and blue-stimulated OSL signals, respectively. Under IR stimulation, the $CaSO_4$:Tm demonstrated a relatively constant OSL response, with respect to the sample period, of approximately 55 counts per channel. Under blue light stimulation, the $CaSO_4$:Tm exhibited a slowly decaying signal over the readout period, starting at approximately 185 counts per channel and decaying to approximately 80 counts per channel. The average data for the ten α-Al_2O_3:C reference samples was

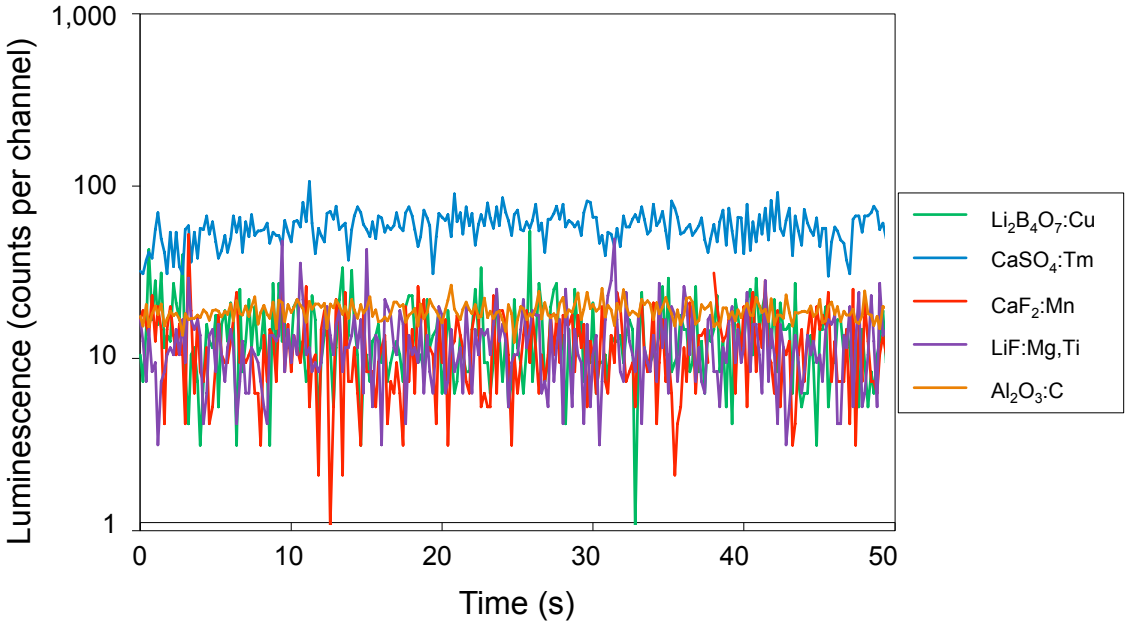

Figure 3.3: Optically stimulated luminescence (OSL) response during infrared light (λ = 830 nm) stimulation of samples irradiated to 15 mGy. Output is shown in counts per channel, with each channel representing 0.2 s.

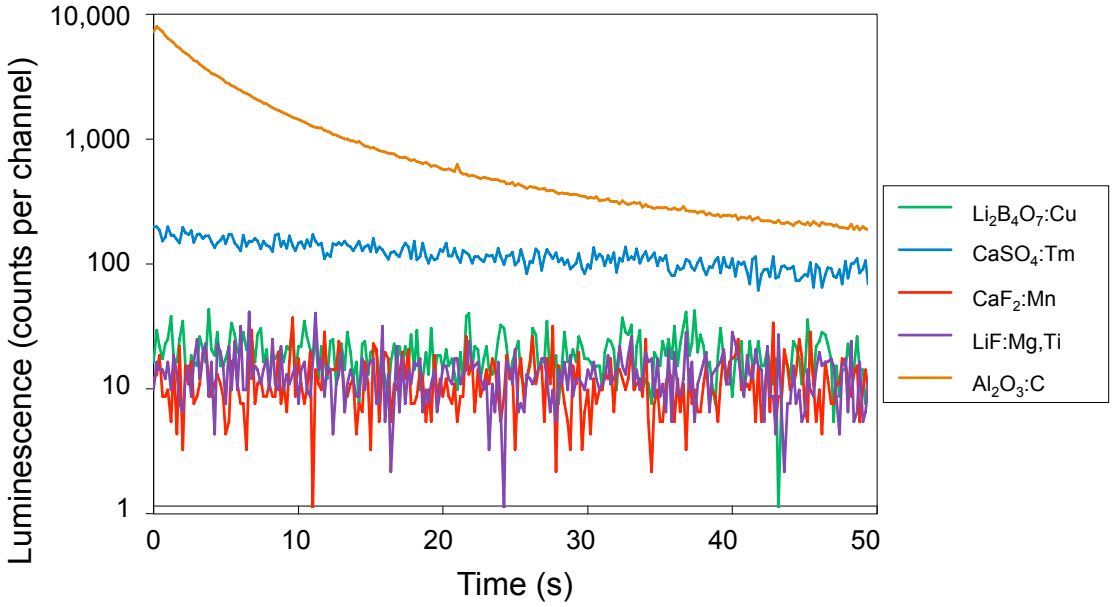

Figure 3.4: Optically stimulated luminescence (OSL) response during blue light (λ = 470 nm) stimulation of samples irradiated to 15 mGy. Output is shown in counts per channel, with each channel representing 0.2 s.

included on these graphs for comparison. As shown, the initial, or peak, light output from the α-Al_2O_3:C under blue light stimulation is approximately 7,750 counts per channel, or roughly 40 times that of the $CaSO_4$:Tm. However, the decay rate of the signal from α-Al_2O_3:C is much faster than that from the $CaSO_4$:Tm. Specifically, the α-Al_2O_3:C signal drops by half after approximately 3 s of readout, while the $CaSO_4$:Tm signal requires approximately 30 s to do the same. This results in an OSL signal for α-Al_2O_3:C of only about twice that of the $CaSO_4$:Tm, approximately 185 counts per channel, by the end of the 50 s readout period.

Plots of the high, 1.5 Gy dose results under IR and blue light stimulation are shown as Figures 3.5 and 3.6, respectively. These data reveal that all of the investigated

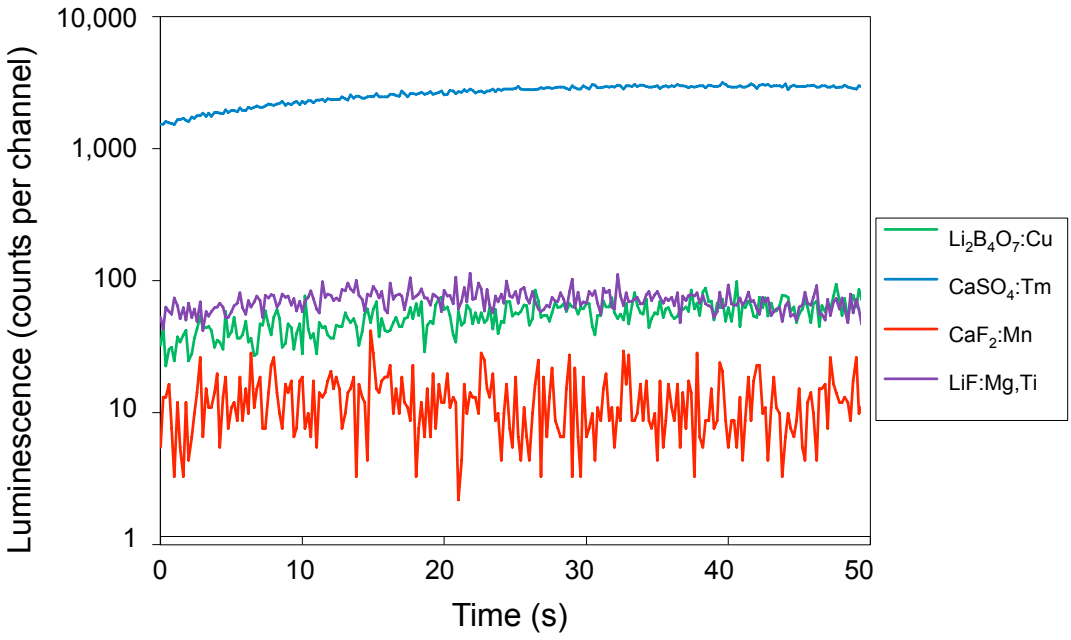

Figure 3.5: Optically stimulated luminescence (OSL) response during infrared light (λ = 830 nm) stimulation of samples irradiated to 1.5 Gy. Output is shown in counts per channel, with each channel representing 0.2 s.

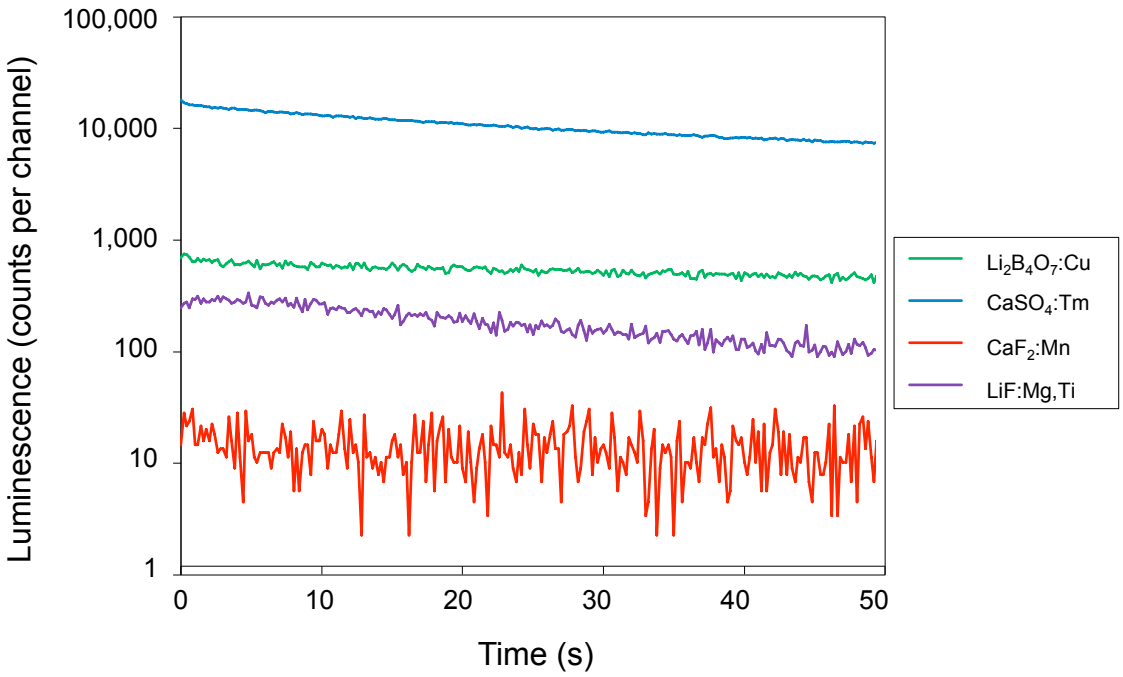

Figure 3.6: Optically stimulated luminescence (OSL) response during blue light (λ = 470 nm) stimulation of samples irradiated to 1.5 Gy. Output is shown in counts per channel, with each channel representing 0.2 s.

TLD materials except for the CaF_2:Mn demonstrated at least some OSL when stimulated by both IR and blue light, though the $CaSO_4$:Tm was an order of magnitude more responsive in this regard.

The plots of the intermediate, 150 mGy dose readouts are not shown, as they were fully consistent with an intermediate position between the low and high dose plots in all cases. That is, all of the materials showed OSL intensities one order of magnitude less than was seen at 1.5 Gy. A plot of the OSL signal peak height versus dose of $CaSO_4$:Tm using both blue light stimulation and IR stimulation is shown as Figure 3.7.

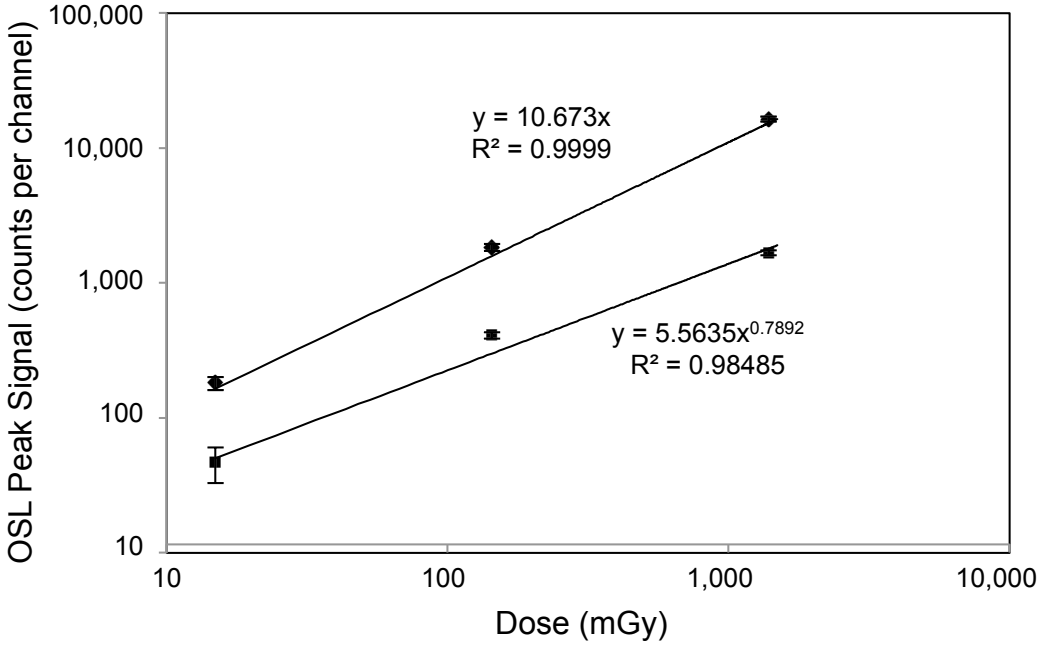

Figure 3.7: Optically stimulated luminescence (OSL) peak signal height versus dose for $CaSO_4$:Tm. Samples were irradiated to 15, 150 and 1,500 mGy and read out using blue light (λ = 470 nm) stimulation (closed diamonds) and infrared light (λ = 830 nm) stimulation (closed squares). Output is shown in counts per channel, with a channel representing 0.2 s. Trendlines are plotted, showing a highly linear dose response under blue light stimulation and a slightly sub-linear dose response under IR stimulation. Error bars are plotted, showing the standard deviation of the signal over 10 count channels, i.e., the statistical counting error.

DISCUSSION

$CaSO_4$:Tm

Based on the results obtained, $CaSO_4$:Tm, exhibits the strongest OSL response of the four materials studied. Although this material's peak luminance under blue light stimulation, shown in Figure 3.4, was approximately a factor of 40 less than that of

α-Al_2O_3:C, it is probable that this OSL sensitivity would be significantly greater with the proper selection of excitation source, detection filter and PMT, not to mention use of a pulsed OSL (POSL) regime, since the primary emission wavelength of $CaSO_4$:Tm is centered at 455 nm and it is a lower-output emission centered at 360 nm[39, 49] that the test equipment most likely picked up. Furthermore, previous investigations have demonstrated that the most effective excitation wavelength for the primary emission at 455 nm is in the region of 355-370 nm, which is well away from the 470 nm LED wavelength[39]. In summary, it appears that the ideal OSL experimental setup for this material would effectively reverse the excitation and emission wavelengths of this OSL reader.

An interesting feature of $CaSO_4$:Tm is that this material was the only one to exhibit an OSL signal in response to 830 nm IR light stimulation as seen in Figures 3.3 and 3.5. This signal, at the highest irradiation dose, increased for the first 30 s of illumination and then appeared to reach a plateau where the signal leveled off. The simplest explanation for this behavior is that this material possesses lower activation energy trap or traps that are read out by the longer-wavelength IR light and that the recombination process occurring as a result demonstrates a metastable state of some type, accounting for its initial rise. It is known that this material possesses a TL glow curve structure with a minor peak in the 145 °C range[37, 41]. The 830 nm excitation light corresponds to a photon energy of approximately 1.49 eV, which may be above the threshold optical ionization energy (E_o) of this trap. This optical ionization energy is not directly comparable with the thermal activation energy of the low-temperature trap since some of an excitation photon's energy is converted in phonon energy, or lattice

vibrations, but it would be a value somewhat larger than the thermal activation energy of the trap, or 0.90 eV. As such, it is hypothesized that the IR light is depopulating this low-temperature trap.

The behavior demonstrated by the $CaSO_4$:Tm under IR stimulation is similar to that of quartz, which experiences an internal transition from a ground state to an excited state at this optical energy, from which subsequent ambient thermal stimulation to the conduction band leads eventually to the production of an OSL signal[1]. The metastable nature of the observed behavior of $CaSO_4$:Tm may indicate the presence of such a delayed thermally-induced clearance mechanism from an excited state. Another possibility is that the IR light itself is causing heating of the material such that TL begins to occur during the readout time. This effect, which could also explain the shape of the OSL curve in this case, cannot be ruled out without further investigations into the sample temperature effects of this OSL reader. A final possibility is that the process involves direct stimulation into the conduction band followed by a metastable recombination process. However, the blue-light OSL signal in this material did not demonstrate such a metastable recombination behavior, making this possibility unlikely. Additionally, the fact that the excitation wavelength is significantly longer than the emission wavelength, i.e., an anti-Stokes shift, makes the possibility that the observed signal results from a simple photoluminescence (PL) process highly improbable[1]. Thus, it is theorized that the origin of the IR-induced signal results from an internal intra-center transition followed by heat-induced elevation into the conduction band. A follow-up experiment performed at cryogenic temperatures would allow a more direct verification of this process.

Dose linearity was also examined for the OSL signals emitted from $CaSO_4$:Tm under both blue light and infrared light stimulation. Figure 3.7 plots the peak OSL signal height, defined in this case as the counts per channel for the first readout channel of the OSL curve, as a function of dose under both illumination sources. The zero dose, or dark count, OSL signal was subtracted from the signals prior to plotting, and a best-fit trendline is shown for both data sets. It is evident from this graph that the peak height of the OSL signal resulting from blue light stimulation is highly linear with respect to dose up to at least 1.5 Gy. The red light-induced OSL signal is slightly sub-linear, suggesting a possible reduction in dose sensitivity at doses in the 1.5 Gy and above range.

CaF_2:Mn

The CaF_2:Mn did not exhibit any detectable OSL signal under either IR or blue light excitation, at any of the utilized radiation doses. This result is likely a reflection more of the experimental setup than of the ability of the material to act as an OSL dosimeter. Previous studies of the optical properties of this substance suggest that the primary photoluminescence emission, due to the Mn^{2+} recombination site, would occur at a longer wavelength, ~500 nm, than the commercial OSL reader used here is able to measure, and furthermore that the excitation wavelengths employed here, 830 nm and 470 nm, are not ideal for OSL in this material [45, 50]. Further investigation of this material using more configurable excitation and emission systems may yield more promising OSL results, and dysprosium-doped and thulium-doped versions of CaF_2, which were not

available for experimentation at the time of this study, could also be investigated in future experiments if desired.

$Li_2B_4O_7$:Cu

With respect to the $Li_2B_4O_7$:Cu, this material's inclusion of boron into the crystal matrix would necessarily make it an attractive detection option for neutrons, since the ^{10}B isotope, which comprises approximately 20% of natural boron, has a very high thermal neutron capture cross-section. However, this material showed an OSL response that was only about 4% that of the $CaSO_4$:Tm under blue light stimulation and was not distinguishable from the instrument background count rate at the 15 mGy dose, leading one to conclude that the utility of a sample of this size and material would not offer a particularly sensitive detection capability at the investigated wavelengths. This material's OSL response to the IR excitation light, which was roughly twice instrument background at 1.5 Gy, supports that conclusion.

The current literature indicates that this material emits light centered at 368 nm[49], which is within the experimental setup's detection window, although not at its most sensitive frequency. With two U-340 ultraviolet-transmitting, visible light-absorbing filters in place at the PMT, the percent transmittance for this wavelength would be approximately 25%. This suggests that with more careful instrument design or with a POSL apparatus, which permits greater OSL detection efficiency, a four-fold increase in sensitivity may be possible from this factor alone. However, this material's optically-induced fading has been shown to be less than 10% after 3000 lx-h of exposure

to room light[32] or to have 85% loss of signal following a week of storage under fluorescent or tungsten lamp lighting[33], which is far less than has been seen in α-Al_2O_3:C[12], indicating that the material likely has a relatively low photoionization cross section and thus OSL potential. Therefore, this experiment and associated literature review shows that the potential for this material as a low-dose OSL dosimetry substance appears to be limited, but that it may warrant further study to determine to what extent it could be useful for high-dose dosimetry applications, particularly those involving neutron fields.

LiF:Mg,Ti

The LiF:Mg,Ti sample demonstrated an extremely weak OSL signal not discernable from background at the 15 mGy dose point under blue light stimulation. This signal has a magnitude approximately 1.4% that of $CaSO_4$:Tm under blue light stimulation, as shown in Figure 3.6. In addition, at the 1.5 Gy irradiation dose, this material exhibited OSL under IR stimulation at a level approximately twice that of instrument background. A review of previously-published emission spectrum data for this material indicates that it emits in a broad range centered at approximately 410 nm and with a FWHM of approximately 110 nm, which does overlap somewhat the OSL reader detection subsystem sensitivity[49]. As such, had the material demonstrated OSL potential to any appreciable degree, it would have been expected to yield a more pronounced signal. The well-known insensitivity of LiF:Mg,Ti to light-induced fading

supports the assertion that the optical stimulation cross-section for this material is unacceptably low for application as an OSL dosimeter.

CONCLUSIONS

While $CaSO_4$:Tm has been studied for its OSL properties to some degree in the published literature, this experiment provides new quantitative information regarding those properties, particularly with respect to this material's OSL sensitivity outside of the optimal stimulation frequencies. Specifically, this experiment indicates that $CaSO_4$:Tm exhibits OSL under both IR and blue light stimulation centered at 830 and 470 nm wavelengths, respectively. This luminescence is easily detectable using a commercial OSL reader utilizing LED-based CW-OSL at irradiation doses of 15 mGy or less. Additionally, the OSL signal peak height when using blue light stimulation is highly linear with respect to dose up to at least 1.5 Gy when using ^{90}Sr beta irradiation. Further investigation of this material's OSL properties is indicated to determine an optimal OSL readout regime and to determine its optimal OSL dose sensitivity and fading properties. In addition, since this experiment analyzed only a single sample for each material, future OSL experiments with this material, as well as with the other materials studied, would benefit from the use of multiple material samples so that sample averages and variances could be determined.

Experimental results for CaF_2:Mn did not show an OSL response at any dose under IR or blue light stimulation; however, additional room-temperature CW-OSL and

POSL experiments at additional excitation and emission frequencies are indicated to more fully characterize the OSL properties of this material.

$Li_2B_4O_7$:Cu demonstrated an OSL signal under blue light excitation that was of significantly lower intensity relative to that of $CaSO_4$:Tm or of α-Al_2O_3:C. Based on these experimental results, as well as on previous published data on the material, $Li_2B_4O_7$:Cu does not show substantial potential as a highly sensitive OSL dosimetry material, though it may have applications in neutron detection applications involving higher doses.

In the case of LiF:Mg,Ti, a very weak OSL response under blue light illumination was seen following irradiation at or above 150 mGy, but the magnitude of this response, in light of previously-published data regarding this material's optical properties, indicate that LiF:Mg,Ti is not an efficient OSL dosimetry material.

ACKNOWLEDGEMENTS

This research would not have been possible without the cooperation and assistance of personnel at Los Alamos National Laboratory. In particular, thanks are given to Dr. David Morris, Dr. Benjamin Warner, Dr. Cathy Wilson, Dr. Kenneth Lepper, Mr. Jeff Hoffman, and Ms. Ricki Sheldon for their constructive comments and assistance with equipment provision and instruction during the course of this research activity. Also, Dr. Eduardo Yukihara's advice and constructive criticism during the execution of this research is greatly appreciated. Finally, Ms. Sara Bernal is recognized

for her assistance with sample preparation and data collection during the conduct of these experiments.

REFERENCES

1. Bøtter-Jensen, L., McKeever, S. W. S. and Wintle, A. G. Optically stimulated luminescence dosimetry. (Amsterdam, The Netherlands: Elsevier Science B.V.) (2003) ISBN 0444506845.

2. Kristianpoller, N., Oster, L. Optically stimulated luminescence in anion-defective carbon doped alpha-Al_2O_3 crystals. Radiation Effects and Defects in Solids. 134, 311-313 (1995).

3. McKeever, S. W. S., Akselrod, M. S. and Markey, B. G. Pulsed optically stimulated luminescence dosimetry using α-Al_2O_3:C. Radiat. Prot. Dosim. 65, 267-272 (1996).

4. Bøtter-Jensen, L. and McKeever, S. W. S. Optically stimulated luminescence dosimetry using natural and synthetic materials. Radiat. Prot. Dosim. 65, 273-280 (1996).

5. Bulur, E. and Göksu, H. Y. Pulsed optically stimulated luminescence from α-Al_2O_3:C using green light emitting diodes. Radiat. Meas. 27, 479-488 (1997).

6. Bøtter-Jensen, L., Larsen, N. A., Markey, B. G. and McKeever, S. W. S. Al_2O_3:C as a sensitive OSL dosimeter for rapid assessment of environmental dose rates. Radiat. Meas. 27, 295-298 (1997).

7. Akselrod, M. S., Lucas, A. C., Polf, J. C. and McKeever, S. W. S. Optically stimulated luminescence of Al_2O_3. Radiat. Meas. 29, 391-399 (1998).

8. McKeever, S. W. S. and Akselrod, M. S. Radiation dosimetry using pulsed optically stimulated luminescence of Al_2O_3:C. Radiat. Prot. Dosim. 84, 317-320 (1999).

9. Bøtter-Jensen, L., Mejdahl, V. and Murray, A. S. New light on OSL. Quaternary Geochronology. 18, 303-309 (1999).

10. Yoder, R. C. A radiation measurement film employing optically stimulated luminescence technology. Landauer, Inc. Glenwood, Illinois. (2000).

11. Akselrod, M. S., Kortov, V. S., Kravetsky, D. J. and Gotlib, V. I. Highly sensitive thermoluminescent anion-defect alpha-Al_2O_3:C single crystal detectors. Radiat. Prot. Dosim. 33, 119-122 (1990).

12. Moscovitch, M., Tawil, R. A. and Svinkin, M. Light induced fading in α-Al_2O_3:C. Radiat. Prot. Dosim. 47, 251-253 (1993).

13. Walker, F. D., Colyott, L. E., Larsen, N. A. and McKeever, S. W. S. The wavelength dependence of light-induced fading of thermoluminescence from α-Al_2O_3:C. Radiat. Meas. 26, 711-718 (1996).

14. West, W. G., Kearfott, K. J. and Bernal, S. M. The sunlight OSL response of a commercially available α-Al_2O_3:C personnel dosimetry material. Radiat. Prot. Dosim. 119, 344-349 (2006).

15. Bøtter-Jensen, L., Markey, B. G. and Agersnap Larsen, N. Retrospective radiation dosimetry using optically stimulated luminescence on natural and synthetic materials. (Horn, Austria: Berger) (1996).

16. Stoneham, D., Bailiff, I. K., Petrov, S., Botter-Jensen, L., Goeksu, Y. and Jungner, H. Retrospective dosimetry: The development of an experimental methodology using luminescence techniques. (Luxembourg, Luxembourg) (1996).

17. Banerjee, D., Boetter-Jensen, L. and Murray, A. S. Retrospective dosimetry: Estimation of the dose to quartz using the single-aliquot regenerative-dose protocol. Applied Radiation and Isotopes. 52, 831-844 (2000).

18. Kanemaki, M., Ninagawa, K., Yamamoto, I., Nakagawa, M., Wada, T., Yamashita, Y. and Endo, K. Red thermoluminescence of volcanic glass fractions from tephras. International Journal of Radiation Applications and Instrumentation. Part D. Nuclear Tracks and Radiation Measurements. 18, 81-88 (1991).

19. Bøtter-Jensen, L., Jungner, H. and Mejdahl, V. Recent developments of OSL techniques for dating quartz and feldspars. Radiation Protection Dosimetry (UK). 47, 643-648 (1993).

20. Banerjee, D. Optical stimulated luminescence (OSL) dating. (Lucas Heights, Australia: Australian Institute of Nuclear Science and Engineering) (1999).

21. Bailey, R. M., Adamiec, G. and Rhodes, E. J. OSL properties of NaCl relative to dating and dosimetry. Radiat. Meas. 32, 717-723 (2000).

22. Huett, G. and Jaek, I. Advances in the luminescence dating: The optically stimulated luminescence based procedures and their physical background. Proceedings of the Estonian Academy of Sciences: Geology. 50, 214-232 (2001).

23. Stokes, S. and Fattahi, M. Red emission luminescence from quartz and feldspar for dating applications: An overview. Radiat. Meas. 37, 383-395 (2003).

24. Takaki, S., Ikeya, M. and Yamanaka, C. Remote TL and OSL for asteroid and meteorite study. Radiat. Meas. 27, 393-397 (1997).

25. Bøtter-Jensen, L. Development of optically stimulated luminescence techniques using natural minerals and ceramics, and their application to retrospective dosimetry. Risø-R-1211(EN). Roskilde, Denmark. (2000).

26. Inrig, E. L., Godfrey-Smith, D. I. and Khanna, S. Optically stimulated luminescence of electronic components for forensic, retrospective, and accident dosimetry. Radiat. Meas. 43, 726-730.

27. Bailiff, I. K. The use of ceramics for retrospective dosimetry in the Chernobyl exclusion zone. Radiat. Meas. 24, 507-511 (1995).

28. Hashimoto, T., Hong, D. G. and Takano, M. Retrospective dosimetry at JCO using luminescence from ceramics pieces and quartz grains. Advances in ESR Applications. 18, 197-202 (2002).

29. Akselrod, M. S., Bøtter-Jensen, L. and McKeever, S. W. S. Optically stimulated luminescence and its use in medical dosimetry. Radiat. Meas. 41, S78-S99 (2006).

30. Gaza, R., McKeever, S. W. S., Akselrod, M. S., Akselrod, A., Underwood, T., Yoder, C., Andersen, C. E., Aznar, M. C., Marckmann, C. J. and Bøtter-Jensen, L. A fiber-dosimetry method based on OSL from Al_2O_3:C for radiotherapy applications. Radiat. Meas. 38, 809-812 (2004).

31. Gaza, R. and McKeever, S. W. S. A real-time, high-resolution optical fibre dosemeter based on optically stimulated luminescence (OSL) of KBr:Eu, for potential use during the radiotherapy of cancer. Radiat. Prot. Dosim. 120, 14-19 (2006).

32. Takenaga, M., Yamamoto, O. and Yamashita, T. A new phosphor $Li_2B_4O_7$:Cu for TLD. Health Phys. 44, 387-393 (1983).

33. Driscoll, C. M. H., Fisher, E. S., Furetta, C., Padovani, R., Richards, D. J. and Wall, B. F. The thermoluminescence properties of lithium borate dosemeters. Radiat Prot Dosimetry. 6, 305-308 (1983).

34. Crittenden, G. C., Townsend, P. D., Gilkes, J. and Wintersgill, M. C. LiF dosimetry: II. The effects of Mg and Ti on the thermoluminescent emission spectra of LiF. J. Phys. D Appl. Phys. 7(1974).

35. Sunta, C. M. O., E.; Lima, J.F.; Yoshimura, E.M. Supralinearity and sensitization of thermoluminescence. II: Interactive trap system model applied to LiF:Mg, Ti. J. Phys. D: Appl. Phys. 27, 2636-2643 (1994).

36. Lee, J. I., Kim, J. L., Pradhan, A. S., Kim, B. H., Chung, K. S. and Choe, H. S. Role of dopants in LiF TLD materials. Radiat. Meas. 43, 303-308 (2008).

37. Nambi, K. S. V. and et al. Thermoluminescence of $CaSO_4$ doped with rare earths. Journal of Physics C: Solid State Physics. 7, 4403 (1974).

38. Iga, K., Yamashita, T., Takenaga, M., Yasuno, Y., Oonishi, H. and Ikedo, M. Composite TLD based on $CaSO_4$:Tm for gamma-rays, x-rays, beta-rays and thermal neutrons. Health Phys. 33, 605-610 (1977).

39. Lewandowski, A. C., Barkyoumb, J.H., Mathur, V.K. Thermoluminescence emission, excitation and stimulation spectra of $CaSO_4$:Dy and $CaSO_4$:Tm. Radiat. Prot. Dosim. 65, 281-286 (1996).

40. Lakshmanan, A. R., Lapraz, D., Prévost, H. and Benabdesselam, M. Thermostimulated luminescence properties of $CaSO_4$:Dy and $CaSO_4$:Tm phosphors annealed at high temperatures. physica status solidi (a). 202, 131-139 (2005).

41. Yamashita, T., Nada, N., Onishi, H. and Kitamura, S. Calcium sulfate activated by thulium or dysprosium for thermoluminescence dosimetry. Health Phys. 21, 295-300 (1971).

42. Pradhan, A. S. Emission spectra and influence of sunlight on thermoluminescence of dysprosium doped $CaSO_4$ and CaF_2. Radiat. Prot. Dosim. 47, 151-154 (1993).

43. Jaek, I., Kerikmae, K., Lust, A. Optically stimulated luminescence of some thermoluminescence detectors as an indicator of absorbed radiation dose. Radiat. Prot. Dosim. 100, 459-462 (2002).

44. Henniger, J., Horlbeck, B., Hubner, K., Prokert, K. The evaluation of CaF_2:Mn-polyethylene detectors with the aid of the optically stimulated luminescence (OSL). Nuclear Instruments and Methods. 204, 209-212 (1982).

45. Allen, P. and McKeever, S. W. S. Studies of PTTL and OSL in TLD-400. Radiat. Prot. Dosim. 33, 19-22 (1990).

46. Miller, S. D., Stahl, K. A., Endres, G. W. R. and McDonald, J. C. Optical annealing of CaF_2:Mn for cooled optically stimulated luminescence. Radiat. Prot. Dosim. 29, 195-198 (1989).

47. Miller, S. D. E., G.W.R. Long-term fading study of the cooled optically stimulated luminescence in CaF_2:Mn. Radiat. Prot. Dosim. 37, 275-277 (1991).

48. Miller, S. D., Endres, G. W. R., McDonald, J. C. and Swinth, K. L. Cooled optically stimulated luminescence in CaF_2:Mn. Radiat. Prot. Dosim. 25, 201-205 (1988).

49. McKeever, S. W. S., Moscovitch, M. and Townsend, P. D. Thermoluminescence dosimetry materials: Properties and uses. (Ashford: Nuclear Technology Publishing) (1995) ISBN 1870965191.

50. McKeever, S. W. S., Brown, M. D., Abbundi, R. J., Chan, H. and Mathur, V. K. Characterization of optically active sites in CaF_2:Ce,Mn from optical spectra. J. Appl. Phys. 60, 2505-2510 (1986).

CHAPTER 4

An Affordable Optically Stimulated Luminescent Dosimeter Reader Utilizing Multiple Excitation Wavelengths

ABSTRACT

Optically stimulated luminescence (OSL) dosimetry using anion-deficient aluminum oxide doped with carbon (α-Al_2O_3:C) has become a widely-used and effective medium for personnel dosimetry applications. The OSL phenomenon involves the illumination of an irradiated sample of an appropriate material to produce a stimulated emission of light whose intensity is indicative of the radiation dose. Commercially-available OSL readers exist, but may be too expensive for many labs beginning OSL research. Furthermore, these readers have been developed primarily for geological dating or simple dosimetric applications and thus offer limited flexibility for researchers who may want to experiment with a variety of excitation light sources, light detection systems, or other aspects of an experimental setup. Faced with these considerations, a lower-cost OSL reader with increased flexibility for pursuing laboratory research into OSL theory and application was designed and constructed. Various methods were used to reduce costs and increase flexibility, including: the use of off-the-shelf optical components, selection of newer higher-power light emitting diodes (LEDs) versus more elaborate light sources such as lasers or broad-spectrum bulbs with

monochromators, and design features that allow simple and rapid changing of key system components. This reader design includes more wavelengths of excitation light than current commercial readers, as well as the ability to swap out filters and other components during an experiment. In spite of these advantages, the total cost of the unit is an order of magnitude lower than commercial alternatives.

INTRODUCTION

During the past ten years, optically stimulated luminescence (OSL) dosimetry using anion-deficient aluminum oxide doped with carbon (α-Al_2O_3:C) has become a widely-used and effective medium for personnel dosimetry applications. The OSL mechanism relies upon the illumination of an irradiated sample with light to produce the stimulated emission of light proportional to the radiation dose that previously caused trapping of electrons in the material[1]. Of course, not all materials exhibit the phenomenon and different materials behave quite differently with respect to the extent to which they exhibit these properties. A great deal of research has been done to identify materials and formulations which produce a strong and stable OSL signal when stimulated with light of convenient wavelengths[2-28].

In addition to the personnel dosimetry application of OSL, the phenomenon has also been harnessed for the purpose of geological dating of soil samples[24, 29-37]. By analyzing the total absorbed dose of an excavated sample of a natural OSL material such as quartz or feldspar, one can determine how long the material has been buried. This is possible because, conveniently, these minerals' OSL signal is "bleached" or reset by prolonged exposure to sunlight[32, 35, 38-41]. As such, the OSL signal's intensity can be

correlated directly to the burial time of the sample. This methodology has also been applied to accident dosimetry scenarios using various building structural materials that exhibit the OSL property[29, 42-45].

The benefits of OSL dosimeters over thermoluminescent dosimeters (TLDs) for dosimetry applications include faster readout, greater dose sensitivity, relative insensitivity to heat and humidity, and the ability to perform multiple read-outs from a single sample[1]. This makes OSL an attractive candidate for further research. However, to date the only OSL readers that can be purchased are either specifically intended for reading one company's α-Al_2O_3:C dosimetric badges (InLight® OSL Readers, Landauer, Inc., 2 Science Road, Glenwood, Illinois, 60425-1586, USA, custserv@landauer.com, +1 800 323 8830, www.landauer.com) or are designed specifically for geologic dating applications and research (Risø Laboratories Model DA-15C/D TL/OSL Reader and Daybreak Model 2200 OSL Reader). As such, these systems' components are optimized for particular materials and read-out protocols. A research laboratory interested in starting an OSL research program could modify an existing system to allow more flexibility in terms of excitation sources (e.g., allowing a variety of wavelengths, intensities, or timing), detection systems (e.g., different types of photo-detectors optimized for different emission wavelengths and intensities), electronics, software, and physical configuration. The most established commercial reader (Model DA-15C/D TL/OSL Reader, Risø National Laboratory, Frederiksborgvej 399, P.O. Box. 49, 4000 Roskilde, Denmark, risoe@risoe.dtu.dk, +45 4677 4677, www.risoe.dtu.dk) utilizes blue and infrared LEDs in its standard configuration and has a 48-sample automated changer[46-48]. This device costs approximately €75,000, which, as of this writing, is

equivalent to approximately US$102,000. This cost does not include the additional expenses that would be required for modifications. The other reader currently available commercially (Model 2200 OSL Reader, Daybreak Nuclear and Medical Systems, Inc., 50 Denison Drive, Guilford, CT, 06437-2344, USA, info@daybreaknuclear.us, +1 203 488 2483, daybreaknuclear.us), has several excitation options available and a 60-sample changer[49]. Finally, bench-top and portable OSL readers are available specifically for dosimetry applications[50], but these devices are closed, specialized designs not intended for general laboratory research. There had previously been one other commercial reader (the ELSEC 9010, produced by Littlemore Scientific Engineering Co, Gutchpool Farm, Gillingham, Dorset SP8 5QP, United Kingdom, elsec@elsec.co.uk, +44 01747 835550, www.elsec.com), but this reader, employing a photomultiplier tube (PMT)-based detection system and interchangeable excitation sources, is no longer produced[51]. For many research laboratories, the expense or the technical limitations of a commercial reader are prohibitive and therefore construction of a lower-cost and/or more customizable lab-built rig becomes necessary. Custom-built OSL readers have been used by various research groups for specific experimental purposes. For example, Gaza et. al. built a custom laser-based OSL system for a fiber optic dosimetry system[52], Schilles et. al. built an early LED-based system for dating of geologic samples[53] and Smetana et. al. built a compact LED-based system for UV dosimetry[54]. The design described herein uses, to the extent possible, off-the-shelf mechanical and optical components, as well as an open table-top design appropriate for a research team desiring to have complete control and upgradeability of reader geometry and subsystems.

This paper reports the design, construction, and initial setup and testing of a novel OSL reader that is designed to allow the maximum amount of experimental flexibility in the research of OSL material properties and physical principles. In addition, some recommendations regarding modifications that could be made to this design to allow various other specific types of experimentation in the field will be included.

OSL READER DESIGN AND CONSTRUCTION

General Design Principles

The design process began with experience using two other commercially available readers, the Risø and the Daybreak (details previously referenced). Though the Risø reader is very well-engineered and well-built for its intended purpose of geological dating, a number of limitations for basic OSL research were identified, including the limited number of excitation wavelengths available and the single available light detection subsystem, consisting of a bialkali PMT behind two high-pass filters. However, it was decided that the basic components of this design, which is very effective at reading α-Al_2O_3:C, would serve as a very good starting point for the design process and also allow for the performance of comparative testing on the reader once finished to validate its proper operation.

The first priority for the reader design was to allow for equipment modularity. Specifically, it was desired to have the ability to add or change excitation light sources, emission light detection systems, and associated filtration quickly and easily. This would

allow the experimenter to swap out various components during a single experiment should that be required and also to change configurations depending on the particular material being researched at the time. To obtain this flexibility, the reader hardware was built on a standard laboratory optical breadboard (Model 07OBK007, CVI Melles Griot, 200 Dorado Place SE, Albuquerque, NM 87123, USA, optics@cvimellesgriot.com, +1 505 296 9541, www.cvimellesgriot.com) and commercially available optical components and fittings were used to the degree possible. This approach allows the use of the extensive range of positioning hardware available for optical components and also provides a very simple horizontally-oriented experimental setup to allow easy component access as well as the option of incorporating large laser light sources. However, there were two significant challenges to this approach. First, unless complicated optics are utilized, a horizontal setup requires a vertical sample mounting system. Such a vertical mounting system is more difficult to implement than a horizontal mounting system in which gravity holds the sample in the sample chamber. Second, using a modular layout versus a custom-machined case means that the optical efficiency of the design is somewhat lower than it would be otherwise. The former issue was addressed by designing and incorporating a vertical sample holder that uses a 120 V alternating current (AC)–powered, low-volume vacuum pump (Renaissance 500, Renaissance International, Inc.) to hold the sample in place. The latter issue was addressed by minimizing the light source-to-sample-to-light detector distance to the extent possible and by simply using somewhat higher experimental radiation doses to samples to create a stronger OSL signal. A rendering of the device, showing its basic layout, was created using a popular computer-aided design program (AutoCAD®, Autodesk, Inc., 111 McInnis Parkway, San

Rafael, CA, 94903, USA, +1 800 964 6432, usa.autodesk.com) and separate rendering software (3D Studio Max, Autodesk, Inc., 111 McInnis Parkway, San Rafael, CA, 94903, USA, +1 800 964 6432, usa.autodesk.com). This rendering is included as Figure 4.1. These same software programs were also used to generate the other renderings included in this paper except for Figure 4.4, which was created and rendered using a different software program (SolidWorks, Dassault Systèmes SolidWorks Corp., 300 Baker Avenue, Concord, MA, 01742, USA, +1 800 693 9000, www.solidworks.com).

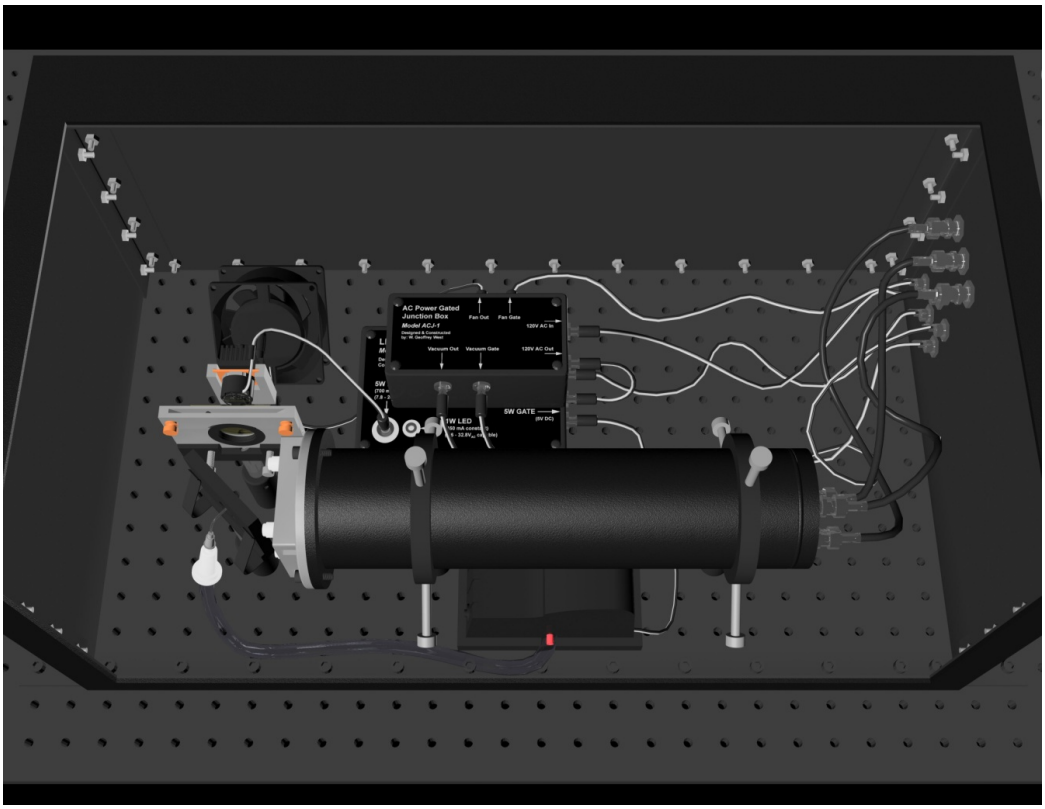

Figure 4.1: Basic layout of the optically stimulated luminescence (OSL) reader. This rendering shows the major system components, including LED source assembly, excitation filter housing and iris assembly, sample holder, PMT with emission filter housing, vacuum pump, fan, project boxes containing power distribution circuitry, and associated wiring.

Once the basic structure of the OSL reader was decided, the initial components to comprise the excitation and detection systems were determined. On the excitation side, LEDs were selected instead of lasers, or broadband bulbs with filters or monochromators, as the light source for a number of reasons: 1) price, 2) speed, 3) complexity, 4) size, and 5) wavelength availability. LEDs are notoriously inexpensive, have very fast turn-on and turn-off times, on the order of tens of nanoseconds, are powered by a simple low-voltage direct current (DC), are compact, and are offered in an increasing assortment of emission wavelengths. Furthermore, LEDs have a very long lifetime and require no maintenance or consumables, such as would be required for a dye laser system, for example. The LEDs chosen for the reader were 1W red, red-orange and amber units, and 5W green, cyan, blue and royal blue units (respectively, Luxeon™ Star Part Nos. LXHL-MD1D, LXHL-MH1D, LXHL-ML1D, LXHL-LM5C, LXHL-LE5C, LXHL-LB5C, LXHL-LR5C, Philips Lumileds Lighting Company, 370 West Trimble Road, San Jose, California, 95131, USA, info@lumileds.com, +1 408 964 2900, www.philipslumileds.com). These LEDs, at the time of construction, boasted the highest light output of any commercially available LED. In particular, the light output of a single 5W blue Luxeon LED substantially exceeds the total light output of all of the 42 Nichia LEDs used in the Risø reader[55]. Calculations demonstrating this relation are shown below.

The Luxeon LED has a rated luminous flux of 48 lm[56] (averaged over its spectrum, which, like the Nichia part, is centered at 470 nm). Each Nichia LED emits approximately 2 cd, or 2 lm sr^{-1} , at an emission angle of 15 degrees[42, 57]. To convert to

lm, one multiplies the luminous intensity in cd by the solid angle of emission in sr. The solid angle can be derived from a plane angle (θ) using the following equation:

$$\text{Solid angle (sr)} = 2 * \pi * [1-\cos(\theta/2)] \quad (1)$$

With an emission angle of 15 degrees, the solid angle would be 0.0538 sr. Multiplying by the 2 Cd-sr^{-1}, the result is 0.108 lumens per LED. Multiplied by the 42 LEDs used, this results in a total luminous flux of approximately 4.5 lm. As such, based on these rough calculations, the available luminance, before other factors such as focusing are considered, is approximately 10 times that of the Risø reader.

Red, red-orange, amber, green, cyan, blue, and royal blue LEDs were all acquired. These LEDs are available in three possible light emission profiles: lambertian, bat-wing, and side-emitting. The lambertian profile was chosen for the LEDs to provide the most directed beam. The center wavelengths and spectral half-widths (i.e., full width at half maximum intensity) of these LEDs are shown in Table 4.1.

Table 4.1: Light emitting diode (LED) emission specifications.

LED Color	Center Wavelength (nm)	Spectral Half-width (nm)
Red (1W)	625	20
Red-Orange (1W)	617	20
Amber (1W)	590	14
Green (5W)	530	35
Cyan (5W)	505	30
Blue (5W)	470	25
Royal Blue (5W)	455	20

On the detection side, a bi-alkali PMT (Model 9235QA with B2F/RFI housing, ADIT Electron Tubes, 300 Crane Street, Sweetwater, Texas, 79556, USA, sales@electrontubes.com, +1 325 235 1418, www.electrontubes.com) selected for a dark count rate of less than 75 counts per second was employed. Like the PMT used in the Risø reader, this unit is configured in a "photon-counting" electrical setup to maximize the sensitivity. One salient difference between this PMT and that of the commercial unit is that an electronic gating circuit (Model GB1BH, ADIT Electron Tubes, 300 Crane Street, Sweetwater, Texas, 79556, USA, sales@electrontubes.com, +1 325 235 1418, www.electrontubes.com) was installed in the tube housing. This was done for two principal reasons: 1) to allow for an additional protective element to prevent over-stimulation of the tube in the event of exposure to room light while high voltage is applied (the gate is configured in a "default-off" state), and 2) to allow for the use of pulsed OSL (POSL) counting methods. The on-off cycle time of this gating circuit is 1.4 μs when set up for pulsed operation, though for initial continuous-operation testing, this gating circuit was used in a DC mode, with a corresponding on-off cycle time of 1.0 ms. This particular detection subsystem allows for excellent quantum efficiency in the shorter-wavelength portion of the visible and near-UV light spectrum between 160 and 550 nm. Should greater sensitivity be desired at some point in the future in the longer-wavelength portion of the spectrum, the modular design of this system would allow the addition or substitution of a PMT more appropriate for that range.

The Excitation System

Figure 4.2 shows a depiction of the OSL reader LED source assembly. This assembly consists generally of an LED "package" mounted in a custom-designed holder. The LED package consists specifically of: 1) the LED with PCB mounting, 2) a heat sink, 3) a collimating lens, 4) a copper mounting plate, and 5) wire leads. The LED is affixed to the copper plate with a thermal adhesive (Thermalbond™, Aavid Thermalloy, LLC, 70 Commercial St., Concord, NH, 03301, USA, +1 603 224 9988, www.aavidthermalloy.com). This adhesive is also used to bond the copper plate to the

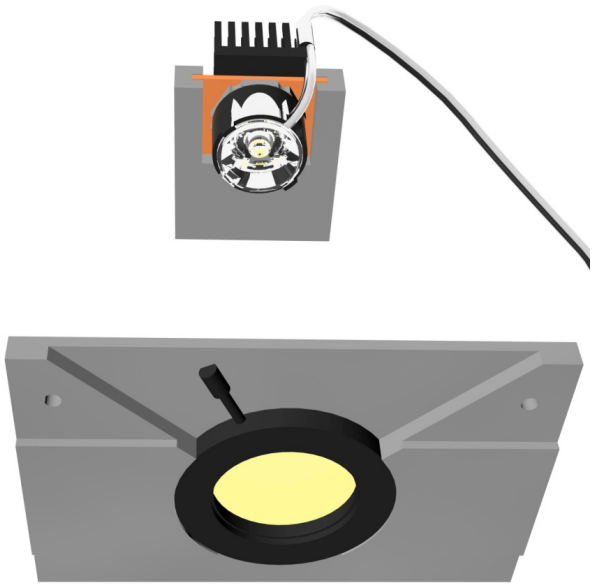

Figure 4.2: Light emitting diode (LED) source assembly and iris plate with iris. The LED source assembly is shown at top and consists of: the heat sink, colored black, the copper mounting plate, colored orange, the LED with PCB mounting, the collimating lens with lens holder and the wire lead. These components rest in a custom holder, colored gray. The iris plate with iris is shown at bottom and consists of the iris, colored black, and the iris plate, colored gray. The excitation lens, colored yellow, is visible through the iris and rests behind it.

heat sink. The collimating lens (Part No. LXHL-NX05, Philips Lumileds Lighting Company, 370 West Trimble Road, San Jose, California, 95131, USA, info@lumileds.com, +1 408 964 2900, www.philipslumileds.com) is held directly on top of the LED by use of a lens holder (Part No. LXHL-NX07, Philips Lumileds Lighting Company, 370 West Trimble Road, San Jose, California, 95131, USA, info@lumileds.com, +1 408 964 2900, www.philipslumileds.com), which is designed to simply snap onto the LED backing. The wire leads were threaded around the lens but inside the lens holder, and then back behind the package by affixing with electrical tape to one corner of the heat sink (Part No. 2317B, Aavid Thermalloy, LLC, 70 Commercial St., Concord, NH, 03301, USA, +1 603 224 9988, www.aavidthermalloy.com). The leads were terminated by use of either a Type M or Type N direct current (DC) barrel plug (Model Nos. 274-1569 and 274-1573, Radio Shack Corporation, 300 RadioShack Circle, Fort Worth, TX, 76102-1964, USA, +1 817 415 3011, www.radioshack.com). The two sizes of plug were used to terminate the 5W and 1W LEDs, respectively, in order to avoid any possibility of powering either wattage LED with the wrong current, which could result in either suboptimal light output or damage to the LED.

The custom-designed holder that holds the LED package consists of a machined aluminum bracket, in which the copper mounting plate slides, affixed to a two-axis optical kinematic mount (Part No.MHT-103, CVI Melles Griot, 200 Dorado Place SE, Albuquerque, NM 87123, USA, optics@cvimellesgriot.com, +1 505 296 9541, www.cvimellesgriot.com) with the thermal adhesive. That mount is then screwed into a post and collar assembly (Part Nos. 07RMH003 and 07PHS013, CVI Melles Griot, 200 Dorado Place SE, Albuquerque, NM 87123, USA, optics@cvimellesgriot.com, +1 505

296 9541, www.cvimellesgriot.com). This is, in turn, screwed into the optical breadboard. This two-part system allows the user to quickly and easily change out the various LED packages, one for each color, between experimental runs.

Though the heat sink for the LED sources was selected based upon heat transfer calculations, detailed below, to allow enough cooling under natural convection conditions, a small AC-powered fan (Model No. 273-242, Radio Shack Corporation, 300 RadioShack Circle, Fort Worth, TX, 76102-1964, USA, +1 817 415 3011, www.radioshack.com) was also installed in the case, pointed at the back of the source assembly heat sink to provide forced convection and thus a margin of safety and thermal stability even under long illumination time experiments.

The maximum allowed junction temperature for the 5 watt LED, the limiting component, is 135 °C, though it was desired to maintain the junction temperature, to levels far below this in order to minimize the negative effect that increased junction temperature has on LED light output[56, 58]. To determine the junction temperature, the following equation is used:

$$T_{Junction} = (R\Theta_{Junction\text{-}Ambient} \times P_d) + T_{Ambient} \quad (2)$$

where $T_{Junction}$ is the LED junction temperature in °C, $R\Theta_{Junction\text{-}Ambient}$ is the overall thermal resistance of the LED plus heat sink in °C W^{-1}, P_d is the power dissipated by the LED in watts, and $T_{Ambient}$ is the surrounding ambient air temperature in °C.

To determine P_d for an LED in W, the following equation is used:

$$P_d = I_f \times V_f \quad (3)$$

where I_f is the forward current of the LED in A, and V_f is the forward voltage of the LED in V.

The total thermal resistance of the LED assembly, $R\Theta_{Junction\text{-}Ambient}$, can be expressed as the sum of the individual resistances of the LED and its heat sink, as follows:

$$R\Theta_{Junction\text{-}Ambient} = R\Theta_{Junction\text{-}Board} + R\Theta_{Board\text{-}Ambient} \quad (4)$$

where $R\Theta_{Junction\text{-}Board}$ is the thermal resistance of all of the components that make up the LED, from junction to aluminum heater spreader, and $R\Theta_{Board\text{-}Ambient}$ is the thermal resistance of the heat sink, including the thermal adhesive used to attach it to the LED.

In order to determine the requirements for the LED heat sink, Equations 3 and 4 are substituted into Equation 2 and solved for $R\Theta_{Board\text{-}Ambient}$:

$$R\Theta_{Board-Ambient} = \frac{T_{Junction} - T_{Ambient}}{I_f \times V_f} - R\Theta_{Junction-Board} \quad (5)$$

The LED manufacturer provides the value of $R\Theta_{Junction\text{-}Board}$ for the 5 W LED, which is the limiting case in terms of heat output, as 11 °C W^{-1}. The manufacturer also provides the values of I_f and V_f as 0.700 A and 6.84 V, respectively. Therefore, to

achieve a temperature of less than 135 °C under continuous operation, and assuming an ambient temperature of 25 °C, these values are substituted into Equation 5 to reach the following result:

$$R\Theta_{Board\text{-}Ambient} \leq 12\ °C\ W^{-1}$$

Upon evaluating the thermal specifications of numerous heat sinks and thermal adhesives, it was determined that a column-type heat sink and low-resistivity thermal adhesive would meet the relevant criterion under free convection conditions.

In addition to the LED source assembly, the excitation system also includes the excitation filter / iris assembly, which was placed directly between the LED source assembly and the sample holder. This assembly consists of a filter holder (Part No. 07HFP002 , CVI Melles Griot, 200 Dorado Place SE, Albuquerque, NM 87123, USA, optics@cvimellesgriot.com, +1 505 296 9541, www.cvimellesgriot.com) on a post and pillar (Part Nos. 07RES002 and 07PHS013, CVI Melles Griot, 200 Dorado Place SE, Albuquerque, NM 87123, USA, optics@cvimellesgriot.com, +1 505 296 9541, www.cvimellesgriot.com) with a filter or filters, and a custom-machined aluminum iris plate measuring approximately 5 cm x 5 cm x 0.3 cm, which fits into the filter holder as a filter would. The iris plate was built from a mechanical iris (Model NT57-582, Edmund Optics, Inc., 101 East Gloucester Pike, Barrington, NJ, 08007-1380, USA, +1 800 363 1992, www.edmundoptics.com), mounted in an aluminum housing. It serves to provide an aperture of selectable size through which the LED excitation light passes. Optimal setting of this aperture size maximizes the ratio of excitation light striking the OSL

sample versus light striking the surrounding sample plate. The aperture assembly was placed towards the sample holder and can be opened or closed using its integral control pin. Once an optimum iris diameter is determined for the reader, there is a control rod cover plate that is installed via two brass thumbscrews on the front of the plate to prevent inadvertent changes to the iris diameter. The iris plate is also shown in Figure 4.2. To eliminate the possibility of unfiltered excitation light from reaching the PMT, a mask of photographic black aluminum foil (Matte Black Cinefoil™, Rosco Laboratories, Inc., 52 Harbor View, Stamford, CT, USA, 06902, info@rosco.com, +1 800 767 2669, www.rosco.com) was placed around the gap between the source LED assembly and the excitation filter / iris assembly. This mask forms a light-tight "tunnel" between these components that can be removed as needed in order to change excitation filters or LEDs.

It should be noted that although the use of a simple plastic collimating lens and aperture provide for focusing of the LED excitation light onto the OSL sample to a fair degree, more effective collimation could be realized by using a more elaborate, and expensive, set of optical lenses. Because more precise focusing using lenses would direct more of the LED output light onto the sample, and less onto the sample holder, this setup would provide a higher signal-to-noise ratio (SNR) during OSL read-outs. This higher SNR would result in a somewhat lower limit of detectability for absorbed dose to a sample. However, it was not utilized in this case in the interest of cost savings and simplicity.

The excitation filter used in the initial reader configuration is a single GG420 high-pass filter (Part No. 03FCG059, CVI Melles Griot, 200 Dorado Place SE, Albuquerque, NM 87123, USA, optics@cvimellesgriot.com, +1 505 296 9541,

www.cvimellesgriot.com), selected to remove excitation wavelengths below 420 nm from all of the LED spectra in the interest of reducing excitation light that could penetrate the corresponding complementary filters on the detection side, to be discussed in the next section. This complementary-filter methodology maximizes the ability of the OSL reader to distinguish legitimate OSL signals from excitation light, though an assumption is made with this method that at least some of the OSL light is of a wavelength less than 420 nm. Should this not be the case, the use of other filter combinations can be used to identify and quantify the OSL response.

The Detection System

Figure 4.3 shows a simplified, 'exploded view' of the main components of the OSL reader. This section of the apparatus consists of four primary components: 1) the PMT, 2) the PMT mounts, 3) the emission filter housing, and 4) the emission filters. The PMT is mounted horizontally by means of two 3-screw ring mounts (Model NT36-605, Edmund Optics, Inc., 101 East Gloucester Pike, Barrington, NJ, 08007-1380, USA, +1 800 363 1992, www.edmundoptics.com) affixed to standard optical posts and bases (Part Nos. 07RES002 and 07PHS013, CVI Melles Griot, 200 Dorado Place SE, Albuquerque, NM 87123, USA, optics@cvimellesgriot.com, +1 505 296 9541, www.cvimellesgriot.com) screwed into the optical breadboard. A custom-machined emission filter housing was designed to hold up to three standard 5.08 cm × 5.08 cm × 0.3175 cm optical filters in series immediately in front on the PMT photocathode. This

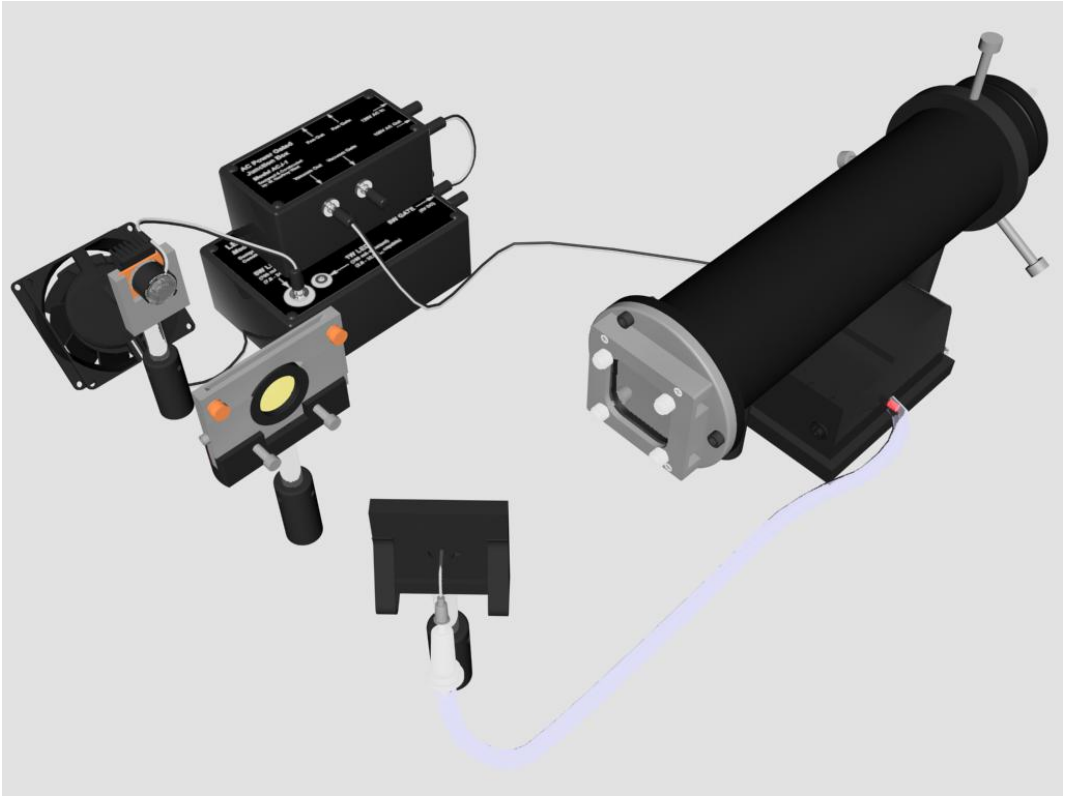

Figure 4.3: 'Exploded view' of the main optically stimulated luminescence (OSL) reader components. From left to right, this rendering shows the cooling fan, light emitting diode (LED) source assembly, iris assembly, power distribution boxes, sample holder, photomultiplier tube (PMT) with emission filter housing, and vacuum pump, located underneath the PMT.

housing was machined to mate securely with the flange on the PMT body. A rendering of this component is shown as Figure 4.4. Note that the design maximizes, to the extent possible the size of the opening through which the emission light will pass. The emission filters are inserted into the side of the housing. This orientation allows easy filter addition or removal while obviating any possibility that a filter will fall from, or into, the assembly and sustain damage. A 0.3175 cm soft 20A-durometer adhesive-backed black polyurethane foam strip was attached to the inside surface of the housing nearest the

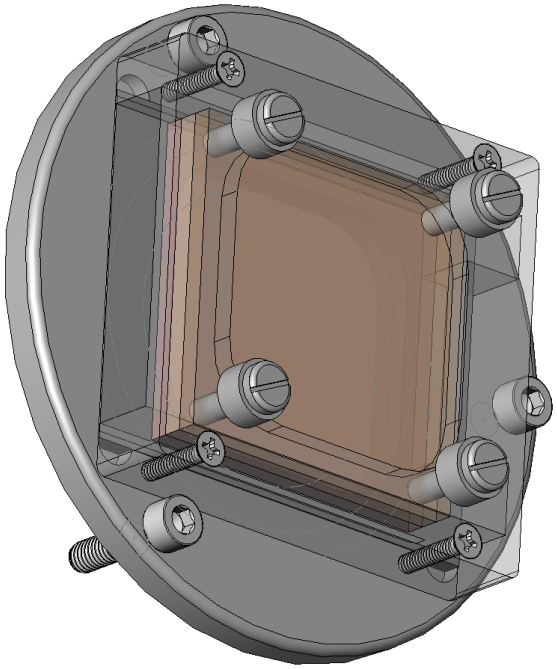

Figure 4.4: Rendering of the optically stimulated luminescence (OSL) reader emission filter housing. The photomultiplier tube (PMT) would be attached behind this component, from this perspective.

PMT for the innermost filter to rest against and the filters are held in place by four plastic set-screws. The gasket and screws are soft enough to avoid any damage to filters under repeated use. Furthermore, the gasket material compresses down below the inside surface of the housing in such a way that a very effective light-tight seal is made once the set screws are tightened. The sides of all filters used in the device were also painted black with common flat black indoor paint that did not demonstrate any fluorescence or phosphorescence during blank runs to keep scattered light ingress to a minimum. The filter housing also has two openings on the side opposite from where the filters are

inserted to allow the insertion of a stylus or other long, thin instrument to push filters out when their removal or change-out is desired.

The emission filters used for instrument setup and testing were the same U340 filters, placed two in series, used in the Risø reader (U340, Hoya Filters, 2-7-5, Naka-Ochiai, Shinjuku-ku, Tokyo, 161-8525, Japan, +813 39521151, www.hoyafilter.com), although on that instrument one of the filters has a metallic coating applied to compensate for a small transmission window in the red portion of the spectrum. If a user is particularly concerned about the contribution of light in the wavelength range 670-810 nm for their experiments, such a coating could be applied in a similar fashion. Of course, other emission filters can be easily substituted in for these filter types, depending on the wavelengths that are of interest. In effect, a series of filter change-outs can provide OSL emission spectroscopic information if the proper selections are made. A solid, opaque block of material was also cut in the size of a filter to provide total light extinction to the PMT for dark count testing and this piece could also be fit quite conveniently in the filter housing.

The Sample Holder

Figure 4.5 shows the sample holder assembly. This device must hold OSL material samples in a stable vertical orientation in close proximity to both the excitation and detection systems. Additionally, the sample holder had to be constructed in such a manner that it both maximized the induced sample OSL light reaching the detector and

Figure 4.5: Rendering of the optically stimulated luminescence (OSL) reader sample holder assembly. The sample is placed in the center of this plate and the vacuum line attaches to the small hole in the center, from behind.

minimized scatter excitation light reaching that same location. For this purpose, a simple 0.635 cm thick aluminum plate measuring 6.35 cm square was milled and mounted in a square filter holder (Part No. 07HFP002, CVI Melles Griot, 200 Dorado Place SE, Albuquerque, NM 87123, USA, optics@cvimellesgriot.com, +1 505 296 9541, www.cvimellesgriot.com) attached to a standard post and pillar (Part Nos. 07RES003 and 07PHS013, CVI Melles Griot, 200 Dorado Place SE, Albuquerque, NM 87123, USA, optics@cvimellesgriot.com, +1 505 296 9541, www.cvimellesgriot.com). The sample plate was painted with a low-reflectance matte black paint to reduce scatter of excitation light into the photomultiplier tube. This plate was milled with a shallow round hole of 1.0 cm diameter on one side of the plate and 0.75 cm diameter on the other side of the plate, in the interest of holding different-sized samples. Additionally, a very small

0.15 cm diameter thru-hole was drilled through the center of the sample holder to accommodate a long, thin nozzle attachment of the vacuum pump. When placed through the back side of the plate on the opposite side of the sample, the pump can be activated to hold the sample (which may be a wafer or a powder mounted on a planchet of some sort) flat against the plate. This system allows for a vertical sample arrangement, and thus a horizontal equipment layout.

For sample mounting and removal, a small notch was placed in the side of each shallow round sample hole to allow access for tweezers to grab the samples. In addition, the sample plate assembly can be rotated about the vertical access to allow easier access to the sample chamber, if necessary.

Electronics

The electronics systems of the OSL Reader can be divided into four primary sub-systems: excitation side electronics, detection side electronics, computer processing electronics including digital acquisition board, and ancillary systems control.

The *excitation side electronics* subsystem is responsible for controlling the timing and cooling of the LEDs. It is composed primarily of the LED power supply. This power supply allows the external digital acquisition (DAQ) board (NI-6020E USB, National Instruments Corporation, 11500 N Mopac Expressway, Austin, TX, 78759-3504, USA, +1 888 280 7645, www.ni.com) to control the LED state. Because the LEDs used are of two different current requirements, two different original equipment manufacturer (OEM) power supplies provide the foundation for this component. The two

power supplies are a 120 V 12 W 700 mA driver, and a 120 V 12 W 350 mA driver (respectively, Part Nos. Xitanium LED120A0700C24F and Xitanium 120A0350C33F, Philips-Advance Transformer, Inc., 10275 West Higgins Road, Rosemont, IL, 60018-5603, USA, +1 847 390 5000, www.advance.philips.com). These drivers feed the 5 W and 1 W LEDs, respectively. Originally, considerable thought was given to driving both LED types with a single higher-current power supply using an appropriate selection of parallel resistors to properly divide the current for the lower-power LEDs. However, it was decided, in the interests of minimizing heat generation and simplifying the circuit design, that both specialized power supplies would be used in the design. Both supplies accept standard 60 Hz, 120 V alternating current (AC) power and output a DC signal of a voltage suitable to drive one or several LEDs in series. It should be noted that consideration was also given to employing power supplies that would allow for variable intensity selection of the LED output, either manually or electronically. It was found, however, that due to a lack of appropriate drivers of this type for these new LEDs, such a power supply would need to be custom-built. This would require considerable additional time. However, this feature was not necessary for the experiments planned for the device in the short term. As such, this more flexible power supply, which would allow for linearly modulated OSL (LM-OSL) techniques on this device, has been left as a future upgrade. Should excitation light intensity reduction be needed on the current equipment setup, neutral density filters could be employed in the excitation filter holder to achieve a measure of control.

In order to turn the LEDs on and off electronically using a 5 V logic pulse from the DAQ board, a switch of some type was needed in-line with the power supplies. It

was decided to employ a switch that would allow rapid pulsing of the LEDs, so transistors and fast reed relays were investigated. In the case of reed relays, no part was identified which could reliably handle the large current draws of the LEDs without resulting in the contacts welding shut within several cycles. Even relays with nominal current capabilities suitable for the task were quickly destroyed. It was determined that LEDs, due to their inductive nature and turn-on spike, present a higher-than expected challenge to a relay. Transistors were also investigated, and would allow the fastest pulsing of the LEDs. These solid-state devices come in thousands of varieties and arriving at correct specifications required study of transistor theory and some consultation with electrical engineers. After repeated attempts to get a transistor-based system to work, it was determined that a confounding factor was that the LED power supply ground potential was not the same as the DAQ board transistor-to-transistor logic (TTL) ground potential in this system. For transistors to operate properly, the ground potential of the gate signal must be the same as that of the power signal. In many cases these grounds can be "bridged," and the power supplies will synchronize their potentials. However, in this case this was simply not possible without extensive redesign of the power systems or elaborate compensatory circuitry. As such, this very high speed pulsing capability, which could be beneficial if very fast POSL techniques were desired to be employed, was also left to a future upgrade and somewhat slower electromechanical relays were utilized which could handle the large currents without damage.

Numerous electromechanical relays were evaluated for the LED switching with the intent of minimizing the switching times while maintaining reliability. After extensive sample testing, relays that optimally balanced switching speed with durability

were identified (Model G6D-1A, Omron Corporation, Shiokoji Horikawa, Shimogyo-ku, Kyoto, 600-8530, Japan, +81-3-3436-7170, www.omron.com) for use on the high-power side of the LED drivers. Switching the low-power side of the drivers was abandoned due to erratic behavior caused by the drivers' automatic voltage regulation capability. The relays are single-pole, single-throw, normally-open units rated to switch up to 2 A and 250 VAC under an inductive load. The switching time (off-on-off) averages 9.8 ms so POSL techniques can still be employed on the reader so long as pulses of shorter duration than this are not needed. In addition to placing the relays in line with the AC power input to the LED drivers, a protection diode (Model No. 1N4148, Radio Shack Corporation, 300 RadioShack Circle, Fort Worth, TX, 76102-1964, USA, +1 817 415 3011, www.radioshack.com) was placed in series with the relay coils to protect the DAQ board digital outputs from relay clamping spikes. The LED drivers, power relays, and protection diodes were wired and placed in a black plastic project box. This box, like all other OSL reader internal components, was kept black to minimize unwanted light scatter. The project box utilizes labeled, non-compatible DC power connectors for all power and signal inputs and outputs. A schematic diagram of the excitation power supply is shown as Figure 4.6.

The *detection side electronics* are responsible for powering the PMT and processing the PMT output into a signal suitable for processing by the DAQ board. For this purpose, Nuclear Instrumentation Module (NIM) components were utilized due to their existing availability to the researchers and the configuration flexibility that a NIM system allows. The components used were: 1) a preamplifier (Model 2005, Canberra

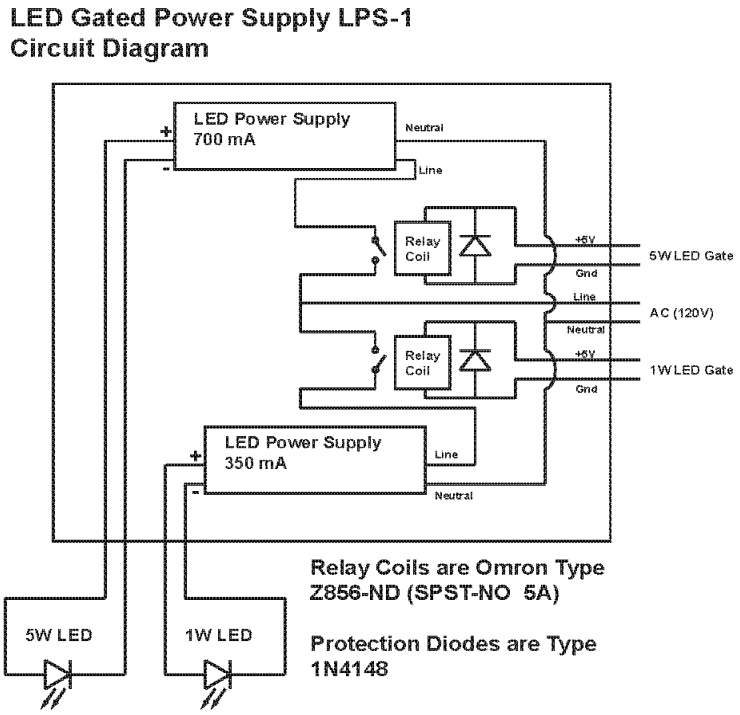

Figure 4.6: Circuit diagram of the excitation power supply.

Industries, Inc., 800 Research Parkway, Meriden, CT, 06450, USA, customersupport@canberra.com, +1 800 243 3955, www.canberra.com), 2) a high voltage power supply (Model 478, Ortec/Advanced Measurement Technology, Inc., 801 South Illinois Avenue, Oak Ridge, TN, 37831-0895, USA, ortec.info@ametek.com, +1 865 482 4411, www.ortec-online.com), 3) an amplifier (Model 575A, Ortec/Advanced Measurement Technology, Inc., 801 South Illinois Avenue, Oak Ridge, TN, 37831-0895, USA, ortec.info@ametek.com, +1 865 482 4411, www.ortec-online.com), and 4) a single-channel analyzer (SCA) (Model 550, Ortec/Advanced Measurement Technology, Inc., 801 South Illinois Avenue, Oak Ridge, TN, 37831-0895, USA, ortec.info@ametek.com, +1 865 482 4411, www.ortec-online.com). The PMT was

powered at its nominal operating voltage of 1,000 V and all other electronics settings, such as SCA window setpoints and amplifier gains, were determined during the reader's initial setup as described later. This signal chain as configured effectively amplified and discriminated the analog PMT output pulses and converted them into 5 V TTL pulses that the DAQ board digital counter inputs could receive and process.

The *DAQ board* possesses 16 analog inputs, 2 analog outputs, 8 digital input/output channels, and 2 up/down counter/timers. This device was selected based on a sufficient number of digital I/O channels, the availability of digital counters, and an acceptable counter maximum source frequency of 20 MHz to accommodate anticipated PMT count rates without difficulty. While some consideration was given to attempting to use the DAQ board's analog inputs to process and count the PMT output pulses directly, a familiarity with NIM electronics made this option unnecessary. However, future iterations of the reader may benefit from this type of sophisticated signal processing in order to afford more portability. For this instrument, the DAQ board's digital channels were used for reader control and signal counting according to Table 4.2. The DAQ board connects to the PC control computer via universal serial bus (USB) cable and is set up and controlled via a custom software program, to be described in the next section.

The *ancillary systems control electronics* consist of a single module that allows on/off switching of the LED cooling fan and the sample vacuum pump. This module, whose circuit diagram is shown as Figure 4.7, consists primarily of two electromechanical relays (Model Z712-ND, Omron Corporation, Shiokoji Horikawa, Shimogyo-ku, Kyoto, 600-8530, Japan, +81-3-3436-7170, www.omron.com) switching

Table 4.2: Digital acquisition (DAQ) board digital channel assignments. All signals use DGND (digital ground) terminals for grounding.

Channel	Function
DIO 0	5 W LED Gating
DIO 1	Unused
DIO 2	PMT Gating
DIO 3	1 W LED Gating
DIO 4	Fan On/Off
DIO 5	Vacuum Pump On/Off
DIO 6	Unused
DIO 7	Unused
PFI 1	PMT Input - Counter

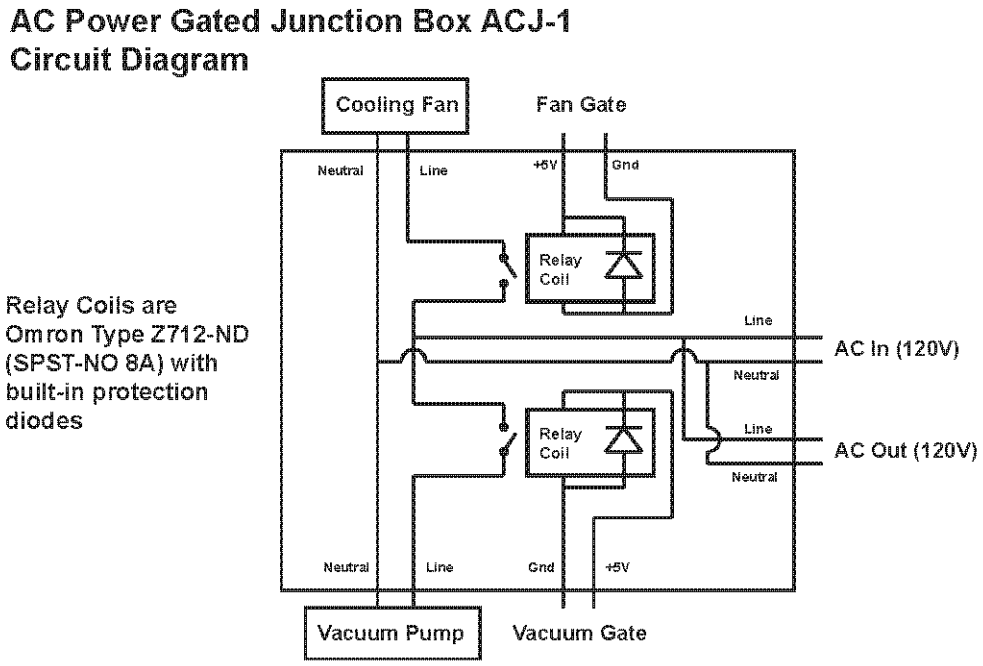

Figure 4.7: Circuit diagram of the cooling fan/vacuum pump control system.

120 VAC power based on the 5 V on/off signals from the DAQ board. These relays are of the single-pole, single-throw, normally-open type and they include built-in protection diodes. Additionally, this control module possesses an AC power pass-through to the LED power supply to minimize wiring clutter inside the OSL reader case.

Case

In order to protect both the PMT and the OSL samples from ambient light during readout cycles, it was necessary to build a light-tight case for the reader. While the OSL reader is currently located in a laboratory darkroom, it was quickly determined that a case would still be needed around the excitation, detection and sample holder systems of the reader to allow the staff to safely view the computer control system screen during

Figure 4.8: Photograph of the optically stimulated luminescence (OSL) reader case when closed.

read-outs and to reduce the PMT light exposure during periods when darkroom lights, both safelights and regular room lights, were required to be on. Though a number of options were considered for case materials, aluminum was eventually settled on for its durability, ease of machining, and complete opacity. Figure 4.8 is a photograph of the OSL reader case.

The case attaches directly to the optical breadboard via mounting screws (Part No. 07AKT005, CVI Melles Griot, 200 Dorado Place SE, Albuquerque, NM 87123, USA, optics@cvimellesgriot.com, +1 505 296 9541, www.cvimellesgriot.com). A black foam rubber gasket material was employed at this interface and the lid interface to allow for light-tightness. The case was designed to minimize the number of seams or penetrations and determination of which components would be internal to the case was made largely based on the number of case penetrations needed. The wiring penetrations through the side of the case were made using various bulkhead adapters – specifically, 2 Bayonet Neill-Concelman (BNC) pass-throughs for PMT gate and signal, 1 miniature high voltage (MHV) pass-through for PMT high voltage, and 5 DC power pass-throughs for AC power, 5 W LED Gating, 1 W LED Gating, Fan On/Off and Vacuum On/Off. Most case seams, such as the back corners, were covered with overlapping aluminum pieces attached using black adhesive caulk to further reduce light ingress. Once built, the inside of the case was painted with a low-reflectance black paint to reduce internal reflections and a multi-layer black polyester cloth cover was sewn to drape over the closed case during operation to further reduce light transmission. The case was tested for light-

tightness after construction and the results of these tests are indicated in the Results section of this paper.

Software

For control of the OSL Reader systems, a Windows®-based (Microsoft Corporation, One Microsoft Way. Redmond, Washington, 98052-6399, USA, www.microsoft.com) personal computer was utilized. This computer interfaces via Universal Serial Bus (USB) connection to the DAQ board. Custom software was developed using the DAQ board manufacturer's application development system (LabVIEW™ Version 7.1, National Instruments Corporation, 11500 N Mopac Expressway, Austin, TX, 78759-3504, USA, +1 888 280 7645, www.ni.com). This software programming tool relies on a visual metaphor to allow for rapid code creation and debugging, and also results in a very extensible product with a clear layout.

The custom software application that was developed allows for individual control of the LED power, PMT gate state, vacuum pump power, and fan power. In addition, this application provides real-time numerical and graphical display of the PMT count rate. Measurement sequences can be specified from the user interface, allowing the designation of excitation durations, PMT sampling rates, and pre- and post-excitation PMT measurement times. The software was programmed to allow for convenient operation of the OSL reader – for example, when the "Start Measurement" icon is clicked, the PMT and LED are turned on and off at the appropriate times automatically and measurements are taken as specified in the respective data input fields. No real-time user intervention is required. Furthermore, the measurement data can be saved either one

measurement run at a time or in measurement run groups at the user's discretion. Header data indicating the experimenter, the LED color, various count time parameters, and the sample type and irradiation level are saved with each measurement. When measurements are saved, they are written to a file named "Reader Output File.txt" in a space-delimited fashion. There is also an empty spreadsheet (Excel™, Microsoft Corporation, One Microsoft Way. Redmond, Washington, 98052-6399, USA, www.microsoft.com) file named "OSL Data Worksheet.xls" that contains a macro that, when activated, reads the reader output file and parses its data into a more readable and formatted spreadsheet structure. This macro also converts the various header data numerical codes, such as operator name code and sample material code, into their easy-to-understand text meanings. After creation of this worksheet, it is saved with an appropriate file name for later analysis. Extensive testing and debugging of the interface software was required in order to arrive at a working version.

The OSL reader control program consists of two main elements: 1) the user interface, which is what the user interacts with to control the reader, and 2) the block diagram, which is the graphical program or code defining how the user interface and the equipment behave. A picture of the user interface is attached as Figure 4.9 and the block diagram is attached as Figure 4.10.

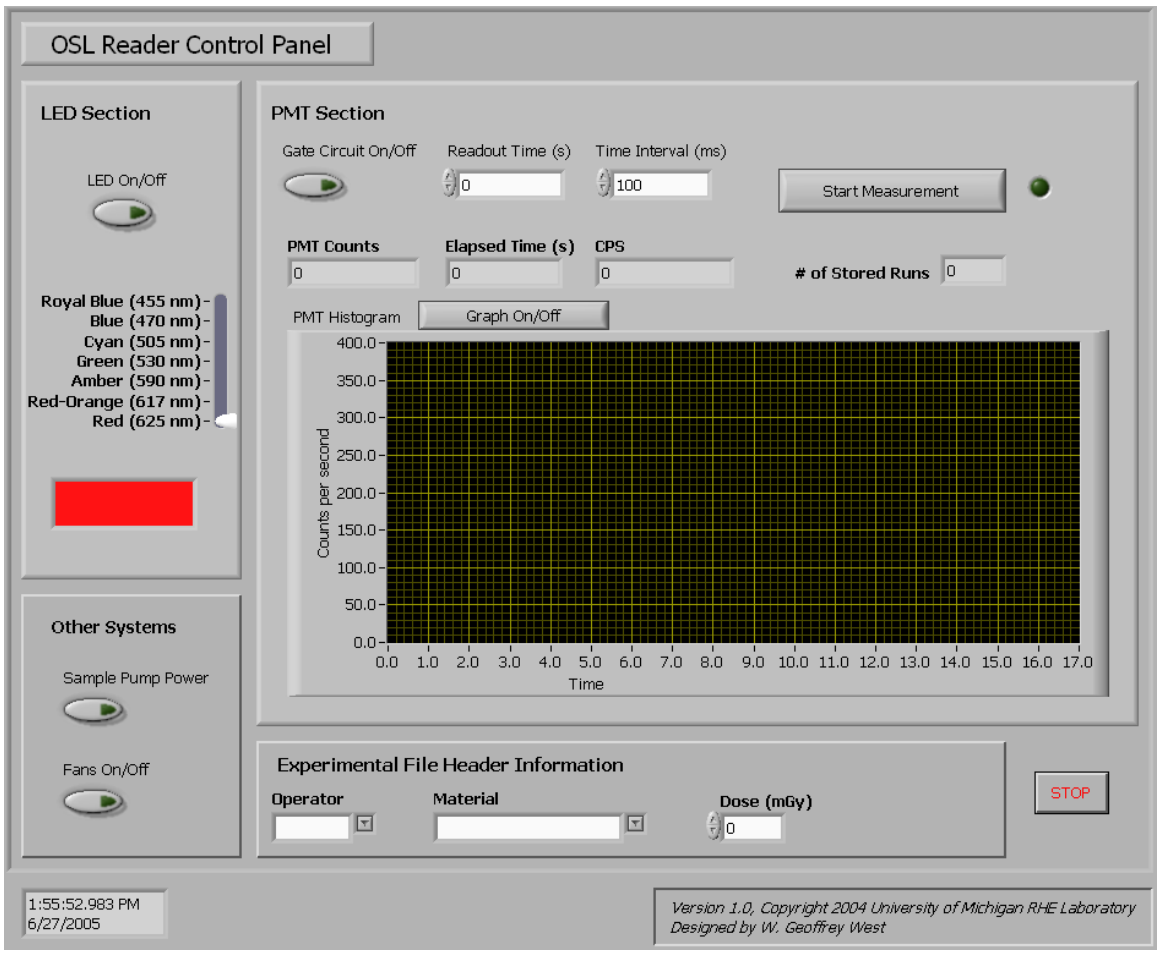

Figure 4.9: Screenshot of the optically stimulated luminescence (OSL) reader software interface.

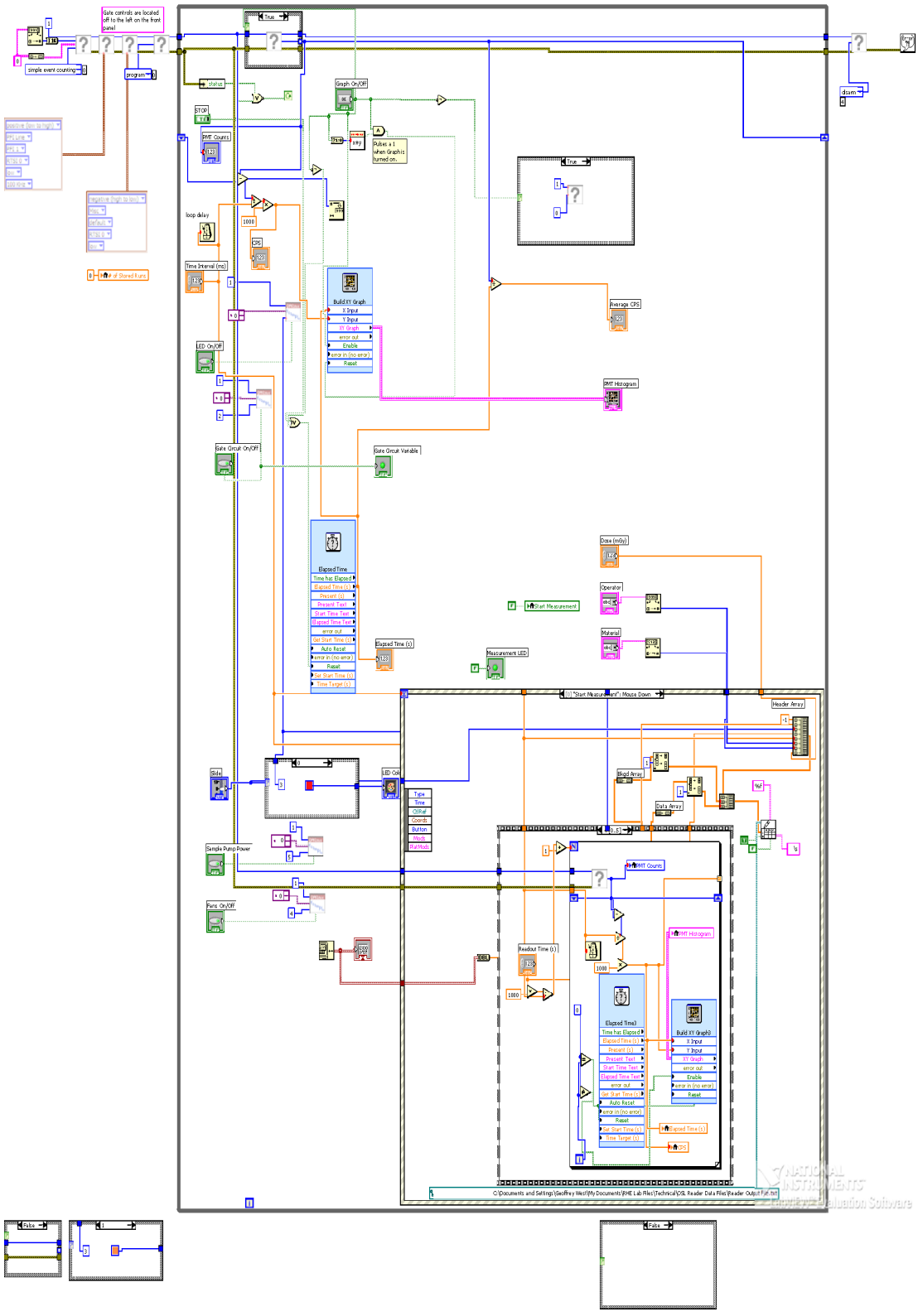

Figure 4.10: Block diagram of the optically stimulated luminescence (OSL) reader software interface.

SETUP AND TESTING

Once design and construction of the OSL reader were complete, testing of the light-tightness of the system was performed, the PMT's operation was validated, and a variety of settings and parameters for optimum operation of the instrument were set. Finally, baseline testing of the reader was performed to determine the reader's performance relative to the commercial alternative. The methodology for accomplishing each of these objectives and the outcome of that methodology is described herein. During this phase of the project, troubleshooting of various electrical and signal problems also occurred. These problems and their solutions will also be described in this section in the interest of helping others to avoid similar time-consuming situations.

Light Leakage Testing

The OSL reader case was first tested for light-tightness by placing a bright, battery-operated light source inside the case while viewing it is a darkened room. This viewing was done after the viewers' eyes had adjusted to complete darkness for 30 min and no light leakage was observed. Once this was done, further testing with bright room lights during PMT operation was performed. Specifically, with the case closed and covered, the PMT count rate was monitored while the room lights were cycled on and off. No impact on PMT count rate was seen.

PMT Performance Testing

Initial testing and setup of the OSL reader PMT consisted of measuring its output signal count rate relative to LED color and on/off status and PMT gate on/off status. For this, the PMT bias voltage was set to a 1,000 V, a safe starting voltage recommended by the manufacturer. Amplifier gain was set to an intermediate value that allowed initial counting to be performed. SCA window settings were set with the lower level above the point where background counts increased noticeably under dark conditions and the upper level was set to its highest point. Once these 'rough' settings were established, the PMT count rate was observed as each LED was powered on and off. Although the emission filters on the OSL reader were selected to filter out light in the visible range, and the PMT photocathode is relatively insensitive at the longer wavelengths of some of the lower-energy LEDs, no filter is 100% effective and the sensitivity of a PMT in photon counting mode is such that some signal does result from each of these very bright sources. The PMT responded positively to light, i.e., the count rate increased significantly when turning on each LED and dropped back to background rates once the LEDs were de-energized.

Once it was verified that the PMT was responding to light, the count rate was observed while the PMT gate circuit was activated and deactivated. The PMT gate circuit seemed to present the reverse type of behavior as expected: when a 5 V TTL signal was applied to the circuit, count rates actually dropped. Further investigation of this behavior showed that the PMT gate circuit was actually de-energizing after 20-30 s of being open, i.e., allowing counts, regardless of the fact that the 5 V control signal

remained on. This de-energization dropped count rates by an order of magnitude or more. In essence, the PMT gate was effective, but closing on its own. Eventually, after consultation with the circuit manufacturer, it was determined that this part actually has two modes of operation: pulsed and DC gating. The circuit had been set up for pulsed operation, but it was exceeding the maximum duty cycle. As such, resistors R2 and R3 were removed and replaced with the proper resistors for DC gating, which successfully allowed constant gate operation. Of course, should very rapid POSL operation be desired in the future, this circuit could be set back to the original mode to reduce the turn-off time from 1.0 ms to 1.2 μs. A diagram of that gating circuit is shown as Figure 4.11.

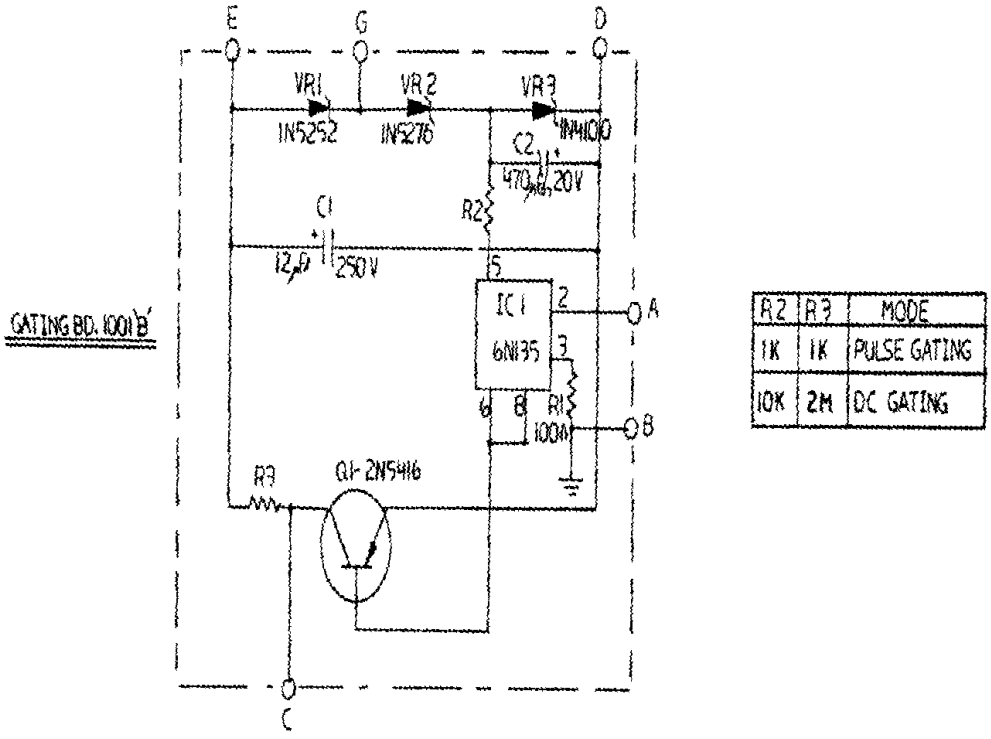

Figure 4.11: Circuit diagram of the photomultiplier tube (PMT) gating circuit. *Figure provided courtesy of ET Enterprises / Electron Tubes.*

Detection Electronics Parameter Optimization

The next step in setting up the OSL reader was to determine the best possible detection electronics chain settings. Specifically, the optimal PMT bias voltage, amplifier settings and SCA window settings needed to be determined.

It is essential in a PMT-based detection instrument to properly bias the PMT for optimal SNR. In order to arrive at this ideal bias voltage, the PMT was first allowed to 'settle' by placement in a completely dark environment, i.e., the light-tight OSL reader case, for over 1 h. This settling process serves to reduce the level of dark counts from the device and thereby maximize the SNR. Dark counts are caused primarily by thermionic emission of electrons from the photocathode and, as such, the temperature of the device will affect this value. In this case, the PMT was expected to be maintained at or near 20 °C during all experiments. Additional contributors to the dark count rate are cosmic radiation and natural radioactivity either in the vicinity of the tube or in the tube itself. None of these contributors depend on device temperature. The settling process reduced the dark counts on the PMT at 1,000 V bias voltage from approximately 200 counts per second (cps) to approximately 70 cps – in line with manufacturer specification.

The initial amplifier settings were a course gain of 100, a fine gain of 2.5, a positive input and unipolar (UNI) output. SCA settings were: normal mode, lower level (LL) of 164, upper level (UL) of 1104 in arbitrary units. These preliminary settings were based upon oscilloscope (Model 434 Storage Oscilloscope, Tektronix, Inc., 14200 SW Karl Braun Drive, P.O. Box 500, Beaverton, OR, 97077, USA, +1 800 833 9200, www.tek.com) viewing during course adjustments while permitting extremely low light

levels into the reader case. Once these preliminary settings were arrived at, the dark count rate settled at approximately 24 cps with the PMT gate open. At this point, a series of tests was begun that involved energizing the blue LED and detecting those few photons that passed through the GG-420 excitation filter and two U-340 emission filters to reach the photocathode; this setup produced a detectable but safe PMT response. The system SNR was then graphed with respect to the SCA LL window setting using the following formula:

$$SNR = \frac{C_L}{\sqrt{C_D}} \tag{6}$$

where C_L is the light count rate in cps and C_D is the dark count rate in cps.

Both light count rates and dark count rates were taken with the PMT gate open. Testing was also conducted using stimulation light at the other available excitation frequencies to confirm the optimal SCA LL window setting as well as to gauge the overall system filtration effectiveness and sensitivity to the excitation sources. The graph showing these results is presented as Figure 4.12. Based on this testing, an ideal SCA setting of 40 was arrived at for this amplifier voltage, producing an SNR of between 380 and 400.

Next, the bias voltage was modulated and SCA window testing was repeated to determine whether modulating the voltage would improve the system SNR. It did not. As such, initially, the PMT will be driven at 1,000 V and the SCA LL set at 40. Setting

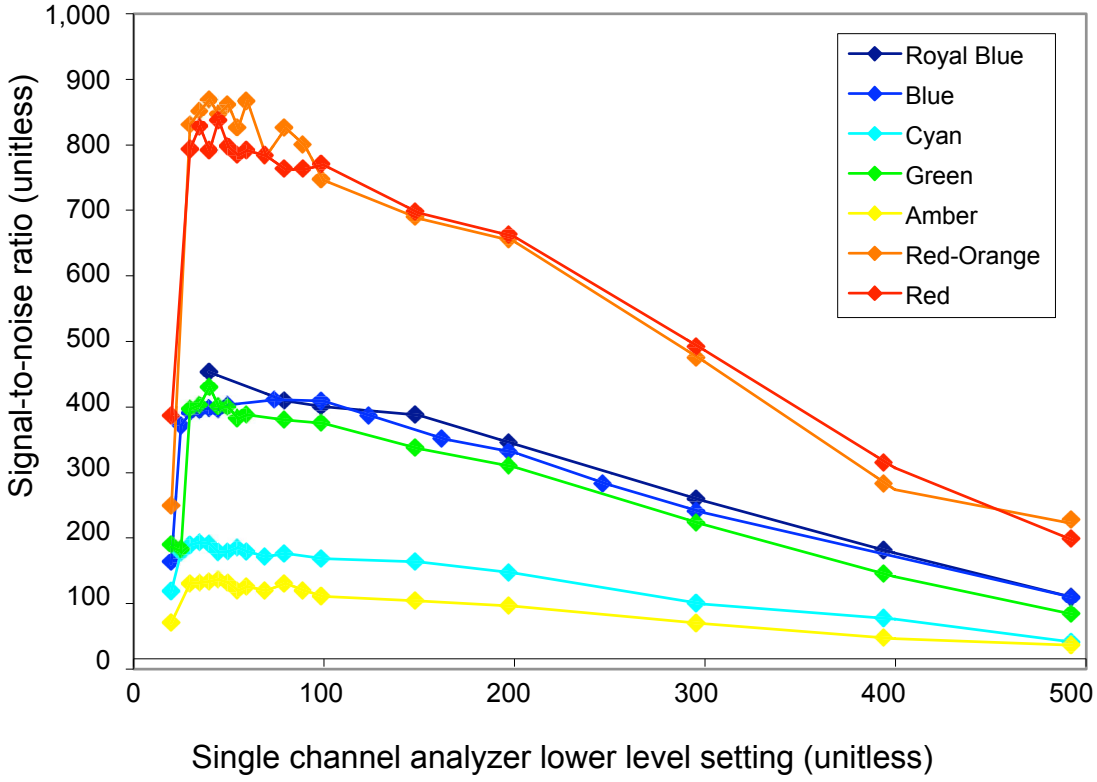

Figure 4.12: Graph showing the results of the single channel analyzer (SCA) setup testing. The signal-to-noise ratio (SNR) is plotted as a function of the SCA lower level setting for all seven light-emitting diode (LED) colors available on the optically stimulated luminescence (OSL) reader.

of the SCA UL window was left at its maximum value of 1104 since this instrument would be used, at least initially, to eliminate the PMT noise floor. Amplifier settings were reviewed as well but found to be sufficient at their initial settings. The only modification to the amplifier setting was to change the pulse profile setting from UNI to bipolar output (BI) during the course of some experiments which exhibited count rate saturation. This change allowed the resolution of higher count rates up to 42,000 cps versus 14,000 cps.

Iris Position Optimization

To maximize system SNR, it is important that the excitation light be focused on the material sample to the maximum extent possible, i.e., the maximum amount of light strikes the sample itself and the minimum amount of light strikes outside the sample. With readers using laser excitation methods, this concern is eliminated due to the inherent spatial coherence of the light beam. However, with an LED light source, even with a collimating lens, the output illumination does not have sharp edges. Therefore, in order to provide additional collimation for the excitation light, an iris was installed between the LED assembly and the sample holder. To determine the optimal aperture setting for this iris, ten 6.35 mm diameter round samples of plastic-laminated α-Al_2O_3:C (Luxel®, Landauer, Inc., 2 Science Road, Glenwood, IL, 60425-1586, USA, custserv@landauer.com, +1 800 323 8830, www.landauer.com) were cut from a single ribbon of material using an office hole punch. This material had accumulated two years of background radiation exposure and presented an OSL signal that was sufficient for testing purposes. Each sample was then 'read out' with the blue LED on the OSL reader, using a slightly different aperture diameter, designated 'iris position 1' through 'iris position 7', with position 1 corresponding to an almost completely closed iris, position 7 corresponding to an almost completely open iris, and positions 2 through 6 corresponding to intermediate settings in between. At each iris setting, the peak OSL count rate was recorded for the background-irradiated sample, as was the peak count rate for an identically-sized 'blank' α-Al_2O_3:C sample that had previously been optically annealed

by prolonged exposure to light from the blue LED. The SNR was calculated at each iris position using the following equation:

$$SNR = \frac{S_B}{\sqrt{S_A}} \tag{7}$$

where S_B is the peak signal from the background dose sample and S_A is the peak signal from the annealed or 'blank' sample.

Plotting of this output data, shown as Figure 4.13, demonstrated that the SNR was maximized at an aperture setting designated 'iris position 2'. As such, the iris was fixed in this position for future experiments.

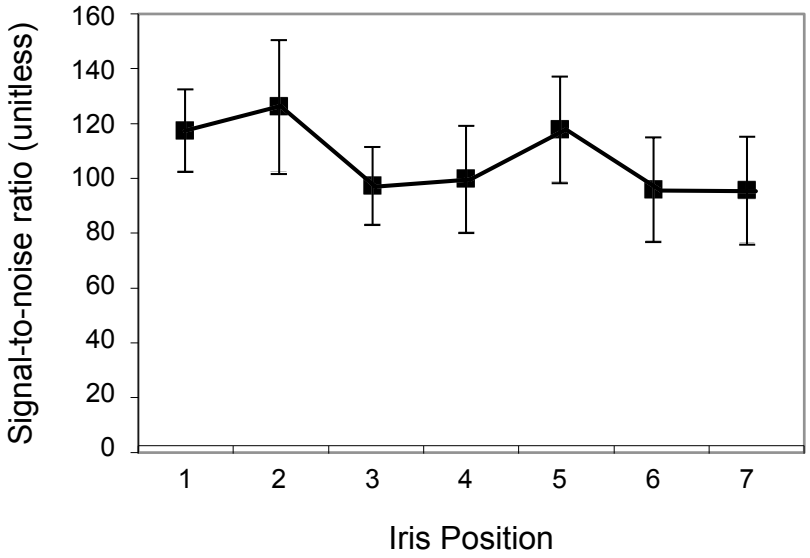

Figure 4.13: Graph showing the results of the iris position optimization testing. The signal-to-noise ratio (SNR) of the optically stimulated luminescence (OSL) peak output signal is plotted as a function of the iris position, with iris position 1 corresponding to an almost completely closed iris, position 7 corresponding to an almost completely open iris, and positions 2 through 6 corresponding to intermediate settings in between. Error bars reflect the aggregate standard deviation due to both counting statistics and sample-to-sample variation in OSL dose sensitivity.

Baseline Data Collection

The final step in the process of OSL reader setup and testing was to irradiate a number of OSL samples to known radiation doses and to then read them out to determine the performance of the reader relative to commercially available apparatus. For this step, commercially available α-Al_2O_3:C was used as the experimental medium, since it is a very well-characterized and efficient OSL material. Eight 6.35 mm diameter round samples of α-Al_2O_3:C were irradiated using a Cs-137 source (Model 28-6B beam calibrator, J. L. Shepherd & Associates, 1010 Arroyo Avenue, San Fernando, CA, 91340-8122, USA, info@jlshepherd.com, +1 818 898 2361, www.jlshepherd.com), four samples to 2.5 mGy and four samples to 5.0 mGy. These samples were then read out using the blue excitation source on the OSL reader. Each readout consisted of a 10 s dark count collection immediately followed by a 50 s continuous-wave OSL (CW-OSL) 'light count', using a sampling interval of 200 ms. The dark count averages were then subtracted from the light counts to produce a graph of the net light counts as a function of time, i.e., the OSL glow curve, shown in Figure 4.14.

RESULTS

The OSL material samples used to set the optimal iris position produced the very first OSL 'glow curves' from the reader. These curves exhibited a roughly exponential decay behavior. The peak signal amplitude was approximately 5,000 – 7,000 cps, while

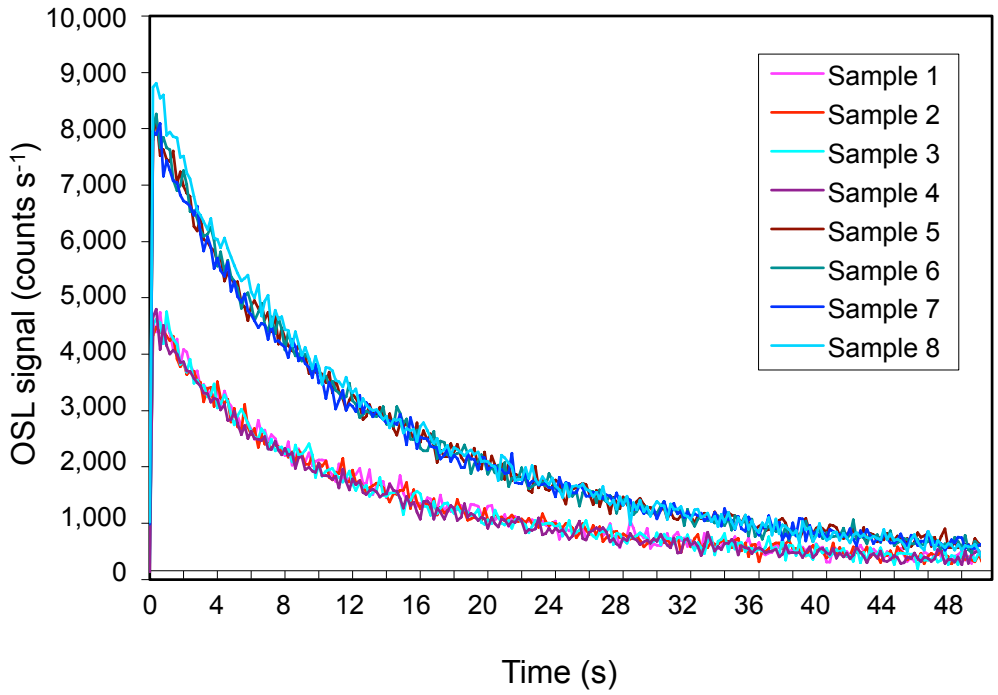

Figure 4.14: Optically stimulated luminescence (OSL) output graph from the OSL reader for samples of Luxel™ irradiated to 250 mGy and 500 mGy using Cs-137 gamma rays. Though error bars are not plotted due to the continuous nature of this data, the average fractional standard deviation is calculated as 1.7%.

the LED source background was approximately 2,500 cps. Therefore, after approximately 1 y of assembly and iterative design, this first result confirmed that the OSL reader was capable of producing meaningful experimental data.

With respect to the glow curves resulting from the final testing phase, these curves exhibit good sample-to-sample consistency, with sample's total OSL output over the readout period varying on average only 1.7% from the mean, as well as good dose-response linearity. That is, the peak OSL signal of the samples irradiated to 5.0 mGy is roughly double the peak OSL signal of the samples irradiated to 2.5 mGy. Specifically,

the height of the OSL peaks is approximately 4,500 cps for the 2.5 mGy sample and 8,250 cps for the 5.0 mGy sample. This equates to a peak height of 1,650-1,800 cps mGy^{-1}. For the sake of comparison, using the commercially available Risø reader, under blue light stimulation, an α-Al_2O_3:C sample irradiated to 15 mGy showed a peak height of roughly 37,500 cps, or 2,500 cps mGy^{-1}, approximately 45% higher than the constructed reader[59]. Even though the excitation light source is significantly more intense than that of the Risø reader, thereby stimulating the production of the OSL signal more quickly, the Risø reader's use of an automated turntable and precision machining and robotics allows for a superior light collection efficiency due to the more favorable excitation light/sample holder/PMT geometry. That increased collection efficiency apparently slightly more than counteracts the decreased excitation source luminance. For this reason, the custom-built OSL reader produces a signal, and a corresponding SNR, similar to but somewhat lower than this commercial reader but certainly at a level fully sufficient for useful OSL research. With additional systematic improvements, discussed in the next section, even greater efficiency should be realized.

Baseline testing was also performed using the other excitation wavelengths and the results of those tests indicated that the reader works reliably and consistently.

POTENTIAL MODIFCATIONS AND FUTURE PLANS

While the constructed OSL reader is capable of performing a great many experiments into the OSL phenomenon, numerous short- and long-term improvements

and enhancements to the design are considered in order to further increase its operational gamut. Short-term modifications anticipated for the reader include:

- Fast transistor-based LED pulsing electronics, to allow for fast pulsed operation of the instrument.
- Software control of the high voltage to the PMT as well as an automatic shutter in front of this component, to allow for faster workflow and greater protection for the PMT. Such a shutter would automatically close at the end of each OSL run, allowing some low-intensity room lights to remain on during sample change-outs subject to sample exposure considerations.
- A sample holder design which allows for greater rotational stability and rotation about a horizontal axis to provide for easier sample change-outs.
- More advanced optics on the excitation side including a lens system to replace the simple collimator/iris arrangement used now. Precision optics would increase the ratio of light impacting the sample versus light impacting the surrounding sample holder, thus improving the signal-to-noise ratio of the measured signal.
- Addition of a tri-alkali PMT to provide for efficient OSL signal detection in the longer visible wavelengths. While the current system does have some sensitivity in these longer wavelengths, a cooled tri-alkali PMT would be more sensitive to this portion of the spectrum.
- Integration of excitation light feedback electronics. LED light output varies to some degree over time due to thermal effects and electronic variations, in spite of the utilization of conditioned power sources and/or constant-current

power supplies. Though baseline or "blank" runs can be performed prior to each experimental OSL readout in order to quantify this time-varying output, a more precise and efficient solution is to integrate an optical sensor into the reader design in such a way that it modulates the LED currents in real time to assure constant luminance. This would eliminate the need for time-consuming blank runs and improve the consistency of experimental results.

Long-term modifications to the reader could include the following:

- Modification of the design to allow for automated sequential reading of multiple samples. The use of a sample wheel or some other loading mechanism to allow for this type of unattended readout would increase the workload of the instrument substantially and allow for more experiments to be carried out in shorter time periods. A software upgrade would be needed as part of this enhancement to allow for programming of unique read-out protocols for individual samples.
- Automated selection of LED color. Creation of an LED assembly which would obviate the need to manually change LEDs and manually designate the correct color on the user interface would allow for quicker experimentation. The OSL reader case would not need to be opened during each LED change and no possibility of marking the OSL output data file with the incorrect LED color would exist. Though various methods were considered during the design phase for implementing this capability, including rotating wheels, fiber light guides, and lens systems, this enhancement has been left to a future upgrade.

- Improved sample holder optics. Construction of an integrating sphere or other reflective case around the sample chamber to direct OSL light to the PMT photocathode would improve the SNR of the system and consequently allow for detection of lower radiation doses on samples.
- Integration of a radiation source into the design. Commercial OSL readers offer the option of irradiating samples in real time using a modest radioactive source at very close range. Integral x-ray generators have also been utilized[60]. This capability allows for greater experimental flexibility and speed since it allows for the detection of radioluminescence as well as OSL and also allows for the detection of OSL signals in traps that quickly decay at room temperature. The current laboratory arrangement and irradiation capabilities at the University of Michigan mean that samples can be read on the OSL reader at approximately 1-2 h post-irradiation at the soonest due to the geographic separation of the irradiation facilities and the OSL laboratory.
- Provision of higher-intensity LEDs or laser-based excitation sources. Since the time of the original design and construction of this reader, newer higher-output LED products have been introduced. Specifically, replacement of the existing LEDs with newer LEDs would increase the typical luminous flux at each existing color by a factor of 2.0-2.5 for the red, red-orange and amber sources, and by a factor of 3.2-5.8 for the green, cyan, blue and royal blue sources[61]. This higher flux would result in faster readouts and higher SNRs. Additionally, should significantly greater monetary resources become available, the replacement of the LED systems with laser-based sources could offer these benefits as well as two

others: 1) multi-wavelength lasers, such as chemical dye lasers, could be utilized to increase the number of color options for excitation, and 2) use of small laser illumination spot sizes would allow for reading of a single sample multiple times or using different excitation wavelengths, thereby eliminating sample-to-sample variability.

- Integration of a more advanced detection system allowing measuring and recording of the OSL material emission spectra. Such systems, employing scanning monochromators[62-63], charge-coupled devices (CCDs)[33, 64] and photodiode arrays[65] have been employed for many years experimentally and would permit a greater range of information to be gleaned from OSL materials.

CONCLUSIONS

The goal of this research and development effort was to design, construct, and test a novel OSL reader that would provide the maximum amount of experimental flexibility in the research of OSL material properties and physical principles. An important challenge during the course of this process was the need to produce such a device within the boundaries of a limited experimental budget far lower than the cost of a commercially-available system. Faced with this challenge, numerous methods were used to reduce costs and increase flexibility, including the use of off-the-shelf optical components; selection of newer higher-power LEDs versus more elaborate light sources such as lasers or broad-spectrum bulbs with monochromators; and integration of design features that allow simple and rapid changing of key system components.

The completed device meets these goals and is able to perform a variety of CW-OSL and POSL experiments. It has subsequently been used for basic research in the area of OSL. While the authors have identified many desired enhancements and improvements for the future, the current design allows the use of more wavelengths of excitation light than current commercial readers, as well as the ability to swap out filters and other components in the midst of an experiment. It is hoped that the information contained in this article will help others to pursue experimentation and exploration in this exciting and worthwhile area of dosimetry research.

ACKNOWLEDGEMENTS

The authors would like to thank the following individuals for their assistance during the design, construction, and testing of the instrument: Mr. Andrew F. Kalchik for his assistance with reader component construction and the production of figures, Dr. David W. Jordan for his assistance with various portions of the electrical work, Michael Reim for his help with the reader case construction, the experts at Electron Tubes for assisting with the comprehension of PMT specifications and circuitry, and the fine folks at LumiLeds Lighting who returned every phone call and fielded many, many questions about optics and lighting.

REFERENCES

1. Bøtter-Jensen, L., McKeever, S. W. S. and Wintle, A. G. Optically stimulated luminescence dosimetry. (Amsterdam, The Netherlands: Elsevier Science B.V.) (2003) ISBN 0444506845.

2. Rao, R. P., de Murcia, M. and Gasiot, J. Optically stimulated luminescence dosimetry. Radiat. Prot. Dosim. 6, 64-66 (1983).

3. Pradhan, A. S. and Ayyangar, K. Radiation dosimetry by photostimulated luminescence of CaSO:Dy. International Journal of Applied Radiation and Isotopes. 28, 534-535 (1977).

4. Henniger, J., Horlbeck, B., Hubner, K., Prokert, K. The evaluation of CaF_2:Mn-polyethylene detectors with the aid of the optically stimulated luminescence (OSL). Nuclear Instruments and Methods. 204, 209-212 (1982).

5. Inabe, K., Miyanaga, T., Takeuchi, N. Optically stimulated luminescence and photoacoustic spectroscopy of NaCl, NaCl:Cu and NaCl:Ca,Cu crystals x-irradiated at room temperature. Journal of Materials Science Letters. 4, 925-927 (1985).

6. Mathur, V. K. G., J.; Abbundi, R.J.; Brown, M.D. Optically stimulated luminescence in MgS:Ce,Sm. Radiat. Prot. Dosim. 17, 333-336 (1986).

7. Pradhan, A. S. Cooled optically stimulated luminsescence of TLDs for radiation dosimetry. Radiat. Prot. Dosim. 29, 213-215 (1989).

8. Allen, P. and McKeever, S. W. S. Studies of PTTL and OSL in TLD-400. Radiat. Prot. Dosim. 33, 19-22 (1990).

9. Miller, S. D. E., G.W.R. Laser-induced optically stimulated m centre luminescence in LiF. Radiat. Prot. Dosim. 33, 59-62 (1990).

10. Miller, S. D. and Eschbach, P. A. Neutron dosimetry using optically stimulated luminescence. (Washington, D.C.: U.S. Department of Energy) (1991).

11. Miller, S. D. High dose dosimetry using optically stimulated luminescence. Radiat. Prot. Dosim. 66, 201-204 (1996).

12. Justus, B. L., Rychnovsky, S., Miller, M.A., Pawlovich, K.J., Huston, A.L Optically stimulated luminescence radiation dosimetry using doped silica glass. Radiat. Prot. Dosim. 74, 151-154 (1997).

13. Akselrod, M. S., Lucas, A. C., Polf, J. C. and McKeever, S. W. S. Optically stimulated luminescence of Al_2O_3. Radiat. Meas. 29, 391-399 (1998).

14. Nanto, H. M., K.; Usuda, T.; Taniguchi, S.; Takeuchi, N. Optically stimulated luminescence in KCl:Eu single crystals. Radiat. Prot. Dosim. 47, 281-284 (1993).

15. Nanto, H., Miyazaki, M., Imai, A., Komori, H., Douguchi, Y., Kusano, E. and Kinbara, A. New photostimulable phosphor materials for digital radiography. (1999).

16. Nanto, H. S., T.; Kashiwagi, N.; Miyazaki, M.; Nasu, S.; Kusano, E. A UV dosemeter utilising photostimulated luminescence in SrS:Eu,Sm phosphor ceramics. Radiat. Prot. Dosim. 85, 305-307 (1999).

17. Nanto, H., Araki, T., Daimon, M., Kusano, E., Kinbara, A., Kawabata, K., Nakano, Y. Optically stimulated luminescence in an imaging plate using BaFl:Eu. Radiat. Prot. Dosim. 100, 385-388 (2002).

18. Kristianpoller, N., Oster, L. Optically stimulated luminescence in anion-defective carbon doped alpha-Al_2O_3 crystals. Radiation Effects and Defects in Solids. 134, 311-313 (1995).

19. Kristianpoller, N., Shmilevich, A., Weiss, D., Chen, R., Khaidukov, N. Study of optical and dosimetric properties of doped fluoride crystals. Optical Materials. 16, 105-110 (2001).

20. Kristianpoller, N., Shmilevich, A., Weiss, D., Chen, R., Khaidukov, N. Luminescence of $LiKyF_5:Pr^{3+}$ crystals. Radiat. Meas. 33, 637-640 (2001).

21. Kristianpoller, N., Weiss, D., Chen, R., Nariyama, N., Khaidukov, N. Luminescence of $CsGd_2F_2$ crystals. Radiat. Prot. Dosim. 100, 207-209 (2002).

22. Hütt, G., Jaek, I. Optically stimulated luminescence materials based on CaS for gamma and fast neutron dosimetry. Radiat. Prot. Dosim. 65, 297-300 (1996).

23. Douguchi, Y., Nanto, H., Sato, T., Imai, A., Nasu, S., Kusano, E., Kinbara, A. Optically stimulated luminescence in Eu-doped KBr phosphor ceramics. Radiat. Prot. Dosim. 84, 143-148 (1999).

24. Bailey, R. M., Adamiec, G. and Rhodes, E. J. OSL properties of NaCl relative to dating and dosimetry. Radiat. Meas. 32, 717-723 (2000).

25. Le Masson, N. J. M. B., A.J.J.; Van Eijk, C.W.E. Optically stimulated luminescence in hydrated magnesium sulfates. Radiat. Meas. 33, 693-697 (2001).

26. Le Masson, N. J. M., Bos, A. J. J., Czapla, Z., Brouwer, J. C. and van Eijk, C. W. E. Fast-neutron OSL sensitivity of thallium-doped ammonium salts. Radiat. Prot. Dosim. 110, 319-323 (2004).

27. Le Masson, N. J. M., Bos, A.J.J., Van Eijk, C.W.E., Furetta, C., Chaminade, J.P. Optically and thermally stimulated luminescence of $KMgF_3:Ce^{3+}$ and $NaMgF_3:Ce^{3+}$. Radiat. Prot. Dosim. 100, 229-234 (2002).

28. Jaek, I., Kerikmae, K., Lust, A. Optically stimulated luminescence of some thermoluminescence detectors as an indicator of absorbed radiation dose. Radiat. Prot. Dosim. 100, 459-462 (2002).

29. Bøtter-Jensen, L., Markey, B. G. and Agersnap Larsen, N. Retrospective radiation dosimetry using optically stimulated luminescence on natural and synthetic materials. (Horn, Austria: Berger) (1996).

30. Stoneham, D., Bailiff, I. K., Petrov, S., Botter-Jensen, L., Goeksu, Y. and Jungner, H. Retrospective dosimetry: The development of an experimental methodology using luminescence techniques. (Luxembourg, Luxembourg) (1996).

31. Bøtter-Jensen, L. and McKeever, S. W. S. Optically stimulated luminescence dosimetry using natural and synthetic materials. Radiat. Prot. Dosim. 65, 273-280 (1996).

32. Banerjee, D., Boetter-Jensen, L. and Murray, A. S. Retrospective dosimetry: Estimation of the dose to quartz using the single-aliquot regenerative-dose protocol. Applied Radiation and Isotopes. 52, 831-844 (2000).

33. Kanemaki, M., Ninagawa, K., Yamamoto, I., Nakagawa, M., Wada, T., Yamashita, Y. and Endo, K. Red thermoluminescence of volcanic glass fractions from tephras. International Journal of Radiation Applications and Instrumentation. Part D. Nuclear Tracks and Radiation Measurements. 18, 81-88 (1991).

34. Bøtter-Jensen, L., Jungner, H. and Mejdahl, V. Recent developments of OSL techniques for dating quartz and feldspars. Radiation Protection Dosimetry (UK). 47, 643-648 (1993).

35. Banerjee, D. Optical stimulated luminescence (OSL) dating. (Lucas Heights, Australia: Australian Institute of Nuclear Science and Engineering) (1999).

36. Huett, G. and Jaek, I. Advances in the luminescence dating: The optically stimulated luminescence based procedures and their physical background. Proceedings of the Estonian Academy of Sciences: Geology. 50, 214-232 (2001).

37. Stokes, S. and Fattahi, M. Red emission luminescence from quartz and feldspar for dating applications: An overview. Radiat. Meas. 37, 383-395 (2003).

38. Singarayer, J. S. and Bailey, R. M. Component-resolved bleaching spectra of quartz optically stimulated luminescence: Preliminary results and implications for dating. Radiat. Meas. 38, 111-118 (2004).

39. Smith, B. W., Aitken, M. J., Rhodes, E. J., Robinson, P. D. and Geldard, D. M. Optical dating: Methodological aspects. Radiat. Prot. Dosim. 17, 229-233 (1986).

40. Aitken, M. J. and Smith, B. W. Optical dating: Recuperation after bleaching. Quaternary Science Reviews. 7, 387-393 (1988).

41. Mejdahl, V. and Christiansen, H. H. Procedures used for luminescence dating of sediments. Quaternary Science Reviews. 13, 403-406 (1994).

42. Bøtter-Jensen, L. Development of optically stimulated luminescence techniques using natural minerals and ceramics, and their application to retrospective dosimetry. Risø-R-1211(EN). Roskilde, Denmark. (2000).

43. Inrig, E. L., Godfrey-Smith, D. I. and Khanna, S. Optically stimulated luminescence of electronic components for forensic, retrospective, and accident dosimetry. Radiat. Meas. 43, 726-730.

44. Bailiff, I. K. The use of ceramics for retrospective dosimetry in the Chernobyl exclusion zone. Radiat. Meas. 24, 507-511 (1995).

45. Hashimoto, T., Hong, D. G. and Takano, M. Retrospective dosimetry at JCO using luminescence from ceramics pieces and quartz grains. Advances in ESR Applications. 18, 197-202 (2002).

46. Markey, B. G., Bøtter-Jensen, L., Poolton, N. R. J., Christiansen, H. E. and Willumsen, F. A new sensitive system for measurement of thermally and optically stimulated luminescence. Radiat. Prot. Dosim. 66, 413-418 (1996).

47. Markey, B. G., Bøtter-Jensen, L. and Duller, G. A. T. A new flexible system for measuring thermally and optically stimulated luminescence. Radiat. Meas. 27, 83-89 (1997).

48. Bøtter-Jensen, L., Andersen, C. E., Duller, G. A. T. and Murray, A. S. Developments in radiation, stimulation and observation facilities in luminescence measurements. Radiat. Meas. 37, 535-541 (2003).

49. Bortolot, V. J. A new modular high capacity OSL reader system. Radiat. Meas. 32, 751-757 (2000).

50. Ford, R. M. and Hanify, R. D. A desktop OSL system for on-site dosimeter processing. Glenwood, IL. (2003).

51. (ELSEC), L. S. Old products. (Dorset, United Kingdom: Littlemore Scientific (ELSEC)) (2009).

52. Gaza, R. and McKeever, S. W. S. A real-time, high-resolution optical fibre dosemeter based on optically stimulated luminescence (OSL) of KBr:Eu, for potential use during the radiotherapy of cancer. Radiat. Prot. Dosim. 120, 14-19 (2006).

53. Schilles, T., Lang, A., Habermann, J. and Riser, U. Improved single aliquot dating applications using a new highly efficient modular luminescence reader. Radiat. Prot. Dosim. 84, 363-366 (1999).

54. Smetana, F., Hajek, M., Bergmann, R., Brusl, H., Fugger, M., Gratzl, W., Kitz, E. and Vana, N. A portable multi-purpose OSL reader for UV dosimetry at workplaces. Radiat. Meas. 43, 516-519 (2008).

55. Bøtter-Jensen, L., Mejdahl, V. and Murray, A. S. New light on OSL. Quaternary Geochronology. 18, 303-309 (1999).

56. Luxeon V Star technical data sheets. DS-30. Philips LumiLeds, San Jose, CA. (2004).

57. Specifications for Nichia blue LED model NSPB500S. STSE-CB2123B.

58. Thermal design considerations for Luxeon 5 watt power light sources. AB23. San Jose, CA. (2002).

59. West, W. G., Kearfott, K. J. and Bernal, S. M. The sunlight OSL response of a commercially available α- Al_2O_3:C personnel dosimetry material. Radiat. Prot. Dosim. 119, 344-349 (2006).

60. Andersen, C. E., Bøtter-Jensen, L. and Murray, A. S. A mini x-ray generator as an alternative to a $^{90}Sr/^{90}Y$ beta source in luminescence dating. Radiat. Meas. 37, 557-561 (2003).

61. Luxeon Rebel color technical datasheet. Philips LumiLeds, (2010).

62. Bøtter-Jensen, L., Poolton, N. R. J., Willumsen, F. and Christiansen, H. A compact design for monochromatic OSL measurements in the wavelength range 380-1020 nm. Radiat. Meas. 23, 519-522 (1994).

63. Crittenden, G. C., Townsend, P. D., Gilkes, J. and Wintersgill, M. C. LiF dosimetry: II. The effects of Mg and Ti on the thermoluminescent emission spectra of LiF. J. Phys. D Appl. Phys. 7(1974).

64. Rhodes, M. W., Wanwilairat, S., Vilaithong, T. and Hoffman, W. Low cost high resolution thermoluminescence spectrometer. Review of Scientific Instruments. 71, 2053-2057 (2000).

65. Piters, T. M., Meulemans, W. H. and Bos, A. J. J. An automated research facility for measuring thermoluminescence emission spectra using an optical multichannel analyzer. Review of Scientific Instruments. 64, 109-117 (1993).

CHAPTER 5

OSL Investigation of KBr, $CaSO_4$:Tm, $CaSO_4$:Dy, $CaSO_4$:Dy+P, LiF:Mg,Cu,Na,Si and LiF:Mg,Cu,Si

ABSTRACT

Optically stimulated luminescence (OSL) dosimetry involves the illumination of an irradiated sample of an appropriate material to produce a stimulated emission of light whose intensity is indicative of the radiation dose. This technique is currently used for personnel dosimetry, environmental dosimetry and geologic dating applications. A great deal of published research has focused on α-Al_2O_3:C, the predominant personnel dosimetry material, and natural materials used for geologic dating, while relatively little published data are available on the OSL properties of other materials with known thermoluminescent (TL) properties that may also exhibit OSL. As such, an experiment was conducted on the following materials to identify and characterize their OSL behavior: KBr, $CaSO_4$:Tm, $CaSO_4$:Dy, $CaSO_4$:Dy+P, LiF:Mg,Cu,Na,Si and LiF:Mg,Cu,Si. Specifically, OSL signals from each material were measured in response to seven excitation wavelengths from 625 nm to 455 nm, at twelve time periods post-irradiation from 6 h to 120 d. The magnitude and fading behaviors of the OSL response of each material were then analyzed and results documented. Based on these

results, it was determined that a significant OSL response exists for $CaSO_4$:Tm, LiF:Mg,Cu,Na,Si and LiF:Mg,Cu,Si. In addition, it was found that the fading rates of OSL signals over time depends upon the excitation wavelength used to elicit the signals, and that these fading rates and the excitation wavelengths that correspond to them correlate well with the TL behavior of the materials.

INTRODUCTION

Optically stimulated luminescence (OSL) dosimetry relies upon the illumination of an irradiated sample with light to produce a stimulated emission of light proportional to the radiation dose which previously caused trapping of electrons in the material[1]. OSL has become an accepted personnel dosimetry method during the past 15 y, as evidenced by the success of a commercially-available dosimeter based upon anion-defective, carbon-doped aluminum oxide, or α-Al_2O_3:C (Luxel®, Landauer, Inc., 2 Science Road, Glenwood, Illinois, 60425-1586, USA, custserv@landauer.com, +1 800 323 8830, www.landauer.com). The use of OSL dosimeters versus other choices, such as thermoluminescent dosimeters (TLDs) or film-based dosimeters, is attractive for a number of technical reasons, including: 1) the current material of choice for this application, α-Al_2O_3:C, is highly sensitive, in that it emits a large amount of stimulated luminescence per unit of radiation dose absorbed[2-8]; 2) the optical readout method is fast and relatively simple[5, 9]; and 3) the OSL technique lends itself to repeat readout of samples, since unlike thermal stimulation as used in TLDs, optical stimulation can be activated and deactivated very quickly, allowing fast readout of the dose information

without a significant depopulation of the dosimetric traps[10]. An additional reason that α-Al_2O_3:C in particular was chosen as a dosimetry material for widespread use is the fact that it exhibits very little fading at room temperature over time, meaning that the accurate estimation of dose is not affected to a large degree by the amount of time elapsed between annealing of the dosimeter and readout[7, 11]. Though OSL dosimeters are frequently susceptible to light-induced fading[12-14], maintaining the material in a light-tight container during use does not present a significant problem in most applications.

In addition to its application in the area of personnel dosimetry, the OSL phenomenon is widely used in the dating of geologic samples[4, 15-23] and has been investigated and used for a variety of other applications, including remote dosimetry[24], retrospective dosimetry[15, 25-28] and medical dosimetry[29-31]. In most of these applications, the material employed is either α-Al_2O_3:C or a natural material such as quartz (SiO_2) or feldspar ($KAlSi_3O_8$, $NaAlSi_3O_8$, or $CaAl_2Si_2O_8$).

Because of the substantial utility of α-Al_2O_3:C, and the prevalence of OSL techniques in geologic dating, a great deal of published research has focused on α-Al_2O_3:C and natural materials, while relatively little published data is available on the OSL properties of other conventional TL materials that may also exhibit OSL. As such, an experiment was conducted to investigate the dose sensitivity and fading behavior of numerous materials that may be of interest, for various reasons, as OSL dosimetry materials. The experiment also seeks to correlate the OSL responses of the materials with their TL response in order to draws some conclusions about their underlying

physical processes. The materials chosen were KBr, $CaSO_4$:Tm, $CaSO_4$:Dy, $CaSO_4$:Dy+P, LiF:Mg,Cu,Na,Si and LiF:Mg,Cu,Si.

In the case of KBr, while this substance has been investigated to a limited degree as an OSL material when doped with europium[31-33], no published research to date has focused on the un-doped material. This substance was originally being considered as a binding agent to produce pressed samples of other materials for OSL experimentation by the authors, but was found to exhibit its own OSL response when blank samples were tested. This experiment will be the first to investigate this material in this manner. In the case of $CaSO_4$:Tm, in spite of its use in commercially-available TLD products, and the presence of substantial published TL data[34-38], no published research exists documenting its OSL properties. However, this material has shown promise as an OSL dosimetry material in recent experiments by the authors[39]. $CaSO_4$:Dy, also a commercially-utilized TL phosphor, has been the focus of substantial TL research[34, 36, 38, 40-44]. Additionally, the material's optically stimulated afterglow (OSA), which is a form of delayed OSL (DOSL), was the subject of one basic experiment, which also investigated its fading properties to a limited degree[45]. A later study examined the OSL response of the material to light of wavelengths of 266 nm and 532 nm and also looked at the fading of this signal from 4 min to 30 min post-irradiation[36]. Finally, a recent study[37] reported on this material's photoluminescence (PL) and photo-transferred thermoluminescence (PTTL) properties, and based on the results, noted the potential for OSL, but did not perform OSL experiments directly. $CaSO_4$:Dy+P, also known as KCT-300, was recently developed by the Korean Atomic Energy Research Institute (KAERI) and mixes $CaSO_4$:Dy with a phosphorus binder to produce a higher-sensitivity

TL phosphor. This material has been investigated using TL techniques[46-48], but not OSL techniques. LiF:Mg,Cu,Na,Si and LiF:Mg,Cu,Si, also known as KLT-300 and New-KLT-300 respectively, were developed at KAERI and have been explored extensively as highly promising TL materials [49-77] but this experiment is the first to investigate their OSL properties.

In order to explore the OSL properties of the candidate materials, a custom-built OSL reader was utilized which could stimulate samples with seven different excitation frequencies. The design, construction and testing of this reader are described elsewhere[78]. The response of each material using the different excitation wavelengths was examined at numerous time periods from 6 h post-irradiation to 120 d post-irradiation. As such, both the magnitude of the OSL response and its fading behavior as a function of excitation energy are determined. By analyzing this fading behavior, it is hoped that it will be shown that the different frequencies of excitation light selectively or preferentially read out different traps in the materials. In so doing, in addition to the primary goal of providing information on the OSL properties of the various materials, a secondary goal could be realized of exploring a method of studying the component elements of aggregated fading behaviors in an OSL material. Finally, TL analysis was performed in parallel for each material at each time period to allow a comparison of the OSL and TL results. A discussion of the theory, methods and results of this experiment follows.

THEORY

Both TL and OSL dosimetry are possible because certain crystalline materials, when exposed to ionizing radiation, trap the resulting freed, i.e. delocalized, electrons and holes at defect sites within the material. The more radiation that the material is exposed to, the more electrons and holes get trapped at these defect, or 'trap', sites. After irradiation, either immediately or at some later time, the material is either heated, in the case of TL, or exposed to light, in the case of OSL. The heating or light exposure excites the electrons in the material, causing the trapped electrons and holes to be freed and, in some cases, they then de-excite in a manner that is accompanied by the release of a photon.

In TL dosimetry, when the irradiated material is heated, the reader produces a 'glow curve', which is simply a graph showing light output and temperature versus time. One or more glow peaks are present on this curve, though in many cases, the peaks become superimposed on one another, leading to the need to deconcolve the curve to see the underlying constituent peaks. It is known that lower-temperature glow peaks in TLD represent lower-energy trapping states and that the fading rate of these peaks is directly related to their energy level, or temperature as it were. Thus, a very low-temperature peak, representing an energy level just below the conduction band of the material, typically fades very quickly at a given temperature, while a higher-temperature peak tends to fade more slowly at the same given temperature. The peak fading half-lives can be estimated by appropriately solving the relevant and well-known first-order model equations[79-80].

To determine the peak half-life, the following equation is used[79]:

$$\tau_{1/2} = \ln(2) \times \tau_f \quad (1)$$

where $\tau_{1/2}$ is the peak half-life and τ_f is the peak mean life, both in units of s. To determine the peak mean life, one uses the following equation[80]:

$$\tau_f = s^{-1} \times \exp(E_t/kT) \quad (2)$$

where s is the attempt-to-escape frequency factor in units of s^{-1}, E_t is the average activation energy, or trap depth, of the peak in units of eV, k is Boltzmann's constant, 8.62×10^{-5} eV K^{-1}, and T is the ambient temperature at which fading is assumed to occur in units of K. This last value is set to 293 K, or 20 °C, in this instance.

The following relation[80] is used to estimate E_t:

$$E_t \approx 25kT_m \quad (4)$$

where k is Boltzmann's constant, 8.62×10^{-5} eV K^{-1}, and T_m is the temperature of the peak at its maximum in unit of K. It is noted that this relation is an approximation which is most accurate when s is $\sim 10^8$ s^{-1}, a typical value for many phosphors. While this value varies somewhat from material to material, it remains a useful starting approximation.

The following equation for s provides an additional relationship linking these variables[79]:

$$s = \beta E / (kT_m^2)(\exp(-E_t/kT_m) \quad (3)$$

where β is the heating rate in units of K s^{-1}, or °C s^{-1}, and is set at 2.5 K s^{-1} to correspond to the heating rate used to establish the $E \approx 25kT_m$ relation, k is Boltzmann's constant, 8.62×10^{-5} eV-K^{-1}, and T_m is the temperature of the peak at its maximum in unit of K.

Solving these equations with the above assumptions and simplifying to express peak half-life in terms of the peak maximum temperature, one arrives at the expression:

$$\tau_{1/2} = (1.54 \times 10^{-13}\ [\text{s K}^{-1}]) \times T_m\ [\text{K}] \times \exp(25T_m\ [\text{K}] / 293\ [\text{K}]) \quad (5)$$

It should be noted that the half-lives calculated above should be considered as estimates only. It has been shown that some materials, such as LiF:Mg,Ti, exhibit fading rates that are significantly different than predicted using this type of first-order method[81]. In addition, it has also been shown that the fading behavior of various materials is affected by the time elapsed between annealing and irradiation[82].

To some extent, low-temperature peaks are confounding elements if the goal is to assure the stability of a dosimeter's dose reading over time. Since glow curves frequently exhibit peaks at different energy levels overlapping each other, the goal in conventional TLD dosimetry is frequently to accurately subtract the contribution of these

low-temperature peaks to assure a time-insensitive dose estimate. However, some research has been performed in the interest of using the fading behaviors of low-temperature peaks as a means to extract time-since-irradiation information from a dosimeter. The theory and methods required to produce such a dosimeter using TLD technology have been discussed to some degree in the literature[42, 83-92].

In OSL, the various trapping states are not accessed by thermal mechanisms, but rather optically. If one uses an excitation light source with enough energy per photon to excite an electron out of a trap, one may then get an emitted, and frequently higher-energy, light output. The excitation light photon energy must at least equal the optical activation energy of the trap. This optical activation energy can be determined using the following equation[1]:

$$E_o = E_t + E_{ph}, \tag{6}$$

where E_o is the optical activation energy of the trap, E_t is the thermal trap depth and E_{ph} is the phonon energy. To determine the phonon energy, the following equation[1] is used:

$$E_{ph} = S\hbar\omega_p \tag{7}$$

where S is the Huang-Rhys factor and ω_p is the phonon vibration frequency.

Each defect in an OSL material will possess a photo-ionization cross section, $\sigma(h\upsilon, E_o)$, that determines the probability of whether a photon of energy $h\upsilon$ will be

absorbed and result in OSL. Depending on the mathematical model used, there are a number of different theorized shapes for this cross section, none of which are a perfect edge, i.e. zero probability of OSL below a photon energy of E_o and maximum probability above[1]. Generally speaking, however, as the excitation light frequency rises, deeper populated traps will begin to produce an OSL signal. Some of the photo-ionization models predict that after the excitation light frequency is raised beyond a certain point, the photo-ionization cross section for a trap will begin to decrease again[93]. Other models predict that it will remain high[94]. In either case, what is important is that by changing the frequency of the excitation light, it should be possible to poll different traps in the material which exhibit different fading rates. Some investigators have proposed a method to separate different components of a quartz OSL signal that could be used for such an application, the stated purpose in their case being to remove the fading signal for more accurate dose estimation[95]. Their proposed method of scanning the excitation light source from long wavelengths to short wavelengths to separate fast and slow components in quartz could, in theory, also be used to selectively scan the relative electron populations of the various fading and non-fading traps in a dosimetry material. This method would provide a greater degree of information regarding the underlying physical processes occurring in the material than would excitation by a single broadband or narrowband light source. Tunable lasers, scanning monochromators, or an appropriate selection of single-frequency light sources may be used for such a purpose.

MATERIAL SAMPLES

Samples of the following six materials were used in this experiment: KBr, $CaSO_4$:Tm, $CaSO_4$:Dy, $CaSO_4$:Dy+P, LiF:Mg,Cu,Na,Si, and LiF:Mg,Cu,Si. The KBr samples consisted of high-purity, spectroscopic-grade powder from a commercial laboratory supply house. One hundred $CaSO_4$:Tm samples were obtained from commercially-available TLD badges (UD-802AQ, Panasonic Industrial Company, 3 Panasonic Way, 7E-6, Secaucus, NJ, 07094, USA, radiationmeasurement@us.panasonic.com, +1 201 348 2517, www.panasonic.com). These samples were in the form of small crystal grains, which were carefully removed from their badge backings. The 25 $CaSO_4$:Dy samples (Thermo Fisher Scientific Inc., 81 Wyman Street, Waltham, MA, 02454, USA, +1 781 622 1000, www.thermoscientific.com), 10 $CaSO_4$:Dy+P samples, 25 LiF:Mg,Cu,Na,Si and 25 LiF:Mg,Cu,Si samples (KAERI, Daeduk-Daero 1045, Dukjin-Dong, Yuseong-Gu, Daejeon, South Korea, +82 42 868 2000, www.kaeri.re.kr) were also in the form of small individual pressed crystalline samples.

All samples, excluding the KBr powder, were washed with ethyl alcohol to remove any potentially fluorescent contaminants before use.

METHODS

All of the samples were annealed prior to packaging and irradiation according to standard heating regimes. Specifically, the KBr powder was heated to 500 ºC for 30 min,

the $CaSO_4$:Tm chips were heated to 350 ºC for 30 min, and the $CaSO_4$:Dy and $CaSO_4$:Dy+P chips were heated to 300 ºC for 30 min. The LiF:Mg,Cu,Na,Si and LiF:Mg,Cu,Si samples were heated to 300 ºC for 1 h. After annealing, material samples were moved to their light-tight irradiation packaging under low-intensity red light, i.e. darkroom conditions, to avoid any possibility of low-energy defect ionizations in the samples.

The material samples were placed into flat, clear plastic sample holders, each with 100 sample locations arranged in a 10 x 10 grid. The 100 $CaSO_4$:Tm chips occupied one sample holder, the 10 $CaSO_4$:Dy+P and 25 $CaSO_4$:Dy chips were placed into another, and the 25 LiF:Mg,Cu,Na,Si and 25 LiF:Mg,Cu,Si chips were placed into a third. The KBr powder was placed in a thin plastic petri dish and, using a metal spoon, pressed into an ~0.25 cm thick layer with consistent thickness across the dish to ensure even irradiation throughout the material. These sample holders were then wrapped in many layers of black plastic to eliminate light ingress.

The irradiation of all samples was performed 1 d after annealing using an under-table fluoroscopy system (Advantx, GE Healthcare, 3000 North Grandview Blvd., Waukesha, WI, 53188, USA, +1 800 886 0815, www.gehealthcare.com). A dose to the samples of 500 mGy was produced by irradiation at a kVp setting of 120 and a tube current of 1.0 mA. A calibrated x-ray survey meter (Mult-O-Meter, Unfors Instruments AB, Uggledalsvägen 29, SE-427 40, Billdal, Sweden, info@unfors.se, +46 31 719 97 00, www.unfors.com) was used to measure the dose rate at this technique at the sample location, which was the tabletop in this case, and it was determined that a 15-min irradiation would result in a 500 mGy dose in air at the sample location. Due to the slight

variation in dose rate along the x-ray tube axis due to the heel effect, the irradiation was divided into two equal periods and the sample holders were rotated 180 degrees between those periods in order to ensure the proper dose to all the samples. Additionally, after irradiation, the KBr powder was mixed thoroughly to ensure that any self-shielding of even this small thickness in the x-ray beam would not affect inter-sample consistency.

Sample readouts were performed over the course of the 120 d post-irradiation. The OSL and TLD readouts were always performed concurrently and, except in the case of $CaSO_4$:Dy+P, were taken at the following elapsed times after irradiation: 0.25, 0.5, 1, 2, 3, 5, 10, 20, 30, 45, 60, and 120 d. Due to limited sample availability, $CaSO_4$:Dy+P was read out at only the 0.25, 1, 3, 10 and 60 d intervals. While waiting for readout, samples were kept in the dark at a stable temperature of 21ºC in an incubator. No radiation shielding was necessary since potential background dose is far less than the irradiation dose.

OSL readouts were performed using a custom-built OSL reader utilizing light emitting diode (LED)-based excitation and a photomultiplier tube (PMT)-based detection systems. Specifically, this reader utilizes LEDs of seven different colors for its excitation subsystem: red, red-orange, amber, green, cyan, blue and royal blue red, red-orange and amber units, and 5W green, cyan, blue and royal blue units (respectively, Luxeon™ Star Part Nos. LXHL-MD1D, LXHL-MH1D, LXHL-ML1D, LXHL-LM5C, LXHL-LE5C, LXHL-LB5C, LXHL-LR5C, Philips Lumileds Lighting Company, 370 West Trimble Road, San Jose, California, 95131, USA, info@lumileds.com, +1 408 964 2900, www.philipslumileds.com). These colors correspond to center wavelengths of 625, 617, 590, 530, 505, 470 and 455 nm, respectively. The excitation light passes through a single

GG420 high-pass filter (Part No. 03FCG059, CVI Melles Griot, 200 Dorado Place SE, Albuquerque, NM 87123, USA, optics@cvimellesgriot.com, +1 505 296 9541, www.cvimellesgriot.com) to remove excitation wavelengths below 420 nm before striking the sample. The detection subsystem of this OSL/TL reader consists of a low-background bi-alkali photomultiplier tube with a quartz window (Model 9235QA with B2F/RFI housing, ADIT Electron Tubes, 300 Crane Street, Sweetwater, Texas, 79556, USA, sales@electrontubes.com, +1 325 235 1418, www.electrontubes.com), operated in photon counting mode. Two U-340 filters (U340, Hoya Filters, 2-7-5, Naka-Ochiai, Shinjuku-ku, Tokyo, 161-8525, Japan, +813 39521151, www.hoyafilter.com) placed in series are employed to filter the emission spectrum and these filters transmit a light bandwidth centered at 340 nm, with a full width at half maximum (FWHM) value of approximately 80 nm. For additional technical information regarding the specifications of this system, the reader is referred to a separate paper regarding its development and construction[78]. Crystal samples were placed directly on the reader sample holder. For the KBr powder, a small metal disc was coated with medical adhesive and approximately 15 mg of KBr powder was adhered to its surface. It was confirmed in prior experiments that this adhesive exhibited no optically- or thermally-stimulated luminescence. Each sample was read out first using the red LED and then immediately thereafter with each progressively shorter wavelength color.

Before and after each OSL readout, blank runs were performed. That is, a readout with no sample in the sample holder was performed at each excitation wavelength. These blank runs were used during the data analysis phase to cancel out any excitation light output changes and PMT sensitivity changes over time, such as may be caused by

temperature fluctuations or electrical variations. Additionally, zero-dose samples of each material were also read out, along with their own blank runs. These zero-dose samples were used to correct the OSL outputs for the particular reflectivity and absorption of each material type at each excitation wavelength. By normalizing each dosed sample readout using a ratio of blank run counts at sample readout time versus zero-dose readout time, and then subtracting the zero-dose outputs, corrected OSL output curves were produced that more closely reflect the true incremental light output due to irradiation of the material.

All OSL readouts consisted of a 10-s dark count, followed by a 60-s continuous-wave OSL (CW-OSL) light count. The sampling interval was set at 0.2 s. For the LiF:Mg,Cu,Na,Si and LiF:Mg,Cu,Si samples, afterglow readings were also collected for up to 60 s after the excitation light was de-energized.

TLD readouts were performed using an automated TL reader (Harshaw 4500, Thermo Fisher Scientific Inc., 81 Wyman Street, Waltham, MA, 02454, USA, +1 781 622 1000, www.thermoscientific.com) in planchet heating mode. Crystal and powder samples were placed directly on the TLD reader heating planchet. For the KBr powder, an analytical balance was used to weigh out 20 mg of powder for each readout and the planchet was carefully cleaned with alcohol after each use. Prior to each sample readout, PMT noise and reference light readouts were collected. Additionally, zero-dose glow curves were produced for each material. These data were used to normalize resultant glow curves and subtract out any potential light output not resulting from irradiation.

TLD readouts were all 60 s in duration with a heating rate of 10 ºC s^{-1}. The starting temperature was 20 ºC and the ending temperature depended on the material:

400 ºC for KBr, 350 ºC for $CaSO_4$:Tm, 300 ºC for $CaSO_4$:Dy, $CaSO_4$:Dy+P;,LiF:Mg,Cu,Na,Si, and LiF:Mg,Cu,Si. The sampling interval was 0.3 s.

The results of both the OSL and TLD readouts were processed and presented by the respective reader software programs. Those raw data files were converted into spreadsheet (Excel™, Microsoft Corporation, One Microsoft Way. Redmond, Washington, 98052-6399, USA, www.microsoft.com) data files for further analysis and display. The results of these experiments are described below.

RESULTS

For each OSL sample readout, including the zero dose readouts, the raw PMT data was plotted on a single graph with seven lines, each representing a different excitation color. The first step in the analysis of this raw data was to normalize the data to compensate for changes in LED output and PMT sensitivity and to subtract the zero dose OSL signal from the sample signals for times 1 through 12. In addition, for $CaSO_4$:Tm, where there were four OSL samples per time period available, those four signals were averaged. This last operation improved the counting statistics for this material and reduced the effect of any inter-sample variability. Specifically, by using four samples instead of one, the standard deviation of the OSL signal as a percentage of the mean, i.e., the fractional standard deviation, drops by a factor of two. This extra step would have been done for the other materials had supplies of those substances permitted. The above mathematical corrections resulted in corrected OSL curves: one per material per time period. The authors have chosen not to show all of the raw and corrected OSL

curves due to their number but these curves were analyzed visually to look for trends and to assess generalized behavior for each material prior to the production of a secondary analysis.

In addition to curves showing the emission of OSL from each material at each time period and for each excitation wavelength, curves were also produced from the afterglow readouts of LiF:Mg,Cu,Na,Si and LiF:Mg,Cu,Si.

The secondary analysis of the OSL data involved the production of graphs to allow better visualization of the fading behavior of each material as a function of excitation wavelength. Specifically, four values were calculated and plotted from each corrected OSL curve to characterize the shape and intensity of the curve: corrected average signal (CAS), corrected peak signal (CPS), peak-to-end ratio (P/E) and peak-to-end difference (P-E). These values were calculated as follows: CAS is the average of the corrected signal over the 60-s OSL readout. It is a measure of the OSL curve average signal. CPS is the total counts from the first 1 s of corrected OSL output signal after excitation light turn-on. It is a measure of the OSL curve peak signal. P/E is the average signal from the first 1 s of corrected OSL output signal *divided* by the average signal from the last 2 s of corrected output signal. It is a measure of the OSL curve peak signal divided by the end signal. P-E is the average signal from the first 1 s of corrected OSL output signal *minus* the average signal from the last 2 s of corrected output signal. It is a measure of the OSL curve peak signal minus the end signal.

By graphing and studying these secondary values, one can begin to understand the OSL behavior of these materials. The secondary graphs reveal at least some OSL signal for all of the materials with the exception of CaSO4:Dy+P. Additionally, these graphs, to

varying degrees, suggest that the different wavelengths of excitation light are selectively stimulating different traps in the materials. As such, in those cases described below, tertiary graphs were developed showing the ratios of the CAS, CPS, P/E, and/or P-E values for different excitation lights over time. These tertiary graphs permit visualization and quantification of the degree to which increased excitation light frequencies result in OSL from selectively deeper traps with less fading over time.

Finally, TLD curves were produced for each material at each time period and those TLD curves are presented to support the discussion of OSL results from each material. The results obtained are now described in detail for each material.

KBr

Figure 5.1 shows the corrected OSL curves for KBr at the first readout, 6 h post-irradiation. Several aspects of this graph are important: 1) both the red and green excitation lights exhibit a detectable OSL signal, 2) no other excitation lights exhibit a detectable OSL signal, and 3) the magnitude of the OSL signals is low with respect to the noise floor. OSL curves at subsequent time periods exhibit reduced OSL signals at both excitation frequencies and little to no evident OSL signal can be seen past 5 d post-irradiation. Since the magnitudes of the OSL peaks in question are low, the CAS parameter does not reveal useful information for this material. However, a graph of the CPS is presented as Figure 5.2 and shows the height of the peaks relative to the time since irradiation. This graph shows the rapid decay of the OSL signal from the red

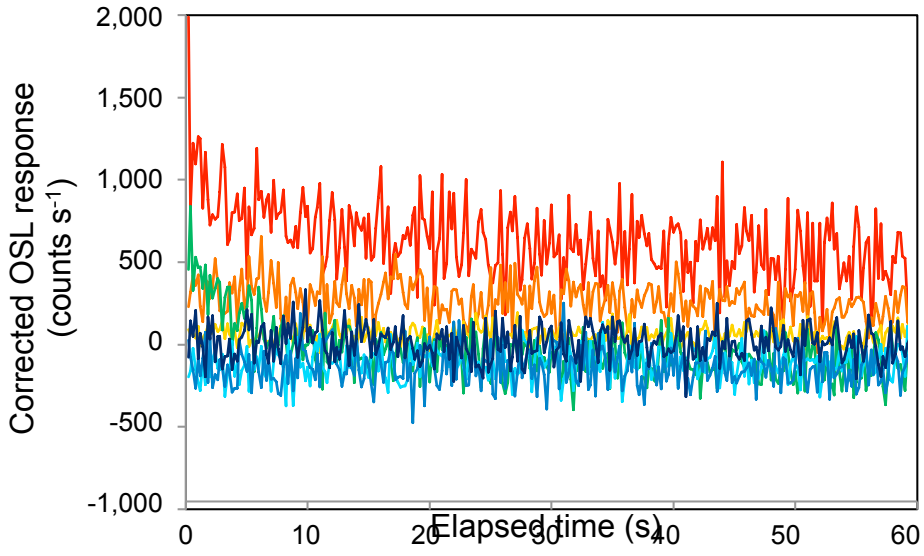

Figure 5.1: Corrected optically stimulated luminescence (OSL) curves for KBr irradiated to 500 mGy dose in air using 120 kVp x-rays, at 6 h post-irradiation. The color of each curve corresponds to the excitation light color: red (λ = 625 nm), red-orange (λ = 617 nm), amber (λ = 590 nm), green (λ = 530 nm), cyan (λ = 505 nm), blue (λ = 470 nm), and royal blue (λ = 455 nm).

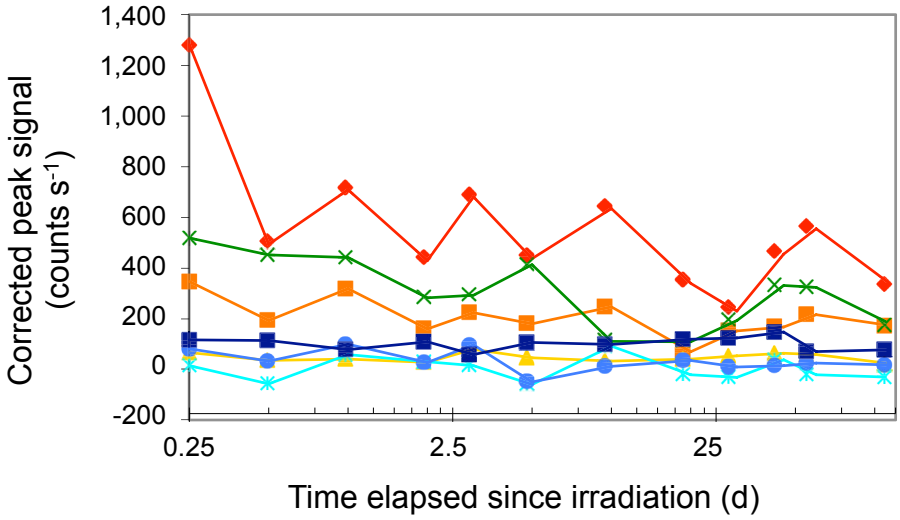

Figure 5.2: Corrected peak signal (CPS) curves for KBr irradiated to 500 mGy dose in air using 120 kVp x-rays. Each data point represents the peak optically stimulated luminescence (OSL) output signal height at a given time since irradiation. The color of each curve corresponds to the excitation light color: red (λ = 625 nm), red-orange (λ = 617 nm), amber (λ = 590 nm), green (λ = 530 nm), cyan (λ = 505 nm), blue (λ = 470 nm), and royal blue (λ = 455 nm).

excitation light, as well as what appears to be a somewhat slower decay of the OSL signal from the green excitation light. Another way to visualize this trend is by looking at the P-E graph for this material, shown as Figure 5.3.

Since at least two excitation light sources exhibited a detectable OSL signal in this material, a tertiary graph was used to compare those two signals, presented as Figure 5.4. Finally, a graph showing the KBr TLD glow curves for each time since irradiation is presented as Figure 5.5. The TL glow curve exhibits one main peak at ~255 ºC, as well as at least two minor peaks at ~115 ºC and ~170 ºC. The significance of these graphs, as well as similar graphs for the other materials tested, will be explored further below.

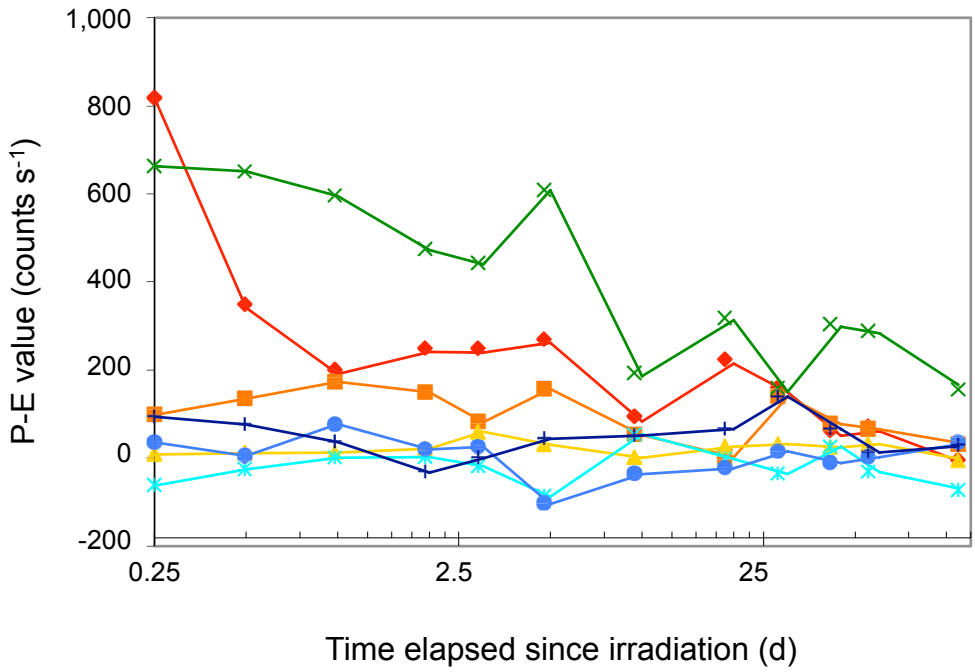

Figure 5.3: Peak signal minus end signal (P-E) curves for KBr irradiated to 500 mGy dose in air using 120 kVp x-rays. Each data point is the calculated difference between the optically stimulated luminescence (OSL) output signal at the beginning of a 60 s readout and the OSL output signal at the end of the readout. The color of each curve corresponds to the excitation light color: red (λ = 625 nm), red-orange (λ = 617 nm), amber (λ = 590 nm), green (λ = 530 nm), cyan (λ = 505 nm), blue (λ = 470 nm), and royal blue (λ = 455 nm).

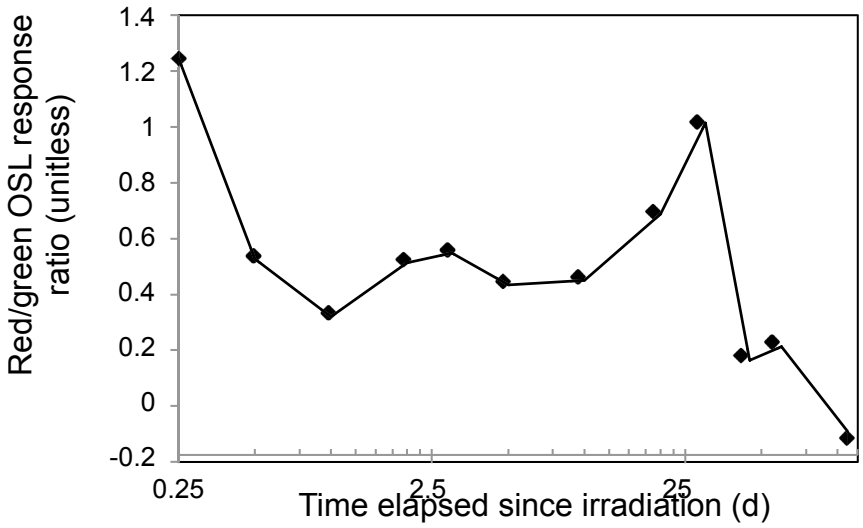

Figure 5.4: Ratio of peak optically stimulated luminescence (OSL) signal minus end signal (P-E) values for KBr under red light excitation (λ = 625 nm) versus green light excitation (λ = 530 nm). Each P-E value is the calculated difference between the optically stimulated luminescence (OSL) output signal at the beginning of a 60 s readout and the OSL output signal at the end of the readout. The KBr was irradiated to 500 mGy dose in air using 120 kVp x-rays.

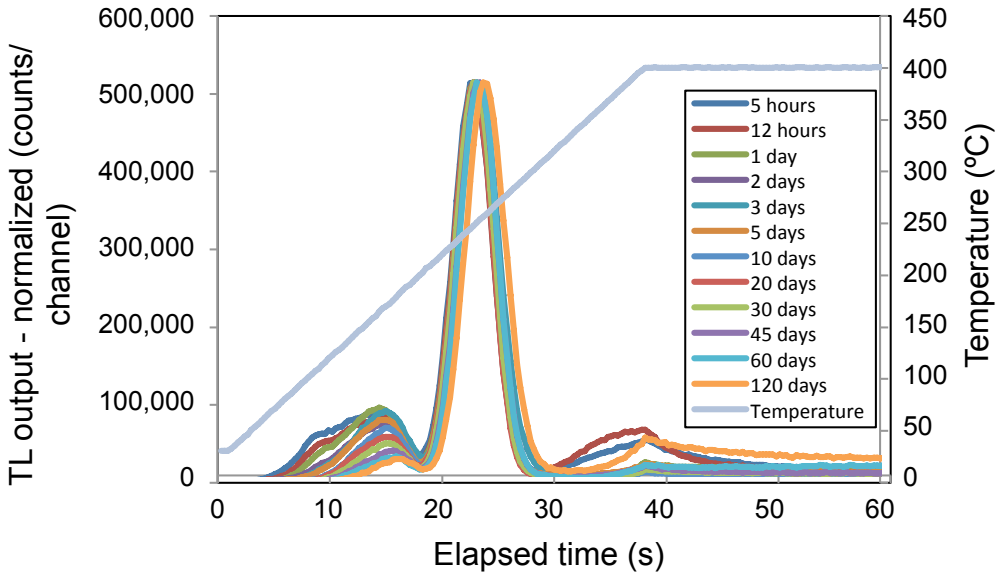

Figure 5.5: Thermoluminescence (TL) glow curves for KBr powder irradiated to 500 mGy dose in air using 120 kVp x-rays. Each colored line represents a TL readout at a different time after irradiation. The curve has been normalized to constant main peak height to eliminate differences due to sample size.

$CaSO_4$:Tm

Figure 5.6 shows the corrected OSL curves for $CaSO_4$:Tm at 6 h post-irradiation. In contrast to the KBr curves, the $CaSO_4$:Tm OSL signal is of far greater magnitude, exhibits with all excitation lights at wavelengths of 530 nm or less, and shows less decay during the readout period. This behavior is indicative of a high trap population relative to the photo-ionization cross section for the trap, as described by other authors[96].

Figures 5.7 and 5.8 show the CAS and CPS curves, and their similarity is a reflection that the OSL signal peak heights are roughly proportional to the average signal heights, indicating that a single trap is being accessed or that multiple traps with similar photo-ionization cross sections are being accessed. Unlike KBr, where the OSL signal

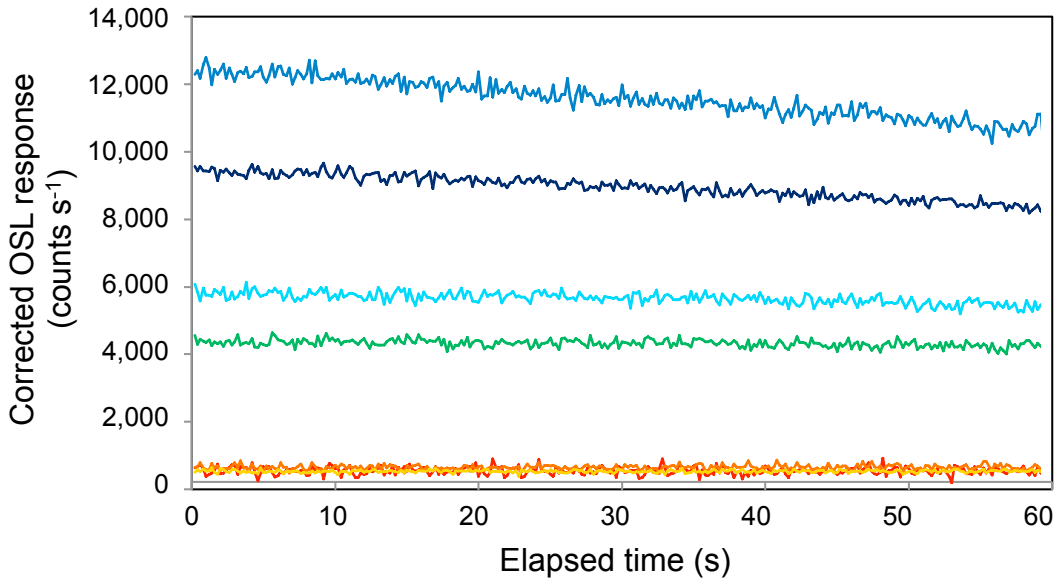

Figure 5.6: Corrected optically stimulated luminescence (OSL) curves for $CaSO_4$:Tm irradiated to 500 mGy dose in air using 120 kVp x-rays, at 6 hours post-irradiation. The color of each curve corresponds to the excitation light color: red (λ = 625 nm), red-orange (λ = 617 nm), amber (λ = 590 nm), green (λ = 530 nm), cyan (λ = 505 nm), blue (λ = 470 nm), and royal blue (λ = 455 nm).

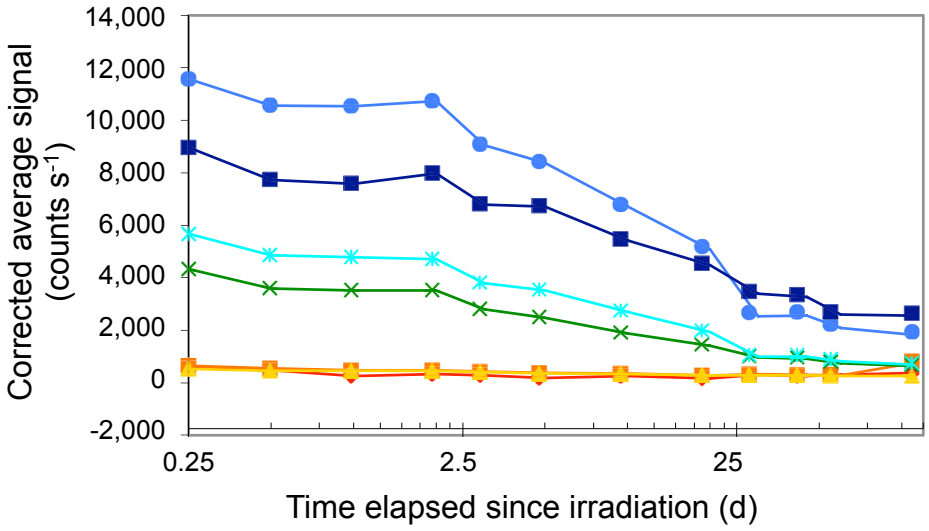

Figure 5.7: Corrected average signal (CAS) curves for $CaSO_4$:Tm irradiated to 500 mGy dose in air using 120 kVp x-rays. Each data point represents the average optically stimulated luminescence (OSL) output signal height at a given time since irradiation. The color of each curve corresponds to the excitation light color: red (λ = 625 nm), red-orange (λ = 617 nm), amber (λ = 590 nm), green (λ = 530 nm), cyan (λ = 505 nm), blue (λ = 470 nm), and royal blue (λ = 455 nm).

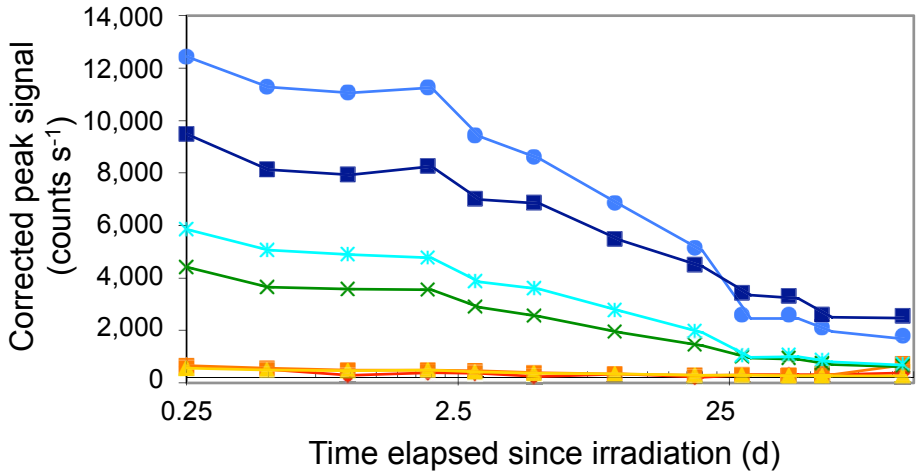

Figure 5.8: Corrected peak signal (CPS) curves for $CaSO_4$:Tm irradiated to 500 mGy dose in air using 120 kVp x-rays. Each data point represents the peak optically stimulated luminescence (OSL) output signal height at a given time since irradiation. The color of each curve corresponds to the excitation light color: red (λ = 625 nm), red-orange (λ = 617 nm), amber (λ = 590 nm), green (λ = 530 nm), cyan (λ = 505 nm), blue (λ = 470 nm), and royal blue (λ = 455 nm).

decayed quickly and much or all of the OSL signal was depleted by the readout, in the case of $CaSO_4$:Tm, there are no pronounced peaks with exponentially-decaying shapes, at least not within the time frame of the readout. Additionally, because of the much higher OSL sensitivity of this material relative to KBr and the concomitantly higher SNR, elaborate data subtraction and correction, in the form of P/E and P-E ratios, are not necessary to analyze the OSL response of this material. As such, Figure 5.9 simply shows the ratios of the green, cyan, and blue CAS values to the royal blue CAS value. This curve shows a reduction in all three ratios with elapsed time. The $CaSO_4$:Tm TLD glow curves for each time since irradiation are presented as Figure 5.10. The glow curves show a major peak at ~275 °C and a minor peak at ~145 °C.

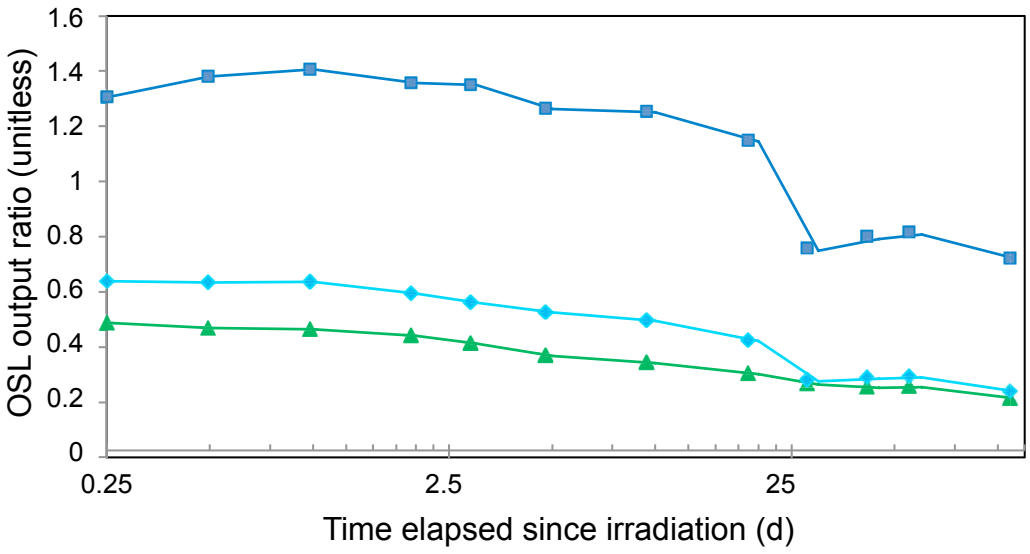

Figure 5.9: Corrected average signal (CAS) output ratios for $CaSO_4$:Tm irradiated to 500 mGy dose in air using 120 kVp x-rays, as a function of time elapsed since irradiation. Each line plots the ratio of the CAS value under the corresponding excitation light, i.e. green, cyan and blue, to the CAS value under royal blue excitation. The CAS value represents the average optically stimulated luminescence (OSL) output signal height at a given time since irradiation.

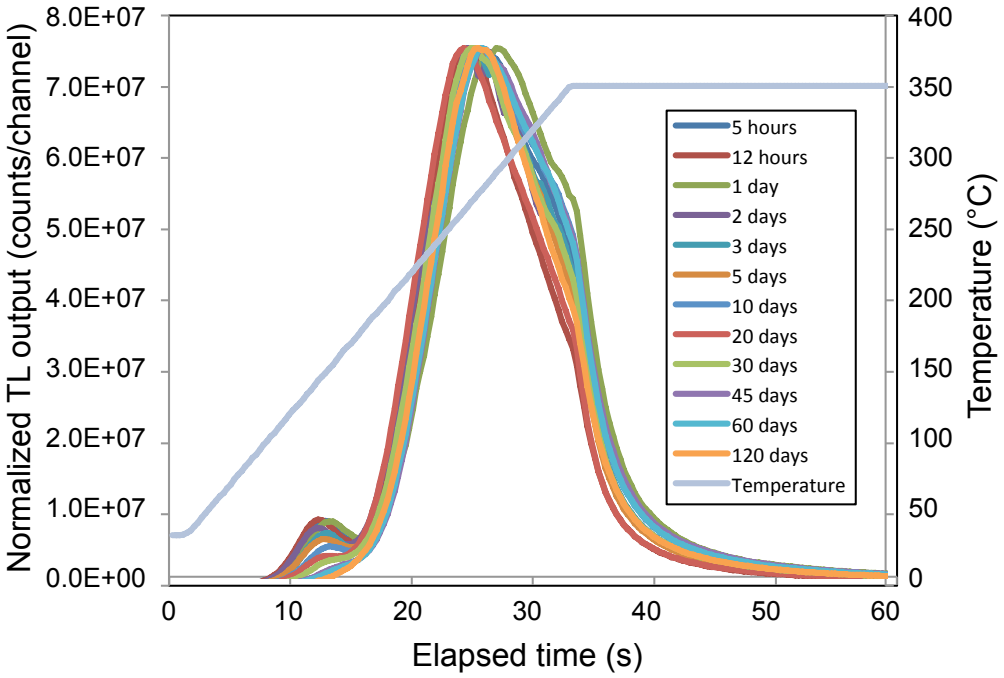

Figure 5.10: Thermoluminescence (TL) glow curves for $CaSO_4$:Tm irradiated to 500 mGy dose in air using 120 kVp x-rays. Each colored line represents a TL readout at a different time after irradiation. The curve has been normalized to constant main peak height to eliminate differences due to sample size.

$CaSO_4$:Dy (TLD-900)

Figure 5.11 shows the corrected OSL curves for $CaSO_4$:Dy at 6 h post-irradiation. The graph shows very little OSL response, just a slightly elevated above noise blue and royal blue line. Review of additional OSL output curves at subsequent time periods show very similar results. Figure 5.12 shows the P-E curve for this material, demonstrating a possible decaying OSL signal with blue light excitation with an approximate half-life on

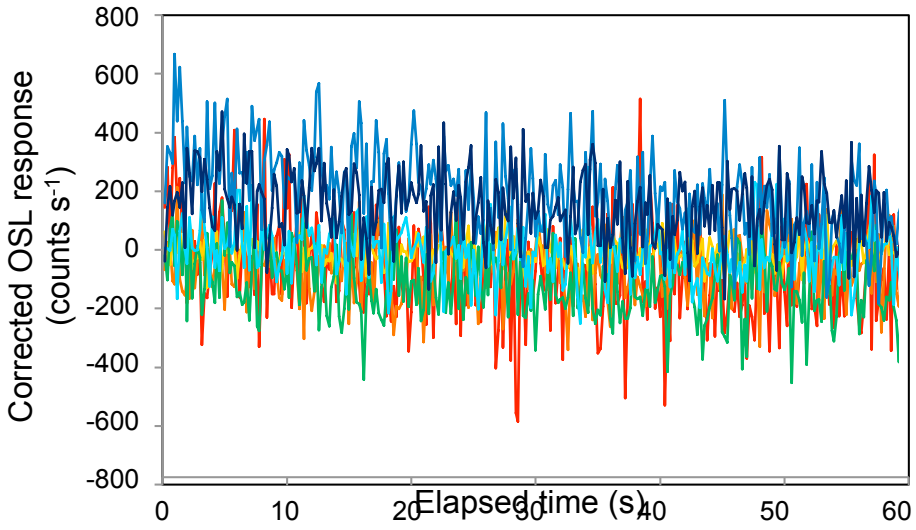

Figure 5.11: Corrected optically stimulated luminescence (OSL) curves for $CaSO_4$:Dy irradiated to 500 mGy dose in air using 120 kVp x-rays, at 6 hours post-irradiation. The color of each curve corresponds to the excitation light color: red (λ = 625 nm), red-orange (λ = 617 nm), amber (λ = 590 nm), green (λ = 530 nm), cyan (λ = 505 nm), blue (λ = 470 nm), and royal blue (λ = 455 nm).

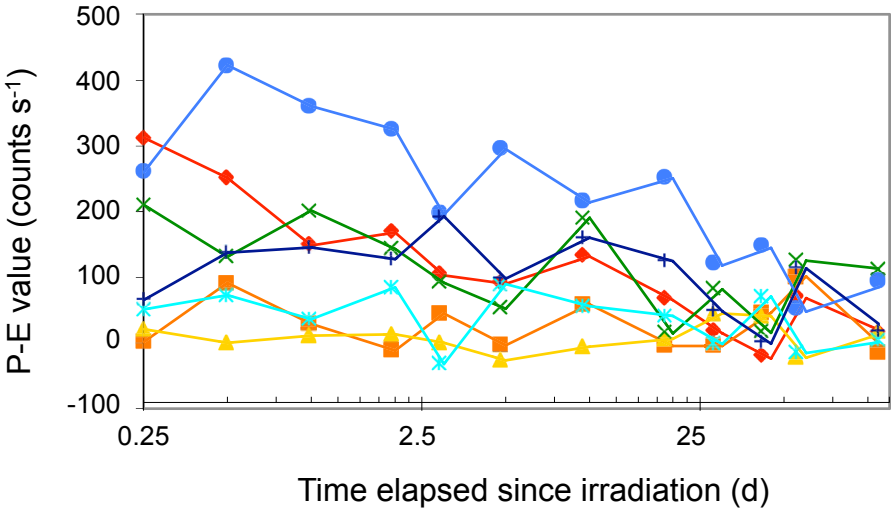

Figure 5.12: Peak signal minus end signal (P-E) curves for $CaSO_4$:Dy irradiated to 500 mGy dose in air using 120 kVp x-rays. Each data point is the calculated difference between the optically stimulated luminescence (OSL) output signal at the beginning of a 60 s readout and the OSL output signal at the end of the readout. The color of each curve corresponds to the excitation light color: red (λ = 625 nm), red-orange (λ = 617 nm), amber (λ = 590 nm), green (λ = 530 nm), cyan (λ = 505 nm), blue (λ = 470 nm), and royal blue (λ = 455 nm).

the order of 10 d. Unfortunately, the OSL signals for this material are below the level at which any meaningful statistical conclusions may be drawn about temporal behavior. As such, no other secondary or tertiary graphs are presented. The $CaSO_4$:Dy TLD glow curves for a selection of times since irradiation are presented as Figure 5.13. These curves show a major peak at ~270 °C and a minor peak at ~160 °C.

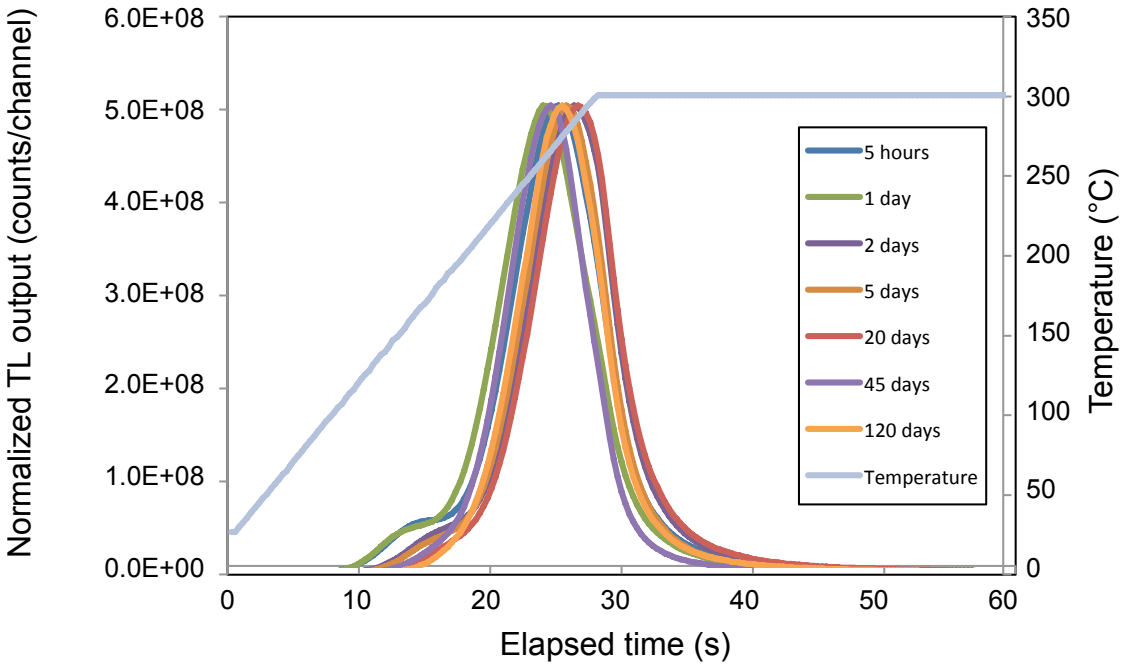

Figure 5.13: Thermoluminescence (TL) glow curves for $CaSO_4$:Dy irradiated to 500 mGy dose in air using 120 kVp x-rays. Each colored line represents a TL readout at a different time after irradiation (some intermediate time periods have been removed in the interest of readability). The curve has been normalized to constant main peak height to eliminate differences due to sample size.

$CaSO_4$:Dy+P

Figure 5.14 shows the corrected OSL curves for $CaSO_4$:Dy+P at 6 h post-irradiation. This graph shows no OSL response whatsoever, at any excitation frequency. Corrected OSL curves at subsequent time periods also show no OSL response. Figure 5.15 shows the TLD glow curves for each time since irradiation for $CaSO_4$:Dy+P.

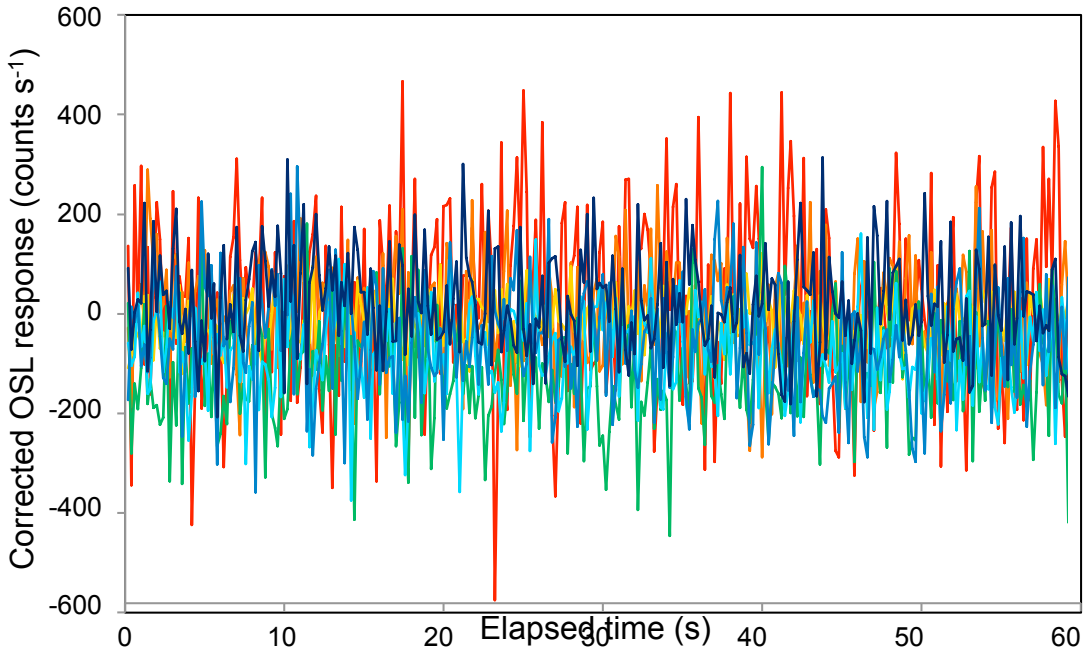

Figure 5.14: Corrected optically stimulated luminescence (OSL) curves for $CaSO_4$:Dy+P irradiated to 500 mGy dose in air using 120 kVp x-rays, at 6 hours post-irradiation. The color of each curve corresponds to the excitation light color: red (λ = 625 nm), red-orange (λ = 617 nm), amber (λ = 590 nm), green (λ = 530 nm), cyan (λ = 505 nm), blue (λ = 470 nm), and royal blue (λ = 455 nm).

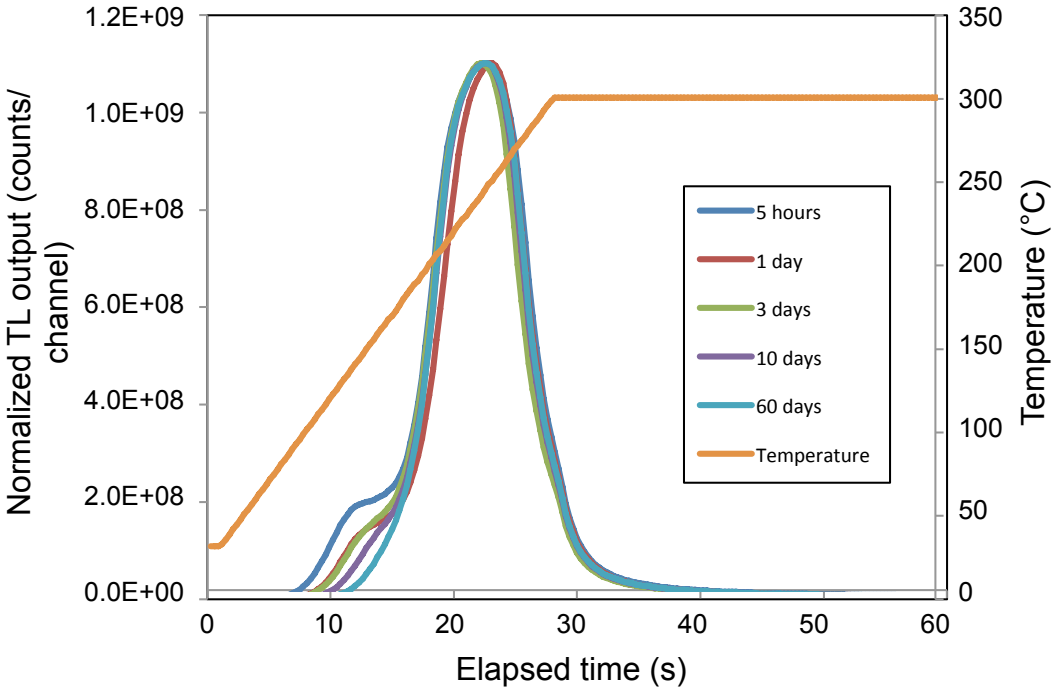

Figure 5.15: Thermoluminescence (TL) glow curves for $CaSO_4$:Dy+P irradiated to 500 mGy dose in air using 120 kVp x-rays. Each colored line represents a TL readout at a different time after irradiation. The curve has been normalized to constant main peak height to eliminate differences due to sample size.

LiF:Mg,Cu,Na,Si (KLT-300)

Figure 5.16 shows the corrected OSL curves for LiF:Mg,Cu,Na,Si at 6 h post-irradiation. An evident OSL signal is produced under stimulation from the green, cyan, blue and royal blue excitation lights. No OSL signal is seen with the red, red-orange or amber excitation lights. Like $CaSO_4$:Tm, the signals, especially those produced by the green and cyan excitation light, decay slowly during the readout period. Additionally, the magnitude of the OSL signals from this material are of the same order of magnitude as those of $CaSO_4$:Tm.

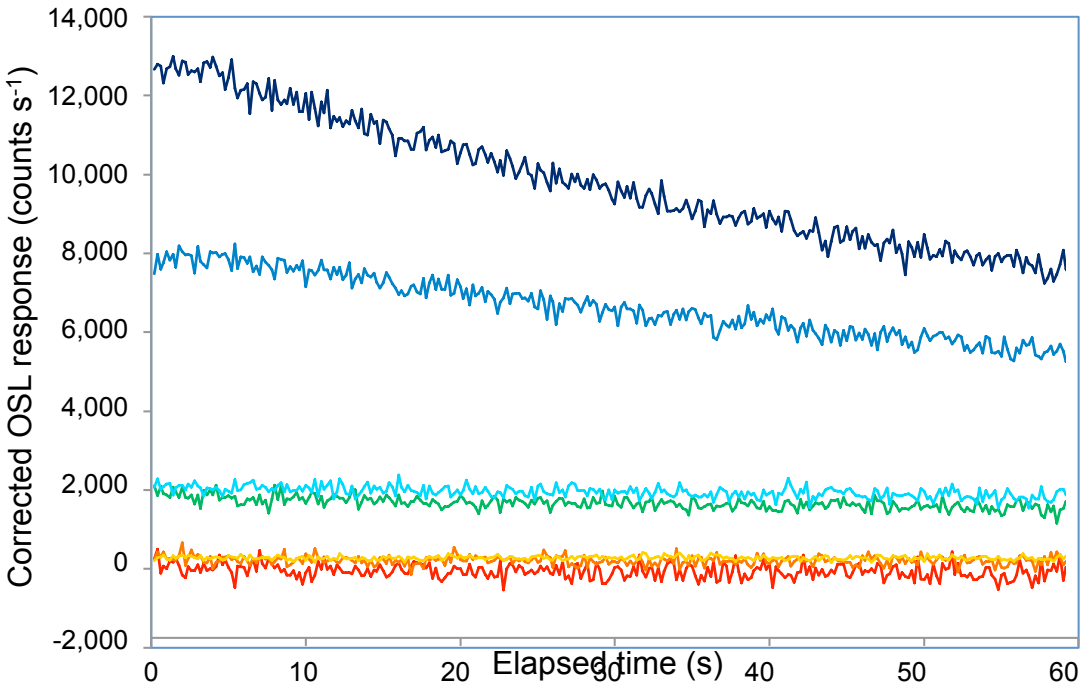

Figure 5.16: Corrected optically stimulated luminescence (OSL) curves for LiF:Mg,Cu,Na,Si irradiated to 500 mGy dose in air using 120 kVp x-rays, at 6 hours post-irradiation. The color of each curve corresponds to the excitation light color: red (λ = 625 nm), red-orange (λ = 617 nm), amber (λ = 590 nm), green (λ = 530 nm), cyan (λ = 505 nm), blue (λ = 470 nm), and royal blue (λ = 455 nm).

Figure 5.17 shows the CAS curves for LiF:Mg,Cu,Na,Si. The CPS curve, shown as Figure 5.18, is virtually identical, indicating that a single trap is being accessed or that multiple traps with similar photo-ionization cross sections are being accessed. Like $CaSO_4$:Tm, there are no pronounced OSL signal peaks with exponentially-decaying shapes within the time frame of the readout. Elaborate data subtraction and correction, in the form of P/E and P-E ratios, is also not necessary due to the relatively high OSL

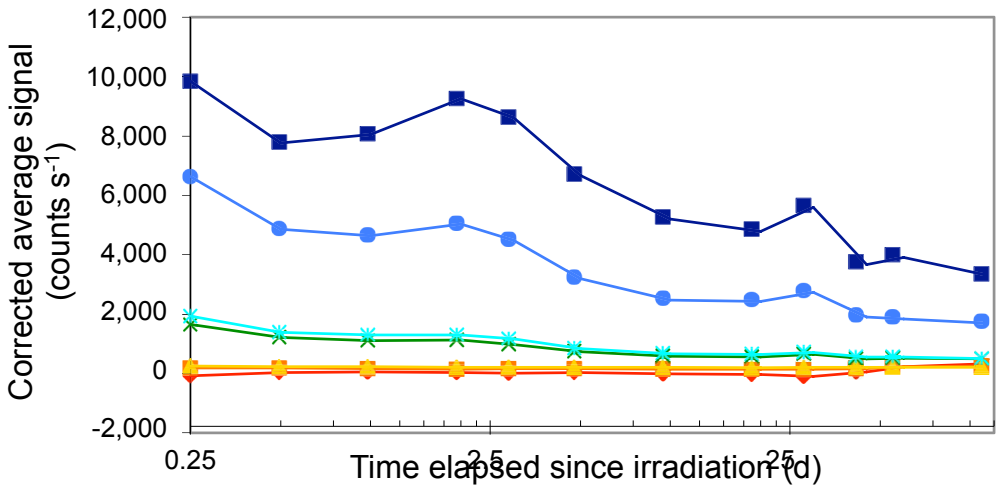

Figure 5.17: Corrected average signal (CAS) curves for LiF:Mg,Cu,Na,Si irradiated to 500 mGy dose in air using 120 kVp x-rays. Each data point represents the average optically stimulated luminescence (OSL) output signal height at a given time since irradiation. The color of each curve corresponds to the excitation light color: red (λ = 625 nm), red-orange (λ = 617 nm), amber (λ = 590 nm), green (λ = 530 nm), cyan (λ = 505 nm), blue (λ = 470 nm), and royal blue (λ = 455 nm).

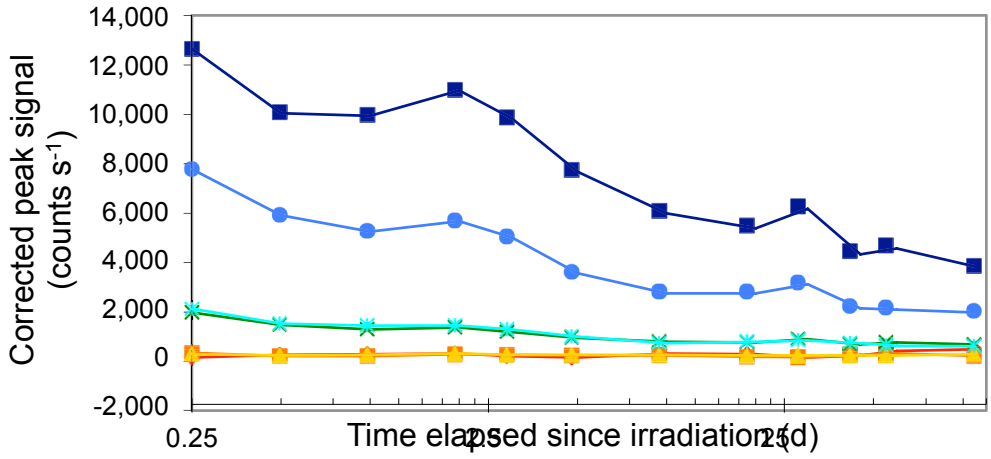

Figure 5.18: Corrected peak signal (CPS) curves for LiF:Mg,Cu,Na,Si irradiated to 500 mGy dose in air using 120 kVp x-rays. Each data point represents the peak optically stimulated luminescence (OSL) output signal height at a given time since irradiation. The color of each curve corresponds to the excitation light color: red (λ = 625 nm), red-orange (λ = 617 nm), amber (λ = 590 nm), green (λ = 530 nm), cyan (λ = 505 nm), blue (λ = 470 nm), and royal blue (λ = 455 nm).

output. Figure 5.19 shows the ratios of the green, cyan and blue CAS values to the royal blue CAS value. These curves trend downward until 5 d post-irradiation and then remain relatively constant thereafter.

LiF:Mg,Cu,Na,Si also exhibited an afterglow signal during the experiments, an example of which is presented as Figure 5.20. This is the OSL output signal collected *after* de-energization of the excitation lights.

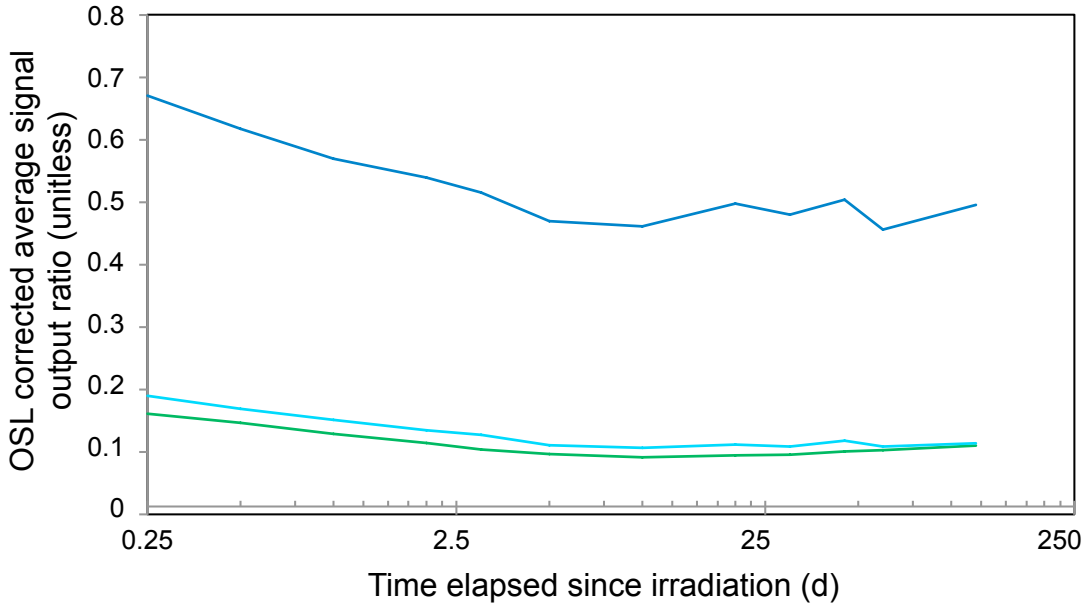

Figure 5.19: Corrected average signal (CAS) output ratios for LiF:Mg,Cu,Na,Si irradiated to 500 mGy dose in air using 120 kVp x-rays. Each line plots the ratio of the CAS value under the corresponding excitation light (green, cyan, blue) to the CAS value under royal blue excitation. The CAS value represents the average optically stimulated luminescence (OSL) output signal height at a given time since irradiation.

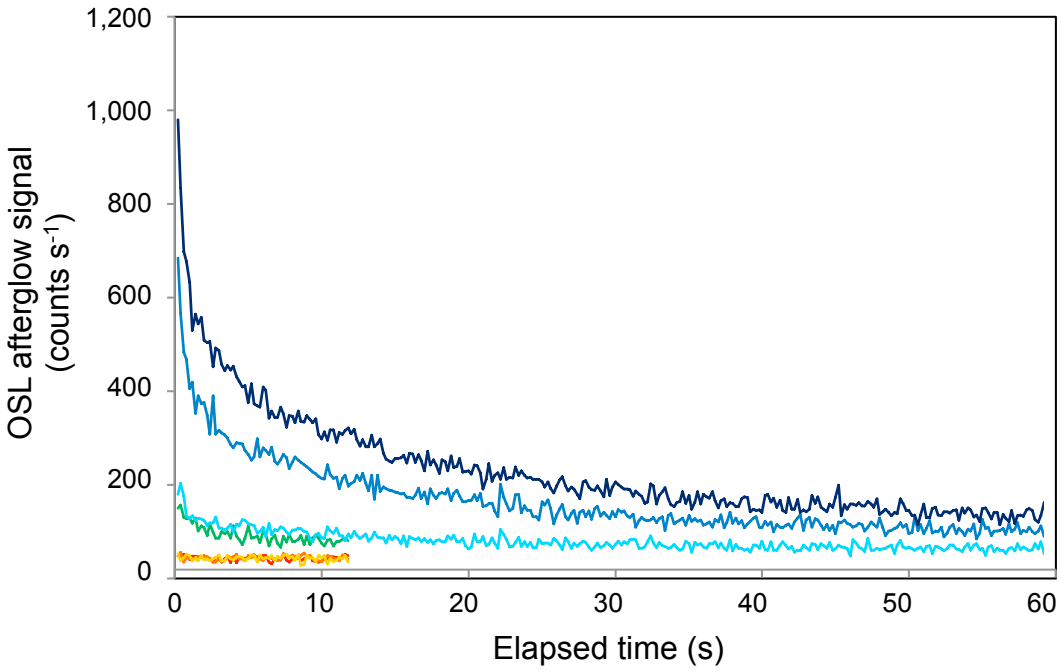

Figure 5.20: Afterglow optically stimulated luminescence (OSL) curves for LiF:Mg,Cu,Na,Si irradiated to 500 mGy dose in air using 120 kVp x-rays, at 6 hours post-irradiation. The color of each curve corresponds to the excitation light color: red (λ = 625 nm), red-orange (λ = 617 nm), amber (λ = 590 nm), green (λ = 530 nm), cyan (λ = 505 nm), blue (λ = 470 nm), and royal blue (λ = 455 nm).

Figure 5.21 shows the TLD glow curves for each time since irradiation for LiF:Mg,Cu,Na,Si, reflecting a major peak at ~230 °C and minor peaks at ~155 °C and 300 °C. Figure 5.22 shows the CAS curves for those excitation frequencies demonstrating an OSL signal, along with fitted logarithmic trendlines, to be used later in this paper.

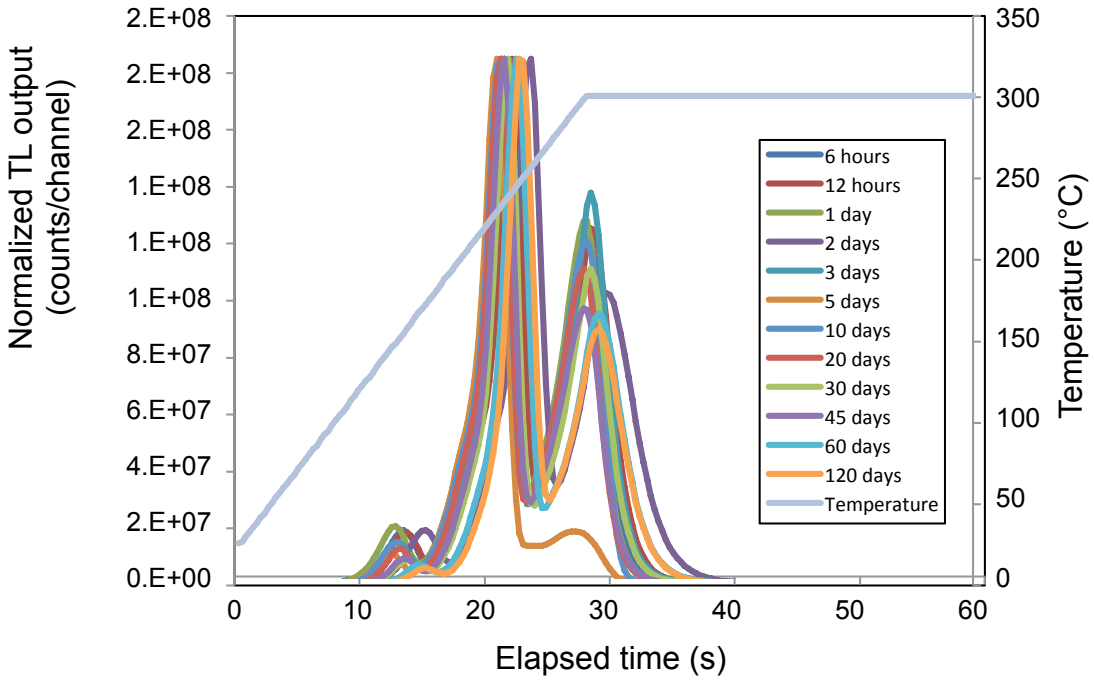

Figure 5.21: Thermoluminescence (TL) glow curves for LiF:Mg,Cu,Na,Si irradiated to 500 mGy dose in air using 120 kVp x-rays. Each colored line represents a TL readout at a different time after irradiation. The curve has been normalized to constant main peak height to eliminate differences due to sample size.

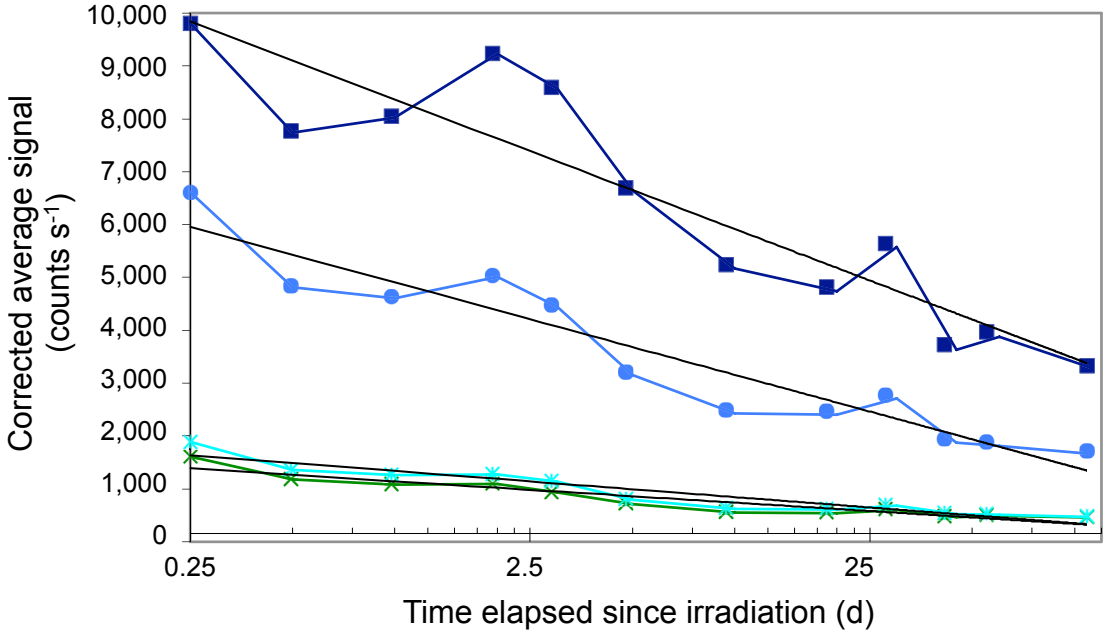

Figure 5.22: Corrected average signal (CAS) curves for LiF:Mg,Cu,Na,Si, irradiated to 500 mGy dose in air using 120 kVp x-rays, with only green, cyan, blue and royal blue curves shown. Each data point represents the average optically stimulated luminescence (OSL) output signal height at a given time since irradiation. Logarithmic trendlines are plotted for each excitation source and the resulting equation and correlation coefficient are as follows: green: $y = -174.7\ln(x) + 1007$; cyan: $y = -214.2\ln(x) + 1205$; blue: $y = -758.7\ln(x) + 4841$; and royal blue: $y = -1063\ln(x) + 8362$. Correlation coefficients (R^2) values for these trendlines are 0.89, 0.90, 0.91 and 0.86, respectively.

LiF:Mg,Cu,Si (New-KLT-300)

Figure 5.23 shows the corrected OSL curves for LiF:Mg,Cu,Si at 6 h post-irradiation. This graph shows a very high OSL signal, relative to the signals of the other materials tested in this experiment, when using green and higher excitation energies. These OSL signals demonstrate no significant decay over the course of the

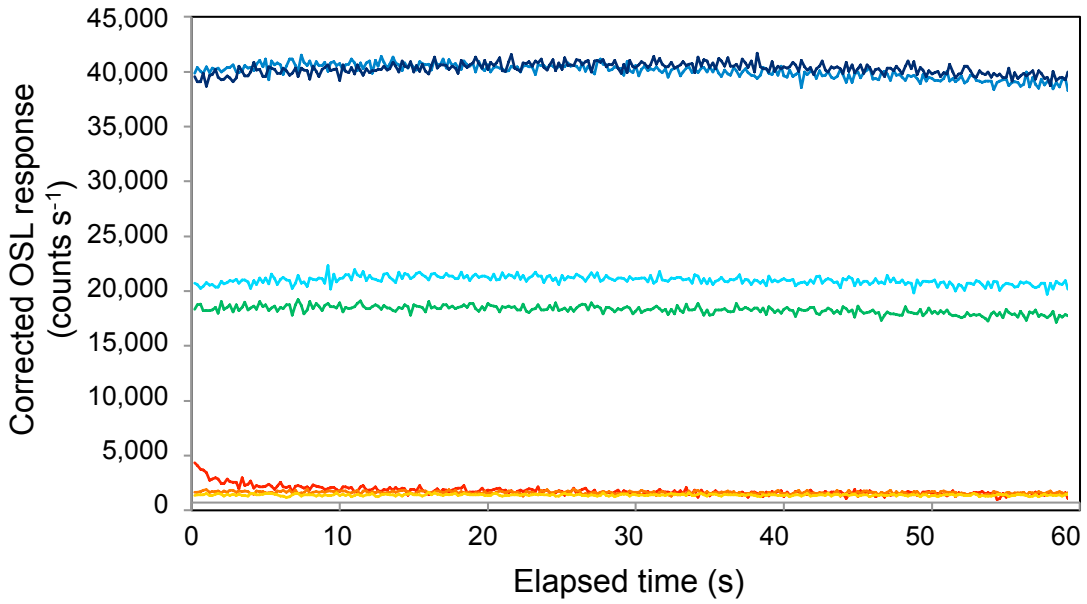

Figure 5.23: Corrected optically stimulated luminescence (OSL) curves for LiF:Mg,Cu,Si irradiated to 500 mGy dose in air using 120 kVp x-rays, at 6 hours post-irradiation. The color of each curve corresponds to the excitation light color: red (λ = 625 nm), red-orange (λ = 617 nm), amber (λ = 590 nm), green (λ = 530 nm), cyan (λ = 505 nm), blue (λ = 470 nm), and royal blue (λ = 455 nm).

readout period, and actually trend upward somewhat for the first 20 s or so. In addition, a red-induced OSL signal is also evident on this graph. Figure 5.24 shows the corrected OSL curves for LiF:Mg,Cu,Si at 30 d post-irradiation. By this point, the OSL signal output has taken on a more 'conventional' appearance, with exponentially-decaying amplitude.

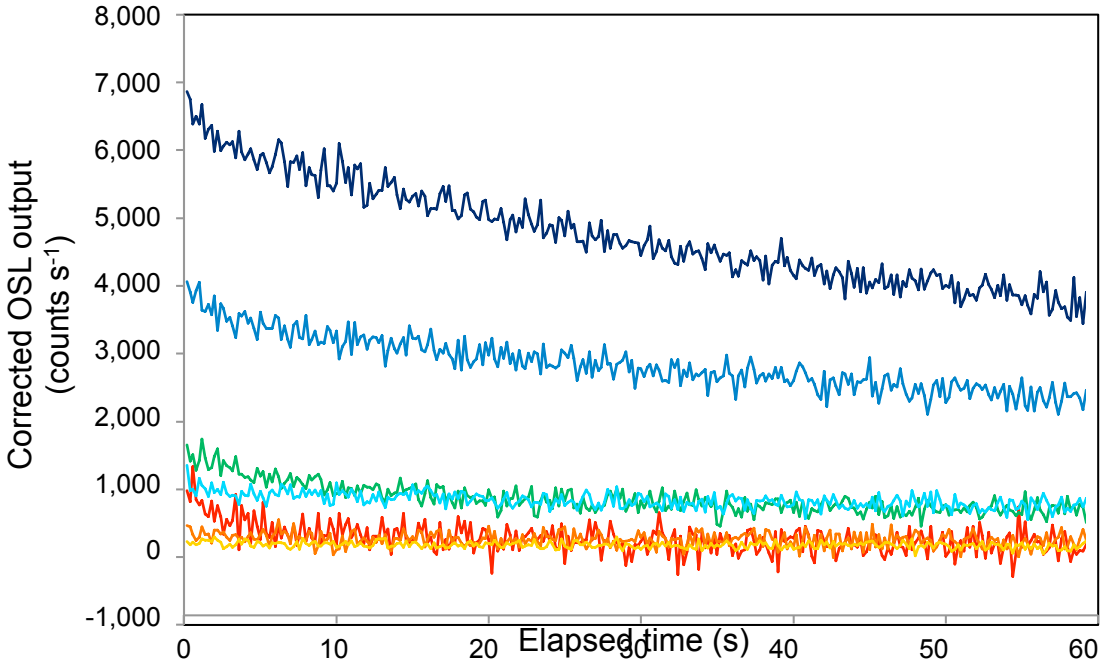

Figure 5.24: Corrected optically stimulated luminescence (OSL) curves for LiF:Mg,Cu,Si, irradiated to 500 mGy dose in air using 120 kVp x-rays, at 30 days post-irradiation. The color of each curve corresponds to the excitation light color: red (λ = 625 nm), red-orange (λ = 617 nm), amber (λ = 590 nm), green (λ = 530 nm), cyan (λ = 505 nm), blue (λ = 470 nm), and royal blue (λ = 455 nm).

Figure 5.25 shows the CAS curve for this material and its appearance is markedly different in one important respect from the CAS curves of the other investigated materials: the blue and royal blue curves remain roughly constant throughout the first 3 d post-irradiation. Based on additional investigation, it was determined that due to saturation of the OSL reader PMT electronics, the OSL light output during these readouts was limited to approximately 20,000 cps net. As such, the data for the initial time periods for these two light sources was compromised by experimental limitations. This

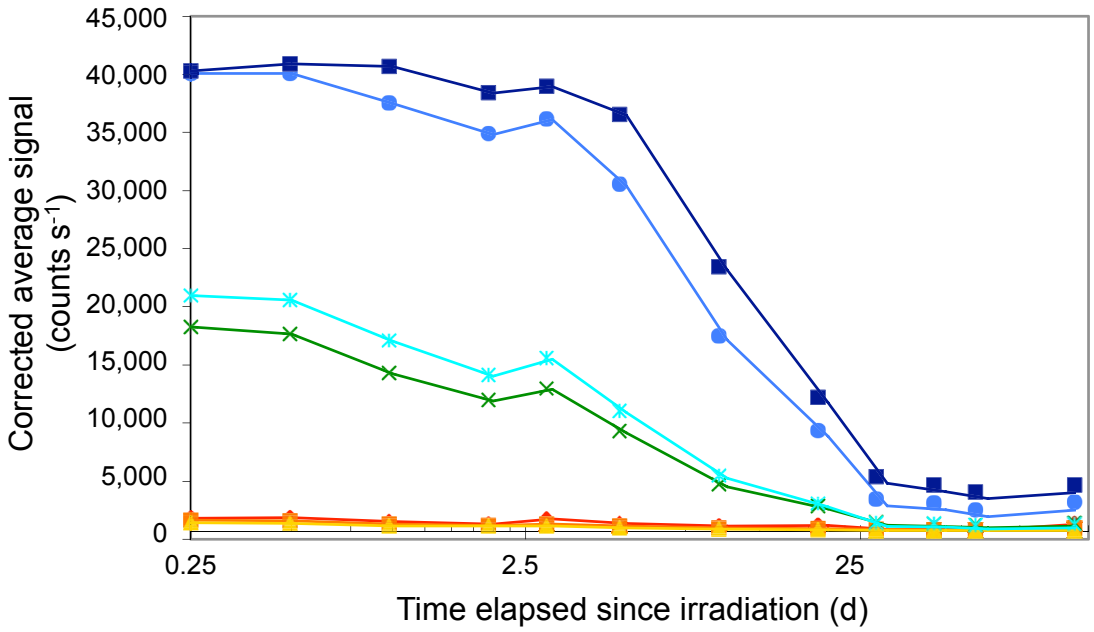

Figure 5.25: Corrected average signal (CAS) curves for LiF:Mg,Cu,Si irradiated to 500 mGy dose in air using 120 kVp x-rays. Each data point represents the average optically stimulated luminescence (OSL) output signal height at a given time since irradiation. The color of each curve corresponds to the excitation light color: red (λ = 625 nm), red-orange (λ = 617 nm), amber (λ = 590 nm), green (λ = 530 nm), cyan (λ = 505 nm), blue (λ = 470 nm), and royal blue (λ = 455 nm).

limitation could be prevented during future experiments by either upgrading the OSL reader detection electronics or by installation of a neutral-density filter to reduce PMT count rates when necessary.

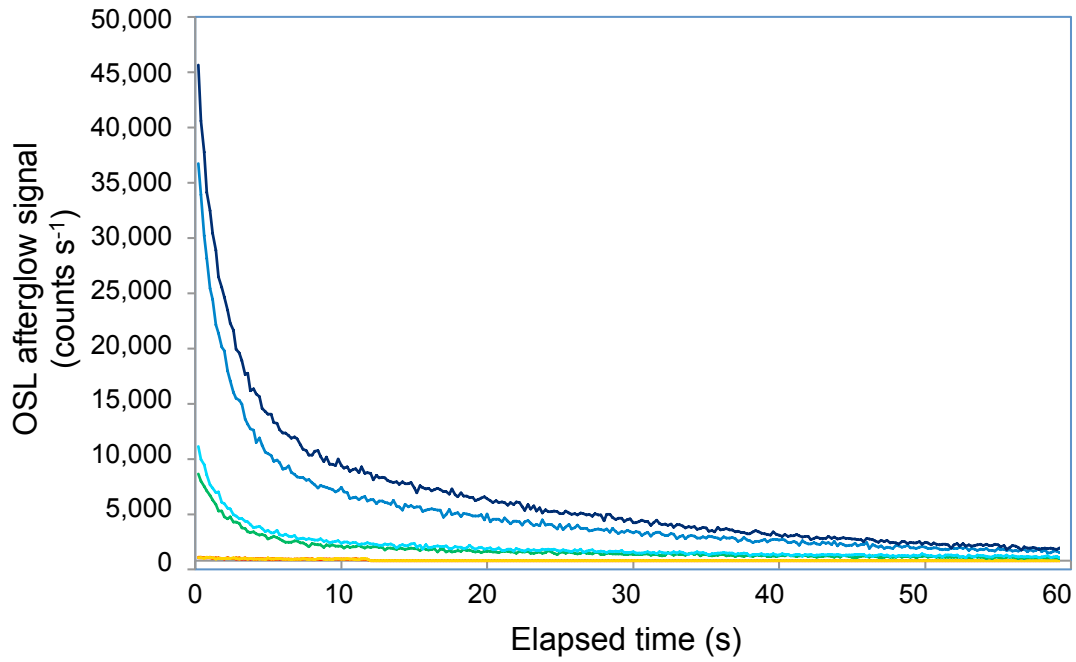

Figure 5.26: Afterglow optically stimulated luminescence (OSL) curves for LiF:Mg,Cu,Si irradiated to 500 mGy dose in air using 120 kVp x-rays, at 5 days post-irradiation. The color of each curve corresponds to the excitation light color: red (λ = 625 nm), red-orange (λ = 617 nm), amber (λ = 590 nm), green (λ = 530 nm), cyan (λ = 505 nm), blue (λ = 470 nm), and royal blue (λ = 455 nm).

Like LiF:Mg,Cu,Na,Si, the LiF:Mg,Cu,Si exhibited OSL light output after de-energization of the excitation lights. This afterglow, an example of which is shown as Figure 5.26, can be used as an alternative method of characterizing the temporal character of this material, as it results in a lower signal that does not saturate the OSL reader electronics. The total area of these afterglow curves were plotted with respect to time since irradiation and that data is shown on the graph in Figure 5.27. Finally, Figure 5.28 shows the ratios of these afterglow curve areas to that of royal blue, in a manner similar to the CAS output ratio graphs presented for the other materials analyzed in this

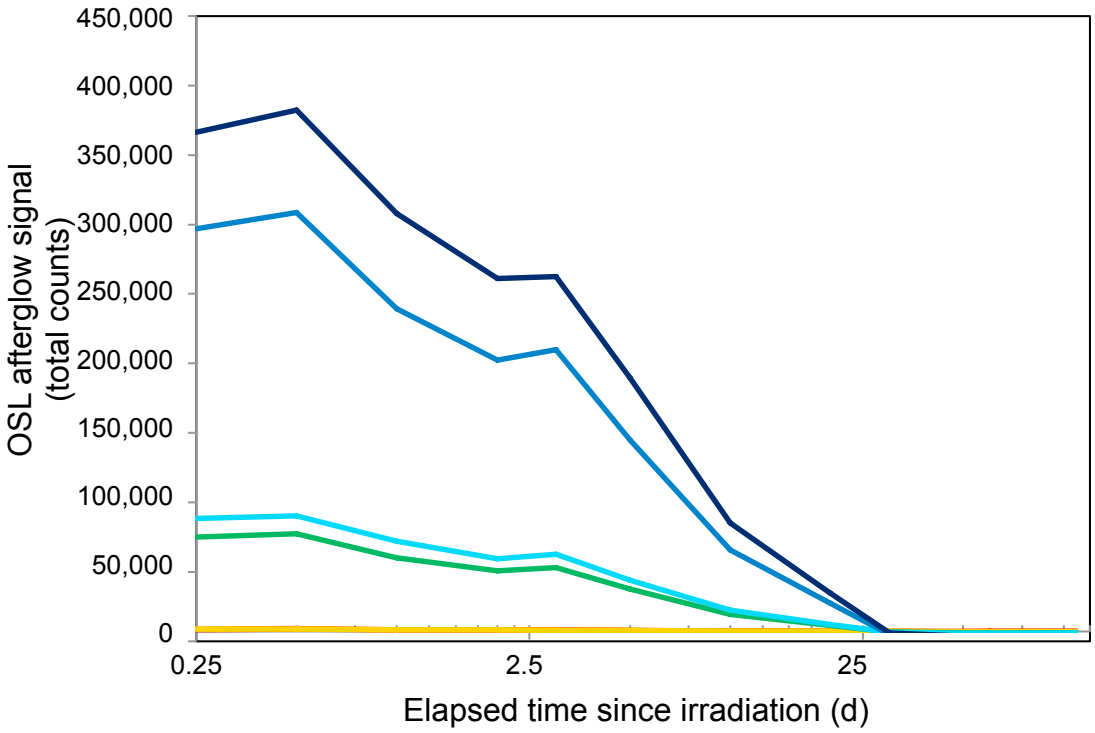

Figure 5.27: Total integrated optically stimulated luminescence (OSL) afterglow signal for LiF:Mg,Cu,Si irradiated to 500 mGy dose in air using 120 kVp x-rays, as a function of time since irradiation. The color of each curve corresponds to the excitation light color: red (λ = 625 nm), red-orange (λ = 617 nm), amber (λ = 590 nm), green (λ = 530 nm), cyan (λ = 505 nm), blue (λ = 470 nm), and royal blue (λ = 455 nm).

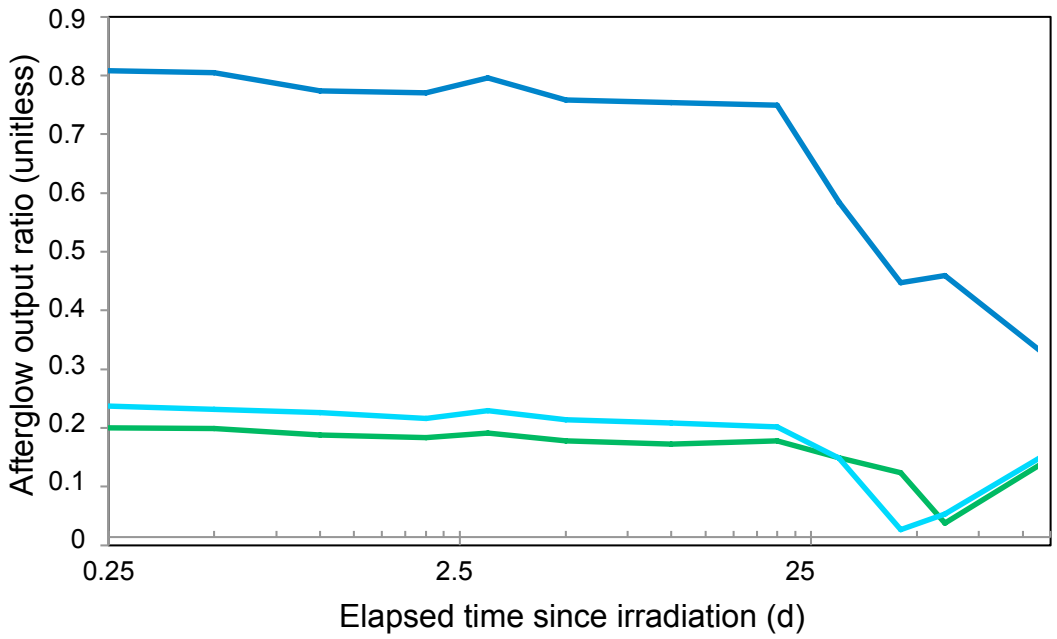

Figure 5.28: Ratio of LiF:Mg,Cu,Si integrated optically stimulated luminescence (OSL) afterglow signals for green, cyan and blue light excitation relative to royal blue light excitation, as a function of time since irradiation. The LiF:Mg,Cu,Si had been irradiated to 500 mGy dose in air using 120 kVp x-rays

experiment. Figure 5.29 shows the TLD glow curves for each time since irradiation for LiF:Mg,Cu,Si. These glow curves show major peaks at ~230 °C and ~205 °C and a minor peak at ~140 °C.

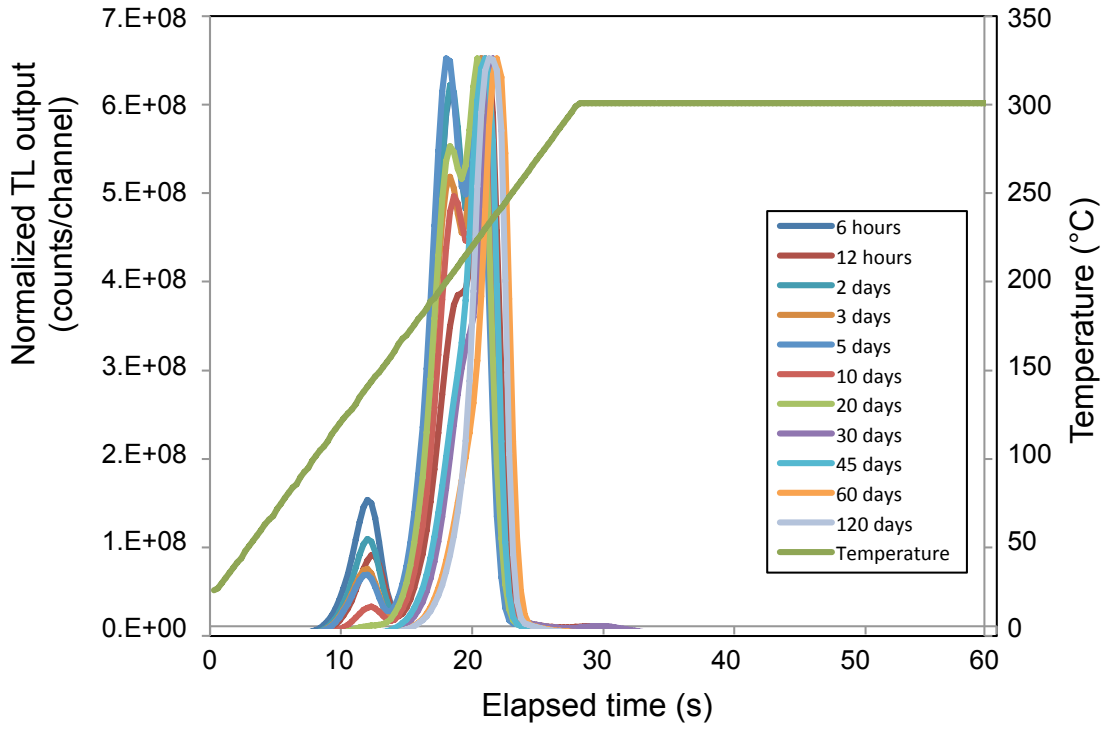

Figure 5.29: Thermoluminescence (TL) glow curves for LiF:Mg,Cu,Si irradiated to 500 mGy dose in air using 120 kVp x-rays. Each colored line represents a TL readout at a different time after irradiation. The curve has been normalized to constant main peak height to eliminate differences due to sample size.

DISCUSSION

The significance of the presented results for each investigated material is discussed below.

KBr

Though un-doped KBr, to date, has not been investigated for its OSL behavior, KBr:Eu has been studied extensively for this purpose due to its use in both medical imaging and environmental radiation dosimetry. It is known that KBr:Eu has a stimulation maximum at 620 nm, i.e., red, corresponding to absorption by neutral Br-vacancy centers, or F-centers[32-33]. It is therefore possible that any dopant/contaminant in this compound could produce a similar response. KBr:Eu has an emission maximum at 420 nm, with a FWHM great enough to pass the custom OSL reader's emission filters and produce a weak PMT signal. As such, the presence of a red-induced OSL signal is logical. Figure 5.2 shows that both red and green excitation lights produced an OSL response from pure KBr. There is also some indication that the red-orange excitation produced an OSL response. It is reasonable that it would, given the similarity in excitation frequencies between the red and red-orange lights, and the fact that its photon energy is higher than that of the red light. Though it is difficult, due to SNR limitations in the data set, to confirm that a bonafide OSL signal results under red-orange excitation, it is likely that since the red-orange excitation of the sample is performed immediately after the red excitation, that the small OSL signal remaining in the material after the red

excitation is being captured by the red-orange light. It is salient to note that no detectable OSL signal is produced by the amber excitation light, and that the green excitation is performed immediately after the amber. As such, it appears that the green excitation light is accessing traps not accessed by the lower-energy lights, as predicted.

Figure 5.3 provides a slightly different view of this behavior. This graph looks at only the difference between the peak height of the OSL curve and the end height. As such, it removes any effects due to variations in baseline corrections at this low signal level, i.e. it is more insensitive to the low SNR. This graph confirms the findings from Figure 5.2 and also suggests a different decay profile versus time for the OSL signal under red excitation versus that produced under green excitation.

Figure 5.4 plots the ratio of the red and green curves from Figure 5.3 to show the relationship of the response over time. While this graph exhibits an exception at time periods 8 and 9, most likely due to suboptimal counting statistics and low SNR in this case, the overall trend appears to be generally downward over time. This suggests that the OSL reader is polling at least two traps, each of which de-populates over time at room temperature with different time constants. This conclusion is further supported by the KBr TL glow curve behavior, shown in Figure 5.5. The TL glow curve consists of one main peak at ~255 ºC, as well as at least two minor peaks at ~115 ºC and ~170 ºC. According to Equation 1, the 115 ºC peak corresponds to a trap half-life of 4 h, the 170 ºC peak corresponds to a trap half-life of 20 d, and the 255 ºC peak corresponds to a trap half-life of 96 y. While the limitations of first-order kinetics as applied to TLD fading rates has already been noted, it is worth mentioning that the half-lives of the 115 ºC and 170 ºC peaks appear to coincide fairly well with the OSL signals resulting from the red

and green light excitation, respectively. It is not yet known to what extent the deep trap contributes to the green light OSL signal, though based on the limited data set, it does not appear that a stable trap is being accessed using OSL in this case.

The results obtained for KBr are interesting and suggestive of a method of obtaining temporal information from this material using, as a start, the ratio of red and green excitation light OSL signals. Further investigation of this material is indicated to produce higher OSL signal intensities for superior counting statistics and data analysis. Since the OSL reader used for these experiments is limited to detection in the UV range only, additional investigation with respect to the OSL emission spectrum of this material is warranted to determine whether the low dose sensitivity found in these experiments was an experimental limitation, as suggested by the emission maximum of KBr:Eu, or a material one.

$CaSO_4$:Tm

$CaSO_4$:Tm was investigated as a potential TL dosimetry material as early as 1970 by Yamashita et. al[38]. Further study on this and other rare--earth--doped calcium sulfates was performed by Nambi et. al.[34] and published in 1974. By 1977, this material was being incorporated by into commercial TLD dosimeters, as related by Iga et. al.[35]. This material remains in use today as a TL phosphor. An initial investigation of its OSL dosimetry potential was only recently performed[39] and this experiment's results seek to extend that investigation.

Based on the previous experiment's results as well as the overall amplitude of the signals shown in Figure 5.6, $CaSO_4$:Tm shows promise as an OSL dosimeter. Previous experiments performed by the authors[39] indicated that although this material's total luminance was approximately a factor of 40 less than that of α-Al_2O_3:C, the OSL sensitivity would likely be significantly greater with more optimal selection of excitation sources, detection filters and PMT.

Figures 5.7 and 5.8 show the OSL signal induced by all excitation wavelengths decreasing as a function of time since irradiation. It is interesting to note that the OSL signal from the blue excitation light decays slightly more rapidly than the OSL signal from the royal blue excitation light. Figure 5.9 shows that this relationship also exists when comparing the green and cyan excitations to royal blue. This suggests that the royal blue excitation light is accessing a deeper, more stable trap to a greater degree than the lower-energy excitation sources. However, the effect is subtle, indicating that there may be a more complex explanation for the behavior than simply two traps with substantially divergent decay constants. One possible explanation is the presence of two or more closely spaced trap sites, with the higher-energy excitation photons accessing the deeper traps slightly more efficiently, leading to a somewhat longer aggregate time constant for the OSL signal decay over elapsed time.

Figure 5.10 shows the TL glow curve for this material, with a major peak at ~275 °C and a minor peak at ~145 °C. This major peak agrees with data previously published by Lewandowski, et. al, who performed a detailed investigation of the TL excitation and emission characteristics of this material[36]. Lewandowski's experiment did not identify a low-temperature peak, however, possibly because of a delay between the irradiation and

readout of the samples; the presence of a low-temperature peak, however, had previously been reported by Nambi et. al. and Yamashita et. al. Yamashita also reported on an even lower-temperature peak at 80 °C that decayed within 2 h post-irradiation, though of course since the first readout was at 6 h post-irradiation, that peak was not measured. According to Equation 1, the 145 °C peak corresponds to a trap half-life of 2.4 d and the 275 °C peak corresponds to a trap half-life of 549 y. The actual half-lives of the OSL signals for all excitation wavelengths were in the 10-20 d range. A complete theoretical discussion of the possible causes for this discrepancy is beyond the scope of this paper but further investigation into the trap structure of this material during the course of future OSL investigations may yield clarifying information.

Lewandowski reported a primary TL emission peak at 455 nm, i.e. blue light, with a moderate peak at 733 nm, and minor peaks at 360 nm, 515 nm, 655 nm and 700 nm[36]. As such, it is likely that the experimental OSL reader setup, exciting from 455-625 nm and detecting at 260-400 nm, is not optimal for this material. Since this material exhibited an afterglow, future experimentation using a pulsed OSL (POSL) technique, combined with a detection system capable of efficiently detecting blue light could yield higher sensitivities and additional useful information.

$CaSO_4$:Dy (TLD-900)

$CaSO_4$:Dy was investigated as a potential TL dosimetry material at the same time as $CaSO_4$:Tm and, in many cases, by the same parties[34, 36, 38]. Its history follows a similar track, with commercial use as a TL dosimetry material. This material has also

been investigated to some degree as a temporal TL dosimeter by Bacci et. al.[40] and, more recently and comprehensively, by Wang et. al.[42]. The positive findings in this regard are part of the impetus for this work. Unlike with $CaSO_4$:Tm, OSL experimentation has been performed on this material, initially by Pradhan, et. al. using broadband stimulation for detection of an afterglow following high irradiation doses[45]. Later, Jaek, et. al[97] used more refined narrow-band light stimulation to investigate the excitation and emission spectra of the material for investigation as an OSL material. Bacci et. al. noted during TL study of the material that no light-induced fading (under laboratory light) of the TL signal was observed[41]. This behavior typically correlates to low or zero OSL response. However, subsequent investigation by Pradhan did show fading of the signal in sunlight[98], and Lewandowski et. al. noted that the primary TL peak was bleached with exposure to 532 nm, i.e. green, light[36], both findings that support the OSL quality of this substance.

A review of Figure 5.12 suggests a meager detected OSL signal induced in $CaSO_4$:Dy with the blue excitation source, decaying with time since irradiation at a half-life on the order of 10 d. This tentative result agrees with the results of the TLD readout of the material, shown in Figure 5.13. A minor peak is exhibited at ~160 °C in addition to the major peak at ~270 °C, which corresponds, using the first-order kinetics equations, to a half-life of approximately 9 d. As such, it is theorized that this trap is capable of being accessed using the higher-energy excitation sources, though to only a limited degree, even at the high irradiation doses utilized.

While this material exhibits a faint OSL signal with the experimental setup, this signal is far too weak to draw any significant material conclusions from. Prior

investigations of the TL and OSL properties of this material[36, 43, 98] reported intense TL emission peaks at 470-480 nm and 570 nm, as well as minor emission peaks at 360 nm, 660 nm and 760 nm. The 360 nm emission is also seen in $CaSO_4$:Tm and in un-doped $CaSO_4$ and is the only one of these emissions that the experimental apparatus can detect. As such, it is likely that utilization of expanded detection capabilities that can detect blue and yellow wavelengths may lead to improved signal amplitudes and allow further and more precise characterization of this substance as an OSL dosimeter.

$CaSO_4$:Dy+P

A description of the development and the TL performance of this new formulation of $CaSO_4$:Dy is described by Yang et. al[47] and further described in a related United States patent[46]. In short, this substance was created to address problems with dose sensitivity reduction in pellets using polytetrafluoroethylene (Teflon) as a binding compound. By substituting phosphorus as a binding agent, TL sensitivity is apparently increased. It is interesting to note that further development of this material has taken place by the addition of lithium isotopes to enhance the neutron sensitivity of the compound[48].

In any event, this material exhibited no detectable OSL signal using the current experimental setup. Based on the experiments of Yang et. al.[47], the TL behavior of this compound should be identical in character, namely peak locations, peak shapes, fading and properties, to that of $CaSO_4$:Dy, though different in magnitude. Specifically, it should exhibit higher signal than other Teflon-based chips but slightly lower signal than

raw powder. In the case of OSL response, it is reasonable to conclude that the addition of the phosphorus has a negative optical impact, either through absorption of the excitation light or the emission light. As with $CaSO_4$:Dy, additional experimentation using other apparatus may yield additional information.

LiF:Mg,Cu,Na,Si (KLT-300)

LiF:Mg,Cu,Na,Si was initially developed by Doh *et al*[59, 63] and further investigated, and dopant concentrations refined, by Nam *et al*[72-75] and Lee *et al*[67]. Based on those investigations, it was found that this material exhibits TL sensitivity approximately twice that of LiF:Mg,Cu,P and has favorable dose linearity, fading and other material characteristics for TL dosimetry. However, to date, no published investigations of this material's OSL behavior exist.

Based on the overall amplitude of the signals shown in Figure 5.16, LiF:Mg,Cu,Na,Si shows promise as an OSL dosimeter. This material's total luminance was approximately a factor of 50 less than that of α-Al_2O_3:C; however, as with $CaSO_4$:Tm, the OSL sensitivity could be somewhat greater with more optimal selection of excitation sources, detection filters and PMT. For instance, Nam *et al* noted that the TL emission in LiF:Mg,Cu,Na,Si runs from approximately 350 nm to 500 nm, with a maximum at 410 nm[75]. As such, the detection system is likely detecting only about half of the output light from the sample since the emission filter low-frequency edge is right at 410 nm.

Figures 5.17 and 5.18 show the OSL signal induced by all excitation wavelengths decreasing as a function of time since irradiation. Figure 5.19 shows that green, cyan and blue-induced OSL in this material decays slightly faster during the first 5 d post-irradiation than the OSL signal induced by royal blue excitation. This suggests that the royal blue excitation light is accessing a deeper, more stable trap to a greater degree than the lower-energy excitation sources.

Figure 5.20 shows the afterglow signal from LiF:Mg,Cu,Na,Si. The height, area and decay properties of the afterglow signals for this material followed closely the CW-OSL signals already analyzed, so an elaborate analysis of afterglow behaviors in LiF:Mg,Cu,Na,Si is not undertaken in this work. However, this information is included to demonstrate that this material is a candidate for POSL, in which the stimulation light is rapidly switched on and off and the emission light is collected only during the intervals when the excitation light is inactive. For materials showing this type of metastable behavior in their OSL output, POSL readout can be a much more sensitive methodology for extracting dose information. Therefore, the presence of a pronounced afterglow signal furthers the notion that LiF:Mg,Cu,Na,Si is a promising candidate for additional OSL investigation.

Figure 5.21 shows the TL glow curve for this material, with a major peak at ~230 °C and minor peaks at ~155 °C and 300 °C. These values agree generally with previously-published TL results[68, 73, 75]. However, the TL curve did not show the 104 °C peak previously seen, likely due to rapid thermally-induced fading. The 300 °C peak has not been previously reported, which may be an avenue for further exploration. According to Equation 1, the 155 °C peak corresponds to a trap half-life of 5.6 d and the

230 °C and 300 °C peaks are essentially stable at the time scale of this experiment. This theoretical behavior is generally supported by the TLD curves. For example, the 155 °C peak is reduced in intensity by approximately half between the 1-d and 5-d post-irradiation readings. The actual half-lives of the OSL signals for the green, cyan, blue and royal blue excitation sources, based on plotting logarithmic trendlines to the CAS data as shown in Figure 5.22, were approximately 8.9, 8.3, 11.9 and 25.3 d, respectively. This behavior supports the theory that the green and cyan excitation lights are primarily accessing this shallow trap and following its decay, while the blue and royal blue excitation lights are beginning to access the deep trap population, thereby extending their time constants as their frequencies increase. Further investigation using higher-frequency light sources could yield additional confirmation of this theory.

LiF:Mg,Cu,Si (New-KLT-300)

LiF:Mg,Cu,Si TL investigations were first published in 1978, by Nakajima et al[55]. However, in those experiments, LiF:Mg,Cu,P was found to be a more sensitive TL dosimetry material and the use of Si as a dopant for LiF was not pursued thereafter, until in 2005, Yang *et al* published an investigation into the thermal stability of several LiF formulations, including LiF:Mg,Cu,Si[57]. This experiment was an attempt to optimize the formulation of the LiF dopants to reduce the drop in sensitivity when the material is annealed at temperatures above 240 °C. However, this new formulation did not change that behavior and, as before, the TL sensitivity remained lower than LiF:Mg,Cu,P. In 2006, researchers at KAERI published the results of experiments on a new formulation of

this material, dubbed New-KLT-300, that involved a somewhat different preparation process[54]. The experimental results described a dosimetry material both more sensitive than LiF:Mg,Cu,P, and with significantly less thermal TL sensitivity loss at high annealing temperatures. Numerous subsequent papers have characterized this new TL material and explored possible formulation improvements[49-53, 56]. However, until now, no OSL investigations of this material have been published.

As discussed in the Results section above, and as evidenced by the obvious differences in OSL signal output characteristics between Figures 5.23 and 5.24, not to mention the CAS curves for this material seen in Figure 5.25, the OSL signal strength of this material was sufficient to saturate the custom OSL reader counting system. This unanticipated result indicates that LiF:Mg,Cu,Si has substantial potential as a sensitive OSL dosimetry material. Based on a simple extrapolation of the CAS curve for the blue excitation light from the time period post-saturation, an estimated OSL signal peak height of ~80,000 cps at 6 h after irradiation is reasonable. Compared to readings with similarly-sized samples of α-Al_2O_3:C[78], this material exhibits an OSL signal at a given dose roughly 10 times weaker than the alumina using the experimental apparatus. However, additional refinement of the readout protocol after further investigation of this material's excitation and emission characteristics could result in substantial improvement of that sensitivity, perhaps resulting in a sensitivity at or near this highly effective OSL material. Also, as evidenced by the presence of a characteristic afterglow signal, this material is a candidate for POSL readout, further increasing its potential utility.

Since investigation using the CW-OSL curves is made difficult by the saturation, investigation of this material's OSL afterglow provides an opportunity to study its

behavior at lower light levels that did not saturate the electronics. Figure 5.27 shows the generally logarithmic decrease in the afterglow intensity as a function of time since irradiation. This behavior parallels normal CW-OSL output behavior. Figure 5.28 presents the ratios of afterglow signal using the green, cyan and blue excitation light, with respect to the afterglow signal using the royal blue excitation light. There is a very gradual decrease in the ratios over time out to 20 d post-irradiation and then a somewhat faster decrease thereafter, though the counting statistics after 20 d increase the uncertainty in this area. Therefore, these results tentatively suggest that there may be some differential fading behavior where the higher-frequency excitation source may be accessing a stable, deeper trap to a slightly greater extent, but the results are inconclusive in this regard. Considering the high OSL sensitivity of this material, the possibility of using POSL techniques, the known trap structure and the excitation-dependent fading behavior measured using afterglow readings, further investigation of LiF:Mg,Cu,Si using lower doses, higher-energy excitation sources, and more flexible detection systems, is indicated.

It is also noted that there does exist a smaller OSL signal resulting from the red light excitation in this material, though it demonstrates a similar time constant as the green and cyan signals, both of which can be estimated since they did not saturate the electronics. Some small degree of red-orange and amber signal also appears to be present, though it is likely that the red excitation would have cleared out to a large extent any trap accessible by the three excitation sources prior to the red-orange and amber excitations.

Figure 5.29 shows the TL glow curve for this material, with major peaks at ~230 °C and ~205 °C and a minor peak at ~140 °C. This glow curve structure is in conformance with previously-published results[54], though the literature also documents a minor peak at 105 °C that is not seen here, most likely due to a fading rate fast enough to eliminate it prior to the first readout. According to Equation 1, the 140 °C peak corresponds to a trap half-life of 1.5 d and the 205 °C peak corresponds to a trap half-life of 445 d. The 230 °C peak is essentially stable at the time scale of this experiment. It is evident from review of the TLD curve behavior that the time constants predicted using first-order kinetic models do not closely match the actual TLD curve decays. The 140 °C peak appears to decay with a half-life of 3-5 d and the 205 °C peak, though harder to measure due to its superposition with the 230 °C peak, has a half-life on the order of 20-45 d. Based on analysis of the CAS values for the red, green and cyan excitation curves, and using logarithmic trendlines as was done with LiF:Mg,Cu,Na,Si, the half-life of both the green- and cyan-induced signals is approximately 4 d, and for the red-induced signal it is approximately 9 d. It is noteworthy that the decay constant for green and cyan-induced OSL matches that of the low-temperature peak in the TL investigation. This suggests that these sources, and also the blue and royal blue sources, are primarily accessing this low-temperature trap. It is not known why the OSL signal resulting from the red excitation light appears to have a longer time constant than the green and cyan curves, other than to theorize that the low signal strength results in poorer counting statistics and that further experimentation with a significantly brighter red excitation source would provide more information. Also, with additional experimentation, it would be possible to determine at what frequency of stimulation light one begins to access the

205 °C and 230 °C traps, and what the relative OSL efficiency of the three traps is in this material, though indications from the afterglow analysis suggest that the royal blue excitation frequency may in fact begin to access the 205 °C and/or 230 °C trap(s).

Finally, Kim *et al* noted that the TL emission spectrum for this material has peaks located at 355, 385 and 440 nm[50]. These first two peaks are well within the detection system window, though the third peak is not. This, in part, provides an explanation for the relatively high OSL signal from this substance. It also suggests that by expanding the detection window from a low-energy edge at 410 nm to perhaps, 450-480 nm, this OSL signal strength would be increased even more. This modification, combined with faster counting electronics, has the potential to yield an exciting new OSL dosimetry method, with the possibility of extracting substantive and valuable information from individual traps.

CONCLUSIONS

$CaSO_4$:Dy and $CaSO_4$:Dy+P showed little to no OSL signal using the experimental apparatus. Additional research at higher excitation frequencies and/or with the capability to measure emission frequencies other than UV would be needed, however, to conclusively rule out these materials' suitability as OSL dosimetry materials. KBr showed low-intensity OSL response using both red and green stimulation light and the relationship between the emitted OSL signals using these sources suggests the possibility that two different traps with different fading rates are being preferentially accessed with the two wavelengths. Specifically, the OSL response resulting from excitation with 625

nm light demonstrated an approximate 10 h half-life, while the OSL response resulting from excitation with 530 nm light demonstrated an approximate 20 d half-life. Further investigation at higher doses, using stronger excitation light sources and/or collecting non-UV emission wavelengths, however, is needed to more precisely characterize and quantify this material's OSL behavior. $CaSO_4$:Tm exhibits significant OSL signal at the experimental dose, as well as some variation in decay rates of OSL signals emitted under different stimulation frequencies. The half-lives of the OSL signals for all excitation wavelengths were in the 10-20 d range. Finally, LiF:Mg,Cu,Na,Si and, to an even greater extent LiF:Mg,Cu,Si, exhibit significant OSL output in the UV range when exposed to visible light. For LiF:Mg,Cu,Na,Si, the half-lives of the OSL signals for the green, cyan, blue and royal blue excitation sources were approximately 8.9, 8.3, 11.9 and 25.3 d, respectively. For LiF:Mg,Cu,Si, the half-life of both the green- and cyan-induced signals is approximately 4 d, and for the red-induced signal it is approximately 9 d though with significantly higher statistical uncertainty. Both of these materials thus exhibit differences in the OSL signals' decay time constants when using lower- versus higher-frequency light excitation, leading to the conclusion that their individual traps may be accessed optically.

It is also interesting to note the consistency to the results of the above-described experiment in terms of which frequencies of excitation light were able to access traps of which temperatures, across all sample materials. Specifically, it was found that OSL emission occurred using red stimulation for materials with traps located at 115 °C and 140 °C, green stimulation produced OSL emission in materials with traps located at 140 °C, 145 °C, 155 °C, 160 °C and 170 °C. Blue stimulation produced OSL emission in

materials with traps located at 230 °C and 245 °C, and no OSL signal was found that corresponded to TL peaks at 255 °C and above. These correlations were further supported by the high degree of matching of fading decay constants between TL and OSL experimental results. Though there will be variation in the optical energy threshold at TL peaks of the same temperature for different materials due to differences in the phonon energy, E_{ph}, associated with the trap, the experimental results indicate a useful range for correlating the OSL excitation spectrum and the TL glow curve of a material. More quantitative exploration of this relationship will require investigation into the phonon vibrational frequencies and Rhys-Huang factors of each material in question, which lies beyond the scope of this work.

In conclusion, $CaSO_4$:Tm, LiF:Mg,Cu,Na,Si and LiF:Mg,Cu,Si exhibit easily detectable OSL signals using the described experimental apparatus at the utilized dose, and OSL fading rates consistent with TL experimental results. In addition, the results provide some evidence that OSL techniques can be used to extract relative individual trap population information from appropriate materials. Specifically, as excitation light increases in frequency, deeper traps in the selected materials are accessed preferentially to contribute to the total OSL light output from the sample.

ACKNOWLEDGEMENTS

The authors would like to thank Andrew F. Kalchik for his assistance during the data collection phase of this series of experiments. In addition, much appreciation is owed to Dr. Jang-Lyul Kim of KAERI, Dr. Kook-Jin Chun of the Korea Research

Institute of Standards and Science (KRISS), and Thermo Fisher Scientific, Inc, for providing material samples.

This research was supported, in part, by a U.S. Department of Homeland Security (DHS) Fellowship administered by the Oak Ridge Institute for Science and Education (ORISE) through an interagency agreement with the U.S Department of Energy (DOE). All opinions expressed in this paper are the author's and do not necessarily reflect the policies and views of DHS, DOE, or ORISE.

REFERENCES

1. Bøtter-Jensen, L., McKeever, S. W. S. and Wintle, A. G. Optically stimulated luminescence dosimetry. (Amsterdam, The Netherlands: Elsevier Science B.V.) (2003) ISBN 0444506845.

2. Kristianpoller, N., Oster, L. Optically stimulated luminescence in anion-defective carbon doped alpha-Al_2O_3 crystals. Radiation Effects and Defects in Solids. 134, 311-313 (1995).

3. McKeever, S. W. S., Akselrod, M. S. and Markey, B. G. Pulsed optically stimulated luminescence dosimetry using α-Al_2O_3:C. Radiat. Prot. Dosim. 65, 267-272 (1996).

4. Bøtter-Jensen, L. and McKeever, S. W. S. Optically stimulated luminescence dosimetry using natural and synthetic materials. Radiat. Prot. Dosim. 65, 273-280 (1996).

5. Bulur, E. and Göksu, H. Y. Pulsed optically stimulated luminescence from α-Al_2O_3:C using green light emitting diodes. Radiat. Meas. 27, 479-488 (1997).

6. Bøtter-Jensen, L., Larsen, N. A., Markey, B. G. and McKeever, S. W. S. Al_2O_3:C as a sensitive OSL dosimeter for rapid assessment of environmental dose rates. Radiat. Meas. 27, 295-298 (1997).

7. Akselrod, M. S., Lucas, A. C., Polf, J. C. and McKeever, S. W. S. Optically stimulated luminescence of Al_2O_3. Radiat. Meas. 29, 391-399 (1998).

8. McKeever, S. W. S. and Akselrod, M. S. Radiation dosimetry using pulsed optically stimulated luminescence of Al_2O_3:C. Radiat. Prot. Dosim. 84, 317-320 (1999).

9. Bøtter-Jensen, L., Mejdahl, V. and Murray, A. S. New light on OSL. Quaternary Geochronology. 18, 303-309 (1999).

10. Yoder, R. C. A radiation measurement film employing optically stimulated luminescence technology. Landauer, I. Glenwood, Illinois. (2000).

11. Akselrod, M. S., Kortov, V. S., Kravetsky, D. J. and Gotlib, V. I. Highly sensitive thermoluminescent anion-defect alpha-Al_2O_3:C single crystal detectors. Radiat. Prot. Dosim. 33, 119-122 (1990).

12. Moscovitch, M., Tawil, R. A. and Svinkin, M. Light induced fading in α-Al_2O_3:C. Radiat. Prot. Dosim. 47, 251-253 (1993).

13. Walker, F. D., Colyott, L. E., Larsen, N. A. and McKeever, S. W. S. The wavelength dependence of light-induced fading of thermoluminescence from α-Al_2O_3:C. Radiat. Meas. 26, 711-718 (1996).

14. West, W. G., Kearfott, K. J. and Bernal, S. M. The sunlight OSL response of a commercially available α-Al_2O_3:C personnel dosimetry material. Radiat. Prot. Dosim. 119, 344-349 (2006).

15. Bøtter-Jensen, L., Markey, B. G. and Agersnap Larsen, N. Retrospective radiation dosimetry using optically stimulated luminescence on natural and synthetic materials. (Horn, Austria: Berger) (1996).

16. Stoneham, D., Bailiff, I. K., Petrov, S., Botter-Jensen, L., Goeksu, Y. and Jungner, H. Retrospective dosimetry: The development of an experimental methodology using luminescence techniques. (Luxembourg, Luxembourg) (1996).

17. Banerjee, D., Boetter-Jensen, L. and Murray, A. S. Retrospective dosimetry: Estimation of the dose to quartz using the single-aliquot regenerative-dose protocol. Applied Radiation and Isotopes. 52, 831-844 (2000).

18. Kanemaki, M., Ninagawa, K., Yamamoto, I., Nakagawa, M., Wada, T., Yamashita, Y. and Endo, K. Red thermoluminescence of volcanic glass fractions from tephras. International Journal of Radiation Applications and Instrumentation. Part D. Nuclear Tracks and Radiation Measurements. 18, 81-88 (1991).

19. Bøtter-Jensen, L., Jungner, H. and Mejdahl, V. Recent developments of OSL techniques for dating quartz and feldspars. Radiation Protection Dosimetry (UK). 47, 643-648 (1993).

20. Banerjee, D. Optical stimulated luminescence (OSL) dating. (Lucas Heights, Australia: Australian Institute of Nuclear Science and Engineering) (1999).

21. Bailey, R. M., Adamiec, G. and Rhodes, E. J. OSL properties of NaCl relative to dating and dosimetry. Radiat. Meas. 32, 717-723 (2000).

22. Huett, G. and Jaek, I. Advances in the luminescence dating: The optically stimulated luminescence based procedures and their physical background. Proceedings of the Estonian Academy of Sciences: Geology. 50, 214-232 (2001).

23. Stokes, S. and Fattahi, M. Red emission luminescence from quartz and feldspar for dating applications: An overview. Radiat. Meas. 37, 383-395 (2003).

24. Takaki, S., Ikeya, M. and Yamanaka, C. Remote TL and OSL for asteroid and meteorite study. Radiat. Meas. 27, 393-397 (1997).

25. Bøtter-Jensen, L. Development of optically stimulated luminescence techniques using natural minerals and ceramics, and their application to retrospective dosimetry. Risø-R-1211(EN). Roskilde, Denmark. (2000).

26. Inrig, E. L., Godfrey-Smith, D. I. and Khanna, S. Optically stimulated luminescence of electronic components for forensic, retrospective, and accident dosimetry. Radiat. Meas. 43, 726-730.

27. Bailiff, I. K. The use of ceramics for retrospective dosimetry in the Chernobyl exclusion zone. Radiat. Meas. 24, 507-511 (1995).

28. Hashimoto, T., Hong, D. G. and Takano, M. Retrospective dosimetry at JCO using luminescence from ceramics pieces and quartz grains. Advances in ESR Applications. 18, 197-202 (2002).

29. Akselrod, M. S., Bøtter-Jensen, L. and McKeever, S. W. S. Optically stimulated luminescence and its use in medical dosimetry. Radiat. Meas. 41, S78-S99 (2006).

30. Gaza, R., McKeever, S. W. S., Akselrod, M. S., Akselrod, A., Underwood, T., Yoder, C., Andersen, C. E., Aznar, M. C., Marckmann, C. J. and Bøtter-Jensen, L. A fiber-dosimetry method based on OSL from Al_2O_3:C for radiotherapy applications. Radiat. Meas. 38, 809-812 (2004).

31. Gaza, R. and McKeever, S. W. S. A real-time, high-resolution optical fibre dosemeter based on optically stimulated luminescence (OSL) of KBr:Eu, for potential use during the radiotherapy of cancer. Radiat. Prot. Dosim. 120, 14-19 (2006).

32. Douguchi, Y., Nanto, H., Sato, T., Imai, A., Nasu, S., Kusano, E., Kinbara, A. Optically stimulated luminescence in Eu-doped KBr phosphor ceramics. Radiat. Prot. Dosim. 84, 143-148 (1999).

33. Nanto, H., Miyazaki, M., Imai, A., Komori, H., Douguchi, Y., Kusano, E. and Kinbara, A. New photostimulable phosphor materials for digital radiography. (1999).

34. Nambi, K. S. V. and et al. Thermoluminescence of $CaSO_4$ doped with rare earths. Journal of Physics C: Solid State Physics. 7, 4403 (1974).

35. Iga, K., Yamashita, T., Takenaga, M., Yasuno, Y., Oonishi, H. and Ikedo, M. Composite TLD based on $CaSO_4$:Tm for gamma-rays, x-rays, beta-rays and thermal neutrons. Health Phys. 33, 605-610 (1977).

36. Lewandowski, A. C., Barkyoumb, J.H., Mathur, V.K. Thermoluminescence emission, excitation and stimulation spectra of $CaSO_4$:Dy and $CaSO_4$:Tm. Radiat. Prot. Dosim. 65, 281-286 (1996).

37. Lakshmanan, A. R., Lapraz, D., Prévost, H. and Benabdesselam, M. Thermostimulated luminescence properties of $CaSO_4$:Dy and $CaSO_4$:Tm phosphors annealed at high temperatures. physica status solidi (a). 202, 131-139 (2005).

38. Yamashita, T., Nada, N., Onishi, H. and Kitamura, S. Calcium sulfate activated by thulium or dysprosium for thermoluminescence dosimetry. Health Phys. 21, 295-300 (1971).

39. West, W. G., Kearfott, K. J. and Bernal, S. M. Optically stimulated luminescence of various TLD materials. (Ann Arbor, Michigan: The University of Michigan) (2011).

40. Bacci, C., Bernabei, R., d'Angelo, S. and Furetta, C. Analysis of TLD-900 glow-curves: Results on single peak properties. Radiation Effects. 69, 127-133 (1983).

41. Bacci, C., Calicchia, A., Pugliani, L., Salvadori, P. and Furetta, C. A preliminary study on the dosimetric properties of $CaSO_4$:Dy ribbon (TLD-900). Health Phys. 38, 21-24 (1980).

42. Wang, T.-K., Hsu, P.-C. and Weng, P.-S. Feasability study of using $CaSO_4$:Dy phosphor for simultaneous estimation of exposure and time elapsed post-exposure. Radiat. Prot. Dosim. 18, 157-161 (1987).

43. Maghrabi, M., Karali, T., Townsend, P. D. and Lakshmanan, A. R. Luminescence spectra of $CaSO_4$ with Ce, Dy, Mn and Ag codopants. J. Phys. D Appl. Phys. 33, 477-484 (2000).

44. Yang, J. S., Kim, D. Y., Chang, S. Y., Nam, Y. M. and Park, J. W. Thermoluminescence characteristics of teflon embedded $CaSO_4$:Dy TLD. Radiat. Prot. Dosim. 100, 337-340 (2002).

45. Pradhan, A. S. and Ayyangar, K. Radiation dosimetry by photostimulated luminescence of CaSO:Dy. International Journal of Applied Radiation and Isotopes. 28, 534-535 (1977).

46. Kim, J.-L., Chang, S.-Y., Jin, D., Yang, J.-S., Nam, Y.-M. and Lee, J.-I. $CaSO_4$ based thermoluminescent detector bonded with P-compound and a method for fabricating thereof. (USA: Korea Atomic Energy Research Institute) (2003) ISBN 6,586,752 B1.

47. Yang, J. S., Kim, D. Y., Kim, J. L., Lee, J. I., Kim, B. W., Chang, S. Y. and Park, J. W. Development of phosphorus-compund $CaSO_4$:Dy(KCT-300) TL pellets. Journal of the Korean Nuclear Society. 34, 142-145 (2002).

48. Yang, J.-S., Kim, J.-L., Kim, D.-y. and Chang, S.-Y. Development of a TL detector for neutron measurement by $CaSO_4$:Dy phosphors. Radiat. Prot. Dosim. 110, 301-304 (2004).

49. Kim, J. L., Lee, J. I., Pradhan, A. S., Chang, I., Kim, B. H., Chung, K. S. and Choe, H. S. Optimization of preparation procedure of LiF:Mg,Cu,Si TLD for improving the reusability. Radiat. Meas. 45, 583-585 (2010).

50. Kim, J. L., Lee, J. I., Pradhan, A. S., Kim, B. H. and Kim, J. S. Further studies on the dosimetric characteristics of LiF:Mg,Cu,Si--a high sensitivity thermoluminescence dosimeter (TLD). Radiat. Meas. 43, 446-449 (2008).

51. Lee, J. I., Kim, J. L., Pradhan, A. S., Kim, B. H., Chung, K. S. and Choe, H. S. Role of dopants in LiF TLD materials. Radiat. Meas. 43, 303-308 (2008).

52. Lee, J. I., Kim, J. L., Rahman, M. S., Chang, S. Y., Chung, K. S. and Choe, H. S. Development of LiF:Mg,Cu,Si TL material (new KLT-300) with a low-residual signal and high-thermal stability. Radiat. Prot. Dosim. 125, 229-232 (2007).

53. Lee, J. I., Kim, J. L., Yang, J. S., Pradhan, A. S., Kim, B. H., Chung, K. S. and Choe, H. S. Dual-step thermal treatment for the stability of glow curve structure and the TL sensitivity of the newly developed LiF:Mg,Cu,Si. Radiat. Meas. 42, 597-600 (2007).

54. Lee, J. I., Yang, J. S., Kim, J. L., Pradhan, A. S., Lee, J. D., Chung, K. S. and Choe, H. S. Dosimetric characteristics of LiF:Mg,Cu,Si thermoluminescent materials. Applied Physics Letters. 89, 094110-094110-3 (2006).

55. Nakajima, T., Murayama, Y., Matsuzawa, T. and Koyano, A. Development of a new highly sensitive LiF thermoluminescence dosimeter and its applications. Nuclear Instruments and Methods. 157, 155-162 (1978).

56. Pradhan, A. S., Lee, J. I., Kim, J. L., Chung, K. S., Choe, H. S. and Lim, K. S. Tl glow curve shape and response of LiF:Mg,Cu,Si--effect of heating rate. Radiat. Meas. 43, 361-364 (2008).

57. Yang, B., Lu, Q., Wang, S. and Townsend, P. D. Studies on the thermoluminescence spectra and thermal stability of LiF:Mg,Cu, LiF:Mg,Cu,Na and LiF:Mg,Cu,Si. Nuclear Instruments and Methods in Physics Research Section B: Beam Interactions with Materials and Atoms. 239, 171-178 (2005).

58. Budzanowski, M., Kim, J. L., Nam, Y. M., Chang, S. Y., Bilski, P. and Olko, P. Dosimetric properties of sintered LiF:Mg,Cu,Na,Si TL detectors. Radiat. Meas. 33, 537-540 (2001).

59. Doh, S. H., Chu, M. C., Chung, W. H., Kim, H. J., Kim, D. S. and Kang, Y. H. Preparation of LiF(Mg,Cu,Na,Si) phosphor and its thermoluminescent characteristics. Korean Journal of Applied Physics. 2, 425-431 (1989).

60. Ha, V. T. T., Hai, N. T. Q., Long, N. N. and Vu, L. V. Preparation and characteristics of LiF:Mg, Cu, Na, Si thermoluminescent material. VNU Journal of Science, Mathematics - Physics. 23, 225-231 (2007).

61. Jung, H., Jai Lee, K., Kim, J.-L. and Lee, S.-Y. Development of a personal dosimeter badge system using sintered LiF:Mg,Cu,Na,Si TL detectors for photon fields. Radiat. Meas. 38, 71-80 (2004).

62. Jung, H., Lee, K. J. and Kim, J. L. A personal thermoluminescence dosimeter using LiF:Mg,Cu,Na,Si detectors for photon fields. Appl Radiat Isot. 59, 87-93 (2003).

63. Kim, H. J., Chung, W. H., Doh, S. H., Chu, M. C., Kim, D. S. and Kang, Y. H. Thermoluminescence dosimetric properties of LiF(Mg,Cu,Na,Si). Journal of the Korean Physical Society. 22, 415-420 (1990).

64. Kim, J. L., Lee, J. I., Chang, S. Y., Chung, K. S. and Choe, H. S. The glow curve structure for the LiF:Mg,Cu,Na,Si TL detector with dopants concentrations and sintering temperatures. Radiat. Meas. 38, 435-438 (2004).

65. Kim, J. L., Lee, J. I., Ji, Y. H., Kim, B. H., Kim, J. S. and Chang, S. Y. Energy responses of the LiF series TL pellets to high-energy photons in the energy range from 1.25 to 21 MV. Radiat. Prot. Dosim. 119, 353-356 (2006).

66. Lee, J. I., Kim, J. L. and Chang, S. Y. Thermoluminescent characteristics of newly developed LiF:Mg,Cu,Na,Si TL detectors. Journal of the Korean Nuclear Society. 36, 6 (2004).

67. Lee, J. I., Kim, J. L., Chang, S. Y., Chung, K. S. and Choe, H. S. Developments in the synthesis of LiF:Mg,Cu,Na,Si TL material. Radiat. Prot. Dosim. 108, 79-83 (2004).

68. Lee, J. I., Kim, J. L., Chang, S. Y., Chung, K. S. and Choe, H. S. Dosimetric properties of the newly developed KLT-300 (LiF:Mg,Cu,Na,Si) TL detector. Radiat. Meas. 38, 439-42 (2004).

69. Lee, J. I., Kim, J. L., Chang, S. Y., Chung, K. S. and Choe, H. S. On the roles of the dopants in LiF:Mg,Cu,Na,Si thermoluminescent material. Radiat. Prot. Dosim. 115, 340-344 (2005).

70. Lee, J. I., Lee, D., Kim, J. L. and Chang, S. Y. Thermoluminescence emission spectra for the LiF:Mg,Cu,Na,Si thermoluminescent materials with various concentrations of the dopants (3-D measurement). Radiat. Prot. Dosim. 119, 293-299 (2006).

71. Miljanić, S., Ranogajec-Komor, M., Knežević, Ž., Štuhec, M. and Prokić, M. Comparative study of LiF:Mg,Cu,Na,Si and $Li_2B_4O_7$:Cu,Ag,P TL detectors. Radiat. Prot. Dosim. 119, 191-196 (2006).

72. Nam, Y. M., Kim, J. L. and Chang, S. Y. Dependence of glow curve structure on the concentration of dopants in LiF:Mg,Cu,Na,Si phosphor. Radiat. Prot. Dosim. 84, 231-234 (1999).

73. Nam, Y. M., Kim, J. L., Chang, S. Y., Kim, B. H. and Kim, H. J. Dosimetric characteristics of LiF:Mg,Cu,Na,Si phosphor. (Hiroshima, Japan: IRPA) (2000).

74. Nam, Y. M., Lee, D. W., Chung, W. H., Doh, S. H., Kim, G. D. and Kim, H. J. Fabrication of LiF:Mg,Cu,Na,Si teflon TLDs and their dosimetric characteristics. Korean Journal of Applied Physics. 11, 102-107 (1998).

75. Nam, Y.-M. and Kim, J.-L. Thermoluminescence properties of LiF:Mg,Cu,Na,Si pellets in radiation dosimetry. Radiat. Prot. Dosim. 100, 467-470 (2002).

76. Tang, K. Dependence of thermoluminescence in LiF:Mg,Cu,Na,Si phosphor on Na dopant concentration and thermal treatment. Radiat. Meas. 37, 133-140 (2003).

77. Tang, K., Zhu, H., Shen, W. and Liu, B. A new high sensitivity thermoluminescent phosphor with low residual signal and good stability to heat treatment: LiF:Mg,Cu,Na,Si. Radiat. Prot. Dosim. 100, 239-242 (2002).

78. West, W. G., Kearfott, K. J. and Kalchik, A. F. An affordable optically stimulated luminescent dosimeter reader utilizing multiple excitation wavelengths. (Ann Arbor, Michigan: The University of Michigan) (2011).

79. McKeever, S. W. S., Moscovitch, M. and Townsend, P. D. Thermoluminescence dosimetry materials: Properties and uses. (Ashford: Nuclear Technology Publishing) (1995) ISBN 1870965191.

80. Randall, J. T. and Wilkins, M. H. F. Phosphorescence and electron traps. I. The study of trap distributions. Proceedings of the Royal Society of London. Series A, Mathematical and Physical Sciences. 184, 365-389 (1945).

81. Horowitz, Y. S. and Yossian, D. Computerised glow curve deconvolution: Application to thermoluminescence dosimetry. Radiat. Prot. Dosim. 60(1995).

82. Harvey, J. A., Haverland, N. P. and Kearfott, K. J. Characterization of the glow peak fading properties of six common thermoluminescent materials. (Ann Arbor, Michigan: The University of Michigan) (2010).

83. Sidran, M. An infrared stimulable phosphor dosimeter with time lapse indication. Applied Optics. 8, 79-84 (1969).

84. Furetta, C., Pani, R., Pellegrini, R. and Driscoll, C. M. H. A computational method to assess the time elapsed since exposure using thermoluminescence dosemeters. Radiation Effects. 88, 59-67 (1986).

85. Budzanowski, M., Vergara, J. C. S., Ryba, E., Bilski, P., Olko, P. and Waligorski, M. P. R. Estimation of the time elapsed between exposure and readout using peak ratios of LiF:Mg, Cu, P (MCP-N, GR200A). Radiat. Prot. Dosim. 85, 149-152 (1999).

86. Spurny, Z. Simultaneous estimation of exposure and time elapsed since exposure using multipeaked thermoluminescent phosphors. Health Phys. 21, 755-761 (1971).

87. Nakajima, T. and Hashizume, T. On applicability of TL fading to estimation of time after irradiation. Health Phys. 16, 782-783 (1969).

88. Moscovitch, M. Automatic method for evaluating elapsed time between irradiation and readout in LiF-TLD. Radiat. Prot. Dosim. 17, 165-169 (1986).

89. Lakshmanan, A. R., Bhatt, B. C. and Bhatt, R. C. Simultaneous determination of dose and elapsed time after radiation exposure using $CaSO_4$:Na,Dy. Radiat. Prot. Dosim. 27, 15-20 (1989).

90. Moscovitch, M. TLD apparatus and method with elapsed time read-out capability. (USA: The Harshaw Chemical Company) (1989) ISBN 4,827,131.

91. Furetta, C., Tuyn, J. W. N., Louis, F., Azorin-Nieto, J., Gutiérrez, A. and Driscoll, C. M. H. A method for determining simultaneously the dose and the elapsed time since irradiation using TLDs. International Journal of Radiation Applications and Instrumentation. Part A. Applied Radiation and Isotopes. 39, 59-69 (1988).

92. Weinstein, M., German, U., Dubinsky, S. and B. Alfassi, Z. On the determination of the post-irradiation time from the glow curve of TLD-100. Radiat. Prot. Dosim. 106, 121-130 (2003).

93. Blakemore, J. S. and Rahimi, S. Models for mid-gap centers in gallium arsenide. (Elsevier) (1984) ISBN 0080-8784.

94. Grimmeiss, H. G. and Ledebo, L. A. Photo-ionization of deep impurity levels in semiconductors with non-parabolic bands. Journal of Physics C: Solid State Physics. 8, 2615 (1975).

95. Singarayer, J. S. and Bailey, R. M. Component-resolved bleaching spectra of quartz optically stimulated luminescence: Preliminary results and implications for dating. Radiat. Meas. 38, 111-118 (2004).

96. Huntley, D. J., Short, M. A. and Dunphy, K. Deep traps in quartz and their use for optical dating. Canadian Journal of Physics. 74, 81-91 (1996).

97. Jaek, I., Kerikmae, K., Lust, A. Optically stimulated luminescence of some thermoluminescence detectors as an indicator of absorbed radiation dose. Radiat. Prot. Dosim. 100, 459-462 (2002).

98. Pradhan, A. S. Emission spectra and influence of sunlight on thermoluminescence of dysprosium doped $CaSO_4$ and CaF_2. Radiat. Prot. Dosim. 47, 151-154 (1993).

CHAPTER 6

CONCLUSIONS

The preceding papers detail a series of experiments ultimately conducted to analyze the OSL properties, using multiple excitation wavelengths, of a number of TL materials. Additionally, the effect of sunlight on the OSL response of α-Al_2O_3:C was explored in detail, and a novel and inexpensive OSL reader with unique capabilities was designed, built and found to be experimentally useful. Ultimately, the course of research detailed herein resulted in several significant observations, described below.

CaF_2:Mn, $Li_2B_4O_7$:Cu, LiF:Mg,Ti, $CaSO_4$:Dy and $CaSO_4$:Dy+P exhibited little to no OSL signal in the UV region, when using visible light stimulation. In the case of CaF_2:Mn, $CaSO_4$:Dy and $CaSO_4$:Dy+P, additional research at higher excitation frequencies and/or with the capability to measure emission frequencies other than UV could reveal an OSL response. In the case of $Li_2B_4O_7$:Cu and LiF:Mg,Ti, the evidence suggests that alternative OSL reader configurations would not result in a favorable OSL sensitivity.

$CaSO_4$:Tm and KBr exhibited relatively modest but detectable OSL responses in the experiments. The presence of OSL signals resulting from different excitation light frequencies in these materials suggested that different electron traps were being accessed by the OSL reader in a manner analogous, and related, to the polling of traps at different temperatures in TL. While their luminance was significantly lower than that of

α-Al_2O_3:C, both materials exhibited different decay rates over time of the OSL signals induced by the different excitation wavelengths. Specifically, the signals resulting from lower-energy stimulation appeared to decay more quickly at room temperature than those resulting from higher-energy stimulation. This behavior supports the correlation between OSL signals resulting from various excitation frequencies and TL peaks resulting from different temperatures. Further investigations at higher doses, using stronger or different-wavelength excitation light sources and/or collecting non-UV emission wavelengths is indicated to more precisely characterize and quantify these materials' OSL behaviors.

LiF:Mg,Cu,Na,Si (KLT-300) and, to an even greater extent, LiF:Mg,Cu,Si, (New-KLT-300) exhibited *significant* OSL output in the UV range when exposed to visible light. The apparent OSL sensitivity of both materials, most especially LiF:Mg,Cu,Si, while less than that of α-Al_2O_3:C using the experimental setup, may ultimately meet or exceed the sensitivity of this commercially-used OSL dosimetry material, given improved experimental conditions. In addition, these materials, like $CaSO_4$:Tm and KBr, also exhibited differences in the OSL signals' decay time constants when using lower- versus higher-frequency light excitation. These differences corresponded in quality and approximate quantity to the trap structure demonstrated by TL measurements of these same materials.

The experiments described above provide substantial new information regarding the OSL properties of a number of substances. Based on these results, it was determined that a significant OSL response exists for $CaSO_4$:Tm, LiF:Mg,Cu,Na,Si and LiF:Mg,Cu,Si. In addition, it was found that the fading rates of OSL signals over time

depends upon the excitation wavelength used to elicit the signals, and that these fading rates and the excitation wavelengths that correspond to them correlate well with the TL behavior of the materials. Further investigation into the OSL properties of $CaSO_4$:Tm, LiF:Mg,Cu,Na,Si and LiF:Mg,Cu,Si is indicated by this research, and it is hoped that the initial work performed during the course of this dissertation may provide a foundation upon which other investigations may be built.

More generally, this dissertation highlights the substantial experimental resources and time required to partially characterize, from an OSL behavior standpoint, a very limited number of candidate materials. Future research in this area would benefit greatly from quicker and more efficient methods of identifying materials that may possess favorable OSL properties. The application of solid state band theory in predicting the energy level structure and recombination properties, as well as the use of recently-developed techniques in the area of computational solid state chemistry, may provide these methods. While much effort has been made in this area related to the development of advanced semiconductors for the electronics and computer industry, and textbooks in this area[1] may focus examples on such materials as gallium arsenide and silicon for that reason, these techniques could theoretically be applied in the radiation dosimetry space. Computational chemistry, in particular, has reached a maturity at which it may be possible for non-materials scientists to predict which materials and dopants will yield the luminescence properties that are desired, and to refine or optimize the existing materials being employed. Codes based on a quantum-mechanical approach to understanding solid state structure, such as the projector-augmented wave (PAW) method and the linearized muffin-tin orbital (LMTO) method, as well as statistical methods such

as Monte Carlo-based and molecular dynamics-based codes, could be employed to predict both optical absorption and luminescence properties[2]. Each of these codes has its particular strengths and weaknesses and the ease of use varies amongst them. As such, while learning to use one or more of them properly and designing a search methodology to identify promising OSL compounds is not a trivial exercise, the long-term benefits to such an effort could be significant.

REFERENCES

1. Singleton, J. Band theory and electronic properties of solids. (Oxford, United Kingdom: Oxford University Press) (2001).

2. Dronskowski, R. Computational chemistry of solid state materials. (Weinheim, Germany: Wiley-VCH) (2005) ISBN 978-3-527-31410-2.